A FINITE ELEMENT ANALYSIS OF A CARBON FIBER COMPOSITE MICRO AIR VEHICLE WING

THESIS

Theodore A. Szelag

AFIT/GAE/ENY/12-M44

DEPARTMENT OF THE AIR FORCE
AIR UNIVERSITY

AIR FORCE INSTITUTE OF TECHNOLOGY

Wright-Patterson Air Force Base, Ohio

AFIT/GAE/ENY/12-M44

A FINITE ELEMENT ANALYSIS OF A CARBON FIBER COMPOSITE MICRO AIR VEHICLE WING

THESIS

Presented to the Faculty

Department of Aeronautics and Astronautics

Graduate School of Engineering and Management

Air Force Institute of Technology

Air University

Air Education and Training Command

In Partial Fulfillment of the Requirements for the

Degree of Master of Science in Aeronautical Engineering

Theodore A. Szelag

March 2012

AFIT/GAE/ENY/12-M44

A FINITE ELEMENT ANALYSIS OF A CARBON FIBER COMPOSITE MICRO AIR VEHICLE WING

Theodore A. Szelag

March 2012

Approved:

//SIGNED 29-FEB-2012//	
Dr. Anthony Palazotto (Chairman)	date
//SIGNED 29-FEB-2012//	
Dr. Robert Brockman (Member)	date
//SIGNED 29-FEB-2012//	
Dr. Donald Kunz (Member)	date

Abstract

Micro-air vehicles (MAV)s provide a valuable and low observable way to do the jobs that the Air Force deems to be dull, dirty and dangerous. Basing the design of an MAV wing on that of a biological counterpart will provide a proven design that is capable of achieving the mission requirements. This research is designed to analyze the design and manufacturing of a wing based off the Manduca Sexta.

Inaccuracies in the fiber orientation can result in substantial changes in the material properties. Experimental vibration data of composite material samples manufactured using a three-ply [0/90/0] small non-homogenous fiber composite provided results that varied over 33 percent from analytical results. Since the material was to be used in the manufacturing of a biologically inspired MAV, it was important to understand the cause of the variance in the measured material properties so that they could be taken into account for the design and manufacturing of the MAV wing.

An analysis was performed on the material to verify that it matched specified material properties. Inaccuracies in the manufacturing of the composite samples were taken into account; specifically ply orientation, cut angle, and material thickness were examined. Using finite element analysis (FEA), it was determined that a misalignment in fiber orientation of less than five degrees combined with resulting short fiber effects accounts for the difference between analytical and experimental results. Using an optical microscope, variances in the ply orientation was observed confirming the FEA results. Possible inaccuracies in the composite material were taken into consideration during the design and construction of the MAV wing.

A FEA model of the engineered MAV wing was developed with the carbon-fiber composites inaccuracies in mind. To allow for changes to the model to be made quickly, the FEA model was generated using a developed MATLAB code that generated finite element input files to be solved using ABAQUS, a finite element program. The developed MATLAB code generated beam cross-sections for the composite material elements based upon the input ply orientations and inaccuracies and assigned corrected densities of each of the beam elements. It also allowed for idiosyncrasies of the composite vein structure of the wing to easily be changed and evaluated. Since multiple FEA input files could be generated quickly, an analysis was performed in order to determine the effects of the misalignment of the ply orientation angles on the MAV wing model.

Acknowledgements

I would like to thank Dr. Palazotto for being my advisor, and giving me the opportunity to study here at AFIT, and Maj. Ryan O'Hara for teaching me the love-hate relationship with MATLAB that was so crucial to this project. Finally, I would like to thank my family and friends, especially Laura Mack, for giving me encouragement and support throughout my time here.

Theodore A. Szelag

Table of Contents

List of Figures

Figure Page

Figure Page

Figure Page

Figure Page

Figure Page

List of Tables

List of Symbols

Symbol:	Definition:
E	Elastic Modulus
E_1	Lamina 0° Tension Modulus
E_2	90° Tension modulus
E/ρ	Specific Modulus
G_{12}	45° in-plane shear modulus
GPa	Giga-Pascal
Hz	Hertz
I	Second Moment of Area
micron	Micrometer
mg	Milligram
mm	Millimeter
υ_{12}	Poisson's Ratio in the x-y plane
θ	Lamina Fiber Orientation Angle
ω	Modal Frequency

List of Abbreviations

Abbreviation:	Meaning:
AFIT	Air Force Institute of Technology
CAD	Computer Automated Design
CT	Computed tomography
CW	Chordwise
DARPA	Defense Advanced Research Projects Agency
DOF	Degrees of Freedom
E	Elastic Modulus
FWMAV	Flapping Wing Micro Air Vehicle
GTOW	Gross Take-Off Weight
ISR	Intelligence, Surveillance and Reconnaissance
MAV	Micro Air Vehicle
MR	Modal Ratio
SLV	Scanning Laser Vibrometer
SW	Spanwise
UAV	Unmanned Aerial Vehicle
USD	United States Dollars

A FINITE ELEMENT ANALYSIS OF A CARBON FIBER COMPOSITE MICRO AIR VEHICLE WING

I. Introduction

1.1. Research Objective

Current research done by O'Hara [1] on the Manduca Sexta has provided a preliminary design for a manufactured bio-inspired Micro Air Vehicle (MAV) wing based upon the structural characteristics of the forewing of the Manduca Sexta. This preliminary design consists of a unidirectional carbon fiber composite vein structure with a Kapton membrane manufactured at the Air Force Institute of Technology (AFIT), see Figure 1.1. The materials for the wing were chosen based upon the need of the MAV wing to have both high strength and low density, successful testing compared to metallic materials and previous research found showing success of carbon fiber wings in other MAV applications [1] [2] [3]. The veins of the wing were cut out of a single sheet of [0/90/0] three-ply unidirectional carbon-fiber composite, based on the geometry of the Manduca Sexta, and a "best guess" method of determine the vein width in order to create a wing that could withstand the stresses and strains of testing.

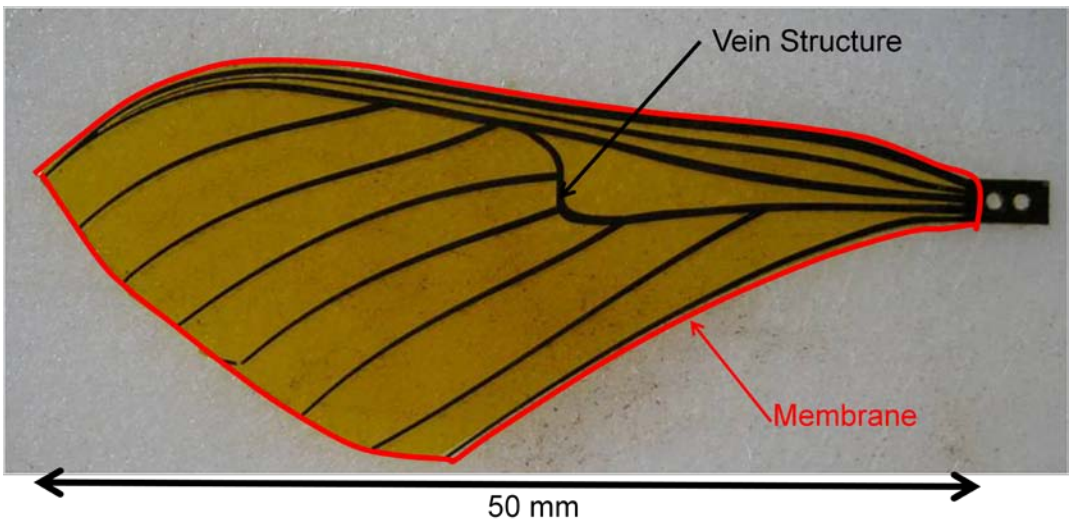

Figure 1.1: Manufactured MAV Wing Developed by O'Hara [2].

While work done by DeLeon has shown that the design of O'Hara's wing shares some characteristics of the hawkmoth wing, some further understanding is necessary to create a manufactured wing that will more closely match the structural characteristics of the Manduca Sexta [1]. It is important that any design changes be made with a full understanding of the structure at hand, so that a better design will result. This will not only lead to a better-designed wing, but also a more efficient design process.

The carbon fiber composite used in the engineered wing allowed for a stiffer, lightweight design. However, there were concerns over the effectiveness of the carbon fiber composite in the wing design. Would the carbon fiber composite retain its material properties given the small size of the veins? How does the fact that the veins are laser cut affect the structure of the engineered wing? How does the anisotropic nature of the composite affect the wing?

These questions are worth looking at if the use of the three-ply unidirectional composite in the MAV wing is to be considered. Therefore, the objective of this thesis is to perform an analysis of the engineered MAV wing structure and the carbon fiber composite material of which it is mainly composed. Furthermore, the generated finite element model should be easily modified so that the effects of design or material changes to the wing can easily be made. This will allow for future designs to be analyzed prior to construction, thus saving considerable time in the design process. In performing the structural analysis using the finite element method, many of the questions above can be answered, and a better understanding of the manufactured MAV wing can be accomplished.

1.2. Background

The demand for unmanned intelligence, surveillance and reconnaissance (ISR) has grown significantly in recent decades. Unmanned aerial vehicles (UAVs) are unrestricted by a pilot's physical limitations and can provide unprecedented loiter times, range, and cost effectiveness. MAVs have been proposed by many due to low cost, tremendous maneuverability and inconspicuous operation, and are seen by many as the next revolution in the field of UAVs. The Defense Advanced Research Agency's (DARPA's) current vision for the optimal MAV is outlined in Table 1.1.

Table 1.1: MAV Design Requirements [4].

Specification	Requirements	Details
Size	<15.24 cm	Maximum Dimension
Weight	~100 g	Objective GTOW
Range	1 to 10 km	Operational Range
Endurance	60 min	Loiter time on station
Altitude	<150 m	Operational ceiling
Speed	15 m/s	Maximum flight speed
Payload	20 g	Mission dependent
Cost	$1,500	Maximum cost, 2009 USD

A quick glance at the requirements will reveal a significant difference between current aircraft requirements and the requirements of an MAV. With such contrast in vehicle requirements, it is only natural that the design of a vehicle will be different. Using nature as a guide, there are many examples of insects that use flapping wings as highly efficient mechanisms for flight [5]. The use of such a flapping mechanism, where the wing would produce thrust as well as generate lift, represents a dramatic shift from the traditional quasi-rigid wing or rotorcraft with a separate propulsion system. Research of the countless number of flying insects present in the world provide examples of structures that are structurally capable of flight and have the potential to meet DARPA's

requirements for MAVs. These structures would provide a valid aerodynamic model for research. This would reduce the significant amount of time associated with solving the low Reynolds's number and unsteady aerodynamics of a flapping MAV. One insect that possesses the capabilities to meet these requirements is the Manduca Sexta, also known as the North American Hawkmoth or simply as the hawkmoth (see Figure 1.2) [6]. Insects such at the Manduca Sexta have the benefit of having undergone millions of years of evolution and have evolved into highly specialized and efficient systems. With such a valid aerodynamic model, if the structural properties of the hawkmoth could be matched, a capable MAV could be developed.

Figure 1.2: An Adult, Female Manduca Sexta (Hawkmoth).

The Manduca Sexta forewing was selected as the basis for the bio-inspired design. The forewing, which produces most of the lift for the moth, has been selected and studied by Norris, and has been determined to be an ideal candidate for a wing [6]. O'Hara has continued the research of Norris and has established general material properties and characteristic dimensions for the hawkmoth wing, and as developed a

preliminary design for an MAV wing based on the his findings, using carbon-fiber and Kapton (see Figure 1.1) [2]. O'Hara's research provides the basis for a bio-inspired MAV wing, and for the objective of this thesis [2].

1.3. Motivation

As war fighters are taxed with ever increasing difficult situations, it is crucial that they be made aware of what is to come; whether it be over a hill, in a cave, or in a room of an unknown building [7]. DARPA's vision for a small, lightweight MAV will allow war fighters to observe the situation while the vehicles small size will allow it to blend in and be nearly indistinguishable from the natural insect population. The capability for a vehicle to be able to observe a situation while hiding in plain sight allows it the ability to gather ISR previously unobtainable by traditional UAVs.

The ability for a vehicle to successfully navigate buildings requires it to be highly maneuverable. This is quite difficult to achieve with traditional quasi-rigid winged vehicles, since forward motion is constantly required to maintain lift. It can be said that in order to meet such a challenging design criteria it is best to turn to nature. Norris et al. stated that current research finds a vested interest in this *flapping wing* MAV (FWMAV), and that science is compelled to mimic the elegant (and efficient) designs that nature has developed for its flapping wing design [8].

Current designs of MAVs, shown in Figure 1.3, show that much research is still required in order to achieve a design that is capable to fulfill DARPA's design criteria.

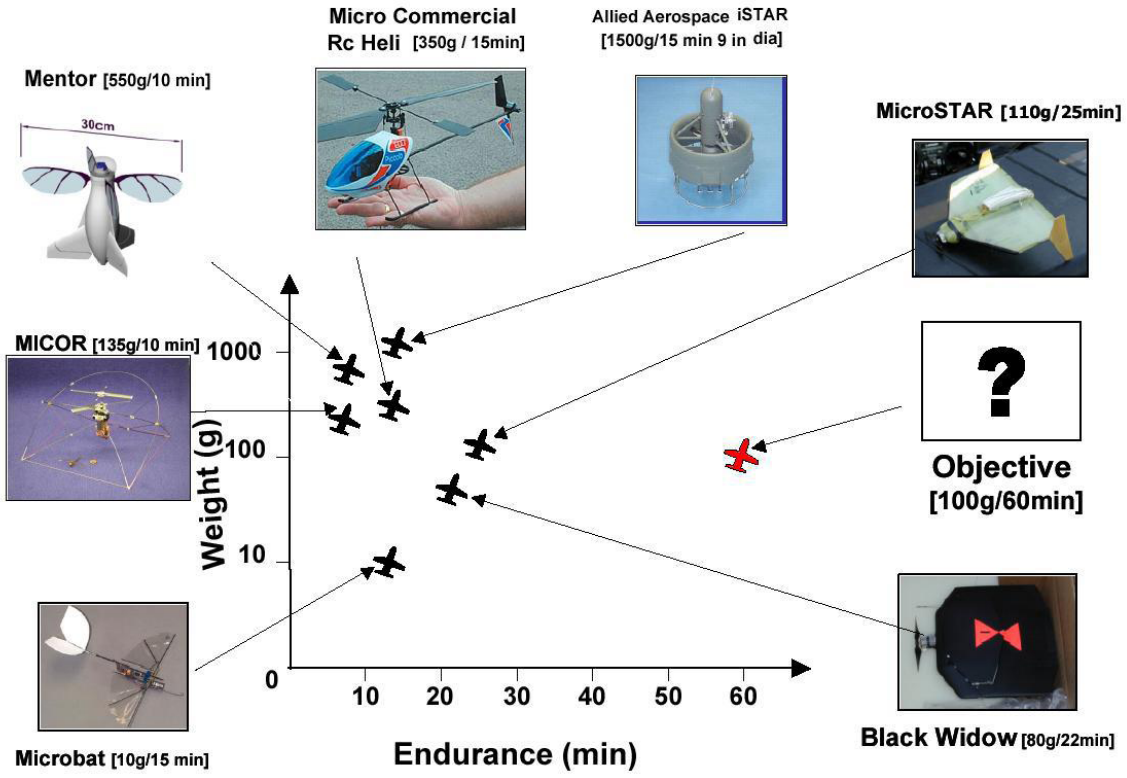

Figure 1.3: View of Recent MAV Developments [9].

1.4. The Concept of Biological Inspiration

Looking to nature's countless examples of flying creatures is not a new concept. The Wright Brothers built and tested airfoil designs based upon the shapes of the wings of birds, eventually leading to the creation of the Wright Flyer. It is easy, however, for scientists to forget about nature's influence on flight and focus energy into determining the 'best way' for something to work, as opposed to examining what is 'known' to work in nature and determining how it works. Without looking at everything that is currently known, many find themselves effectively reinventing the wheel instead of using knowledge and information already known.

Biologically inspired flight can be said to be the foundation of flapping wing flight. Erich von Holst is considered an early pioneer in the study of bio-inspired flapping wing vehicles. He and his colleagues studied the biological and aerodynamics of flying animals in the 1930's and 1940's, even developing several successful flapping vehicles based on the study of birds and insects (See Figure 1.4. [10]).

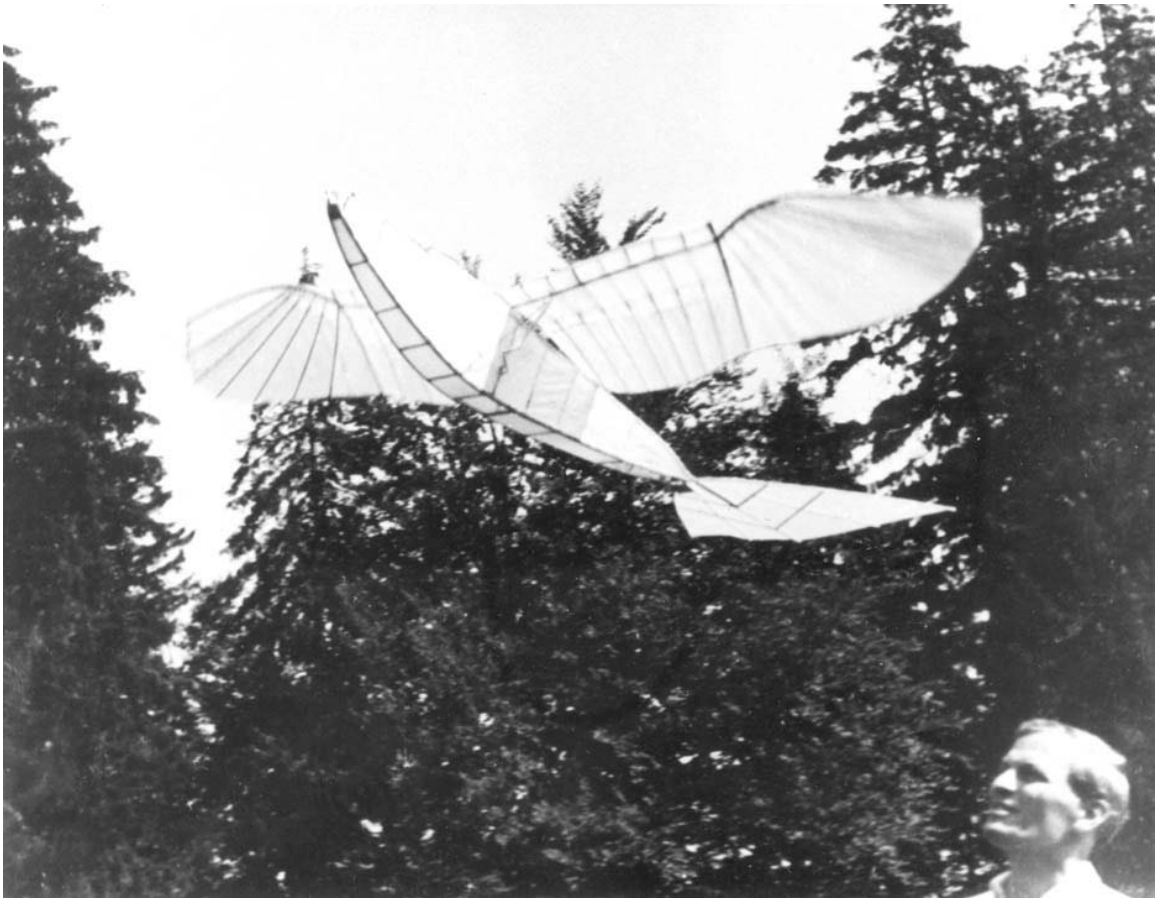

Figure 1.4: Erich von Holst with a Flapping Air Vehicle Based upon a Swan [10].

In the period following World War II, it seems that the importance of bio-inspired work was forgotten until only recently. Aaron Norris found that there was a significant lack of literature present on the area of bio-inspired flight [6]. This especially held true in the area of insects that would likely be mimicked in order to create an MAV based upon

DARPA's criteria. Furthermore, Norris and DeLeon both found that the majority of literature that exists dealt with the aerodynamics associated with MAV, and that there was a significant lack of information about the structures of MAVs [6] (See Figure 1.5. [1]). In order to create a feasible MAV wing, more research was needed.

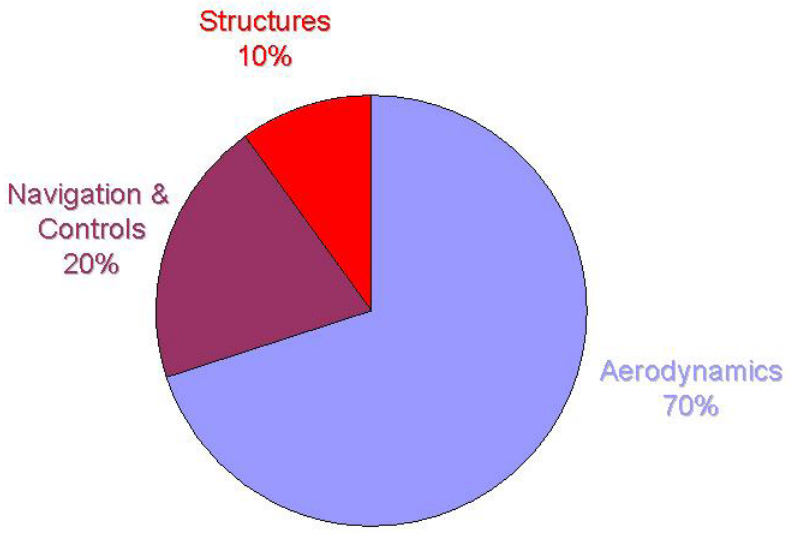

Figure 1.5: Current Research Intrest of Flapping Flight [6].

1.5. A Look at the Manduca Sexta

It is important to look at some of the previous work performed on the Manduca Sexta to better understand what is trying to be matched for the creation of a flapping micro air vehicle (FMAV). Looking at previous work done [1] [2], one will better understand the motivation behind the project, as well as the objectives for an engineered

wing. This section will primarily focus on the work done by Norris and O'Hara, its relation to the Manduca Sexta and application for FWMAVs.

Norris studied the forewing of the Manduca Sexta, selecting the hawkmoth because it was readily available for study and could meet the requirements set forth by DARPA for an MAV. Norris "liberated" (i.e. separated) the wings from a large sample of hawkmoths for study. In order to understand the general characteristics of the wings, Norris performed a frequency analysis of the wing using a scanning laser vibrometer (SLV). Norris vibrated liberated wings from the hawkmoth and vibrated them at various frequencies using an SLV to measure the wing's response in both air and in vacuum. The four mode shapes he determined can be seen below in Figure 1.6. The ratios of these frequencies for the various mode shapes show the relative dynamic stiffness of the wing. These mode shapes were relatively constant across a large sample of wings. Norris identified the first four modes as *flap*, *feather*, *saddle*, and *bisaddle* modes respectively [6].

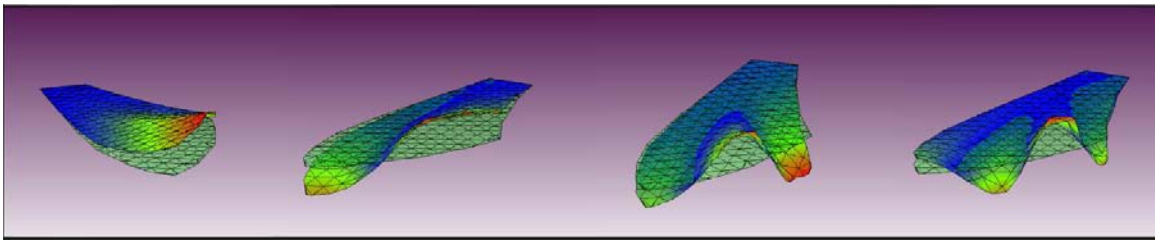

Figure 1.6:The First Four Frequency Modes of the Hawkmoth's Forewing.

Norris used a total of 60 wings to perform his analysis. While the mode shapes remained relatively constant from specimen to specimen, there was some variation [6]. Table 2 below shows the results of Norris' SLV frequency tests. The fact that there is some variation in the results is significant for those wishing to fabricate a bio-inspired wing based on the hawkmoth because it means that the wings do not need to meet exact

specifications in order to produce an artificial wing that can mimic the hawkmoth wing. This degree of tolerance in the fabrication of such an MAV is important, and will be shown to be quite significant later on.

Table 1.2: Summary of the Modal Parameters of a Hawkmoth's Forewing in Air and Vacuum [6]. * Based on 10 samples tested in near vacuum
** Based on 50 samples tested in air

Mode	Structural Behavior	Name	Avg. Freq (Air)** [Hz]	Avg. Freq (Vac)* [Hz]	MR (Air)** [-]	MR (Vac)* [-]	Damp (Air)** [%]	Damp (Vac)* [%]
1	SW Bending	Flap	60	85	1.0	1.0	5.0	2.5
2	SW Torsion	Feather	84	105	1.4	1.3	5.0	2.5
3	CW Bending	Saddle	107	138	1.8	1.6	5.0	2.5
4	CW	BiSaddle	142	170	2.4	2.2	5.0	2.5

O'Hara continued on the work of Norris in hopes of developing a manufactured wing that could be used in an MAV. To successfully understand the structure, it is important to understand the geometry and material proeprties. O'Hara's work looked to provide just that. For his research, the material properties of the wing were broken down into two separate parts, the vien structure and the membrane. Both the membrane and the veins were then characterized using a variety of techniques. Figure 1.7 below shows a venation diagram of the hawkmoth, illustrating the names and locations of the veins in the forewing [11].

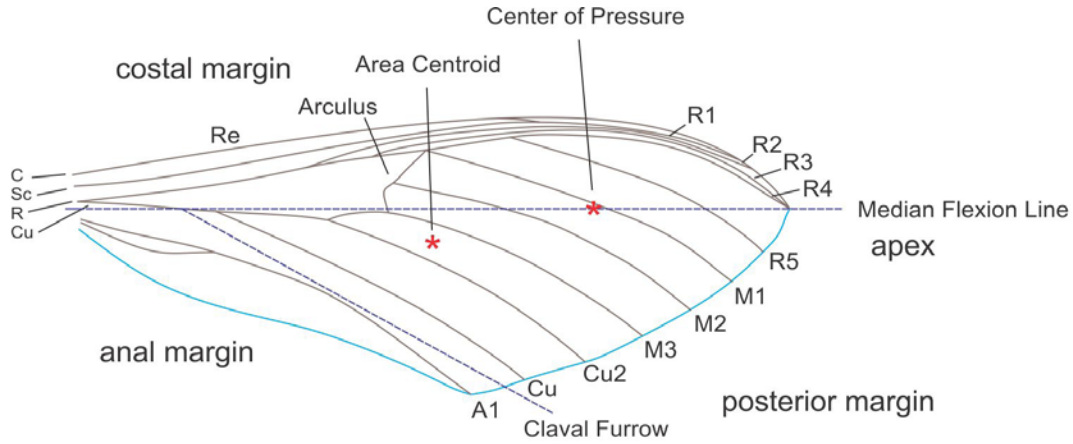

Costa (C) – the leading edge of the wing
Subcosta(Sc) – second longitudinal vein (behind the costa), typically unbranched
Radius (R) – third longitudinal vein, one five branches reach the wing margin
Media (M) – fourth longitudinal vein, one to four branches reach the wing margin
Cubitus (Cu) fifth longitudinal vein, one to three brances reach the wing margin
Anal Vein (A) – unbranched veins behind the cubitus

Figure 1.7: A Venation Diagram of the Manduca Sexta Forewing [11].

In order to determine the material properties of the veins, it was important to first know the vein dimensions. Using Computed Tomography (CT) scan, O'Hara was able to develop a detailed geometry of the venation pattern of the hawkmoth, as well as take measurements of inner and outter diameter of the veins [2]. Using this information, he then cut out individual veins from the liberated wing. Using dynamic forced response, the veins were then tested under simple cantilever beam conditions to predict the elastic modulus, E, of the structure. This was done using laser vibrometry and modal analysis. A section of the vein was clamped and psuedo-randomly vibrated. The frequency of the first bend was measured using a laser vibrometer (See Figure 1.8 for setup and results [2]).

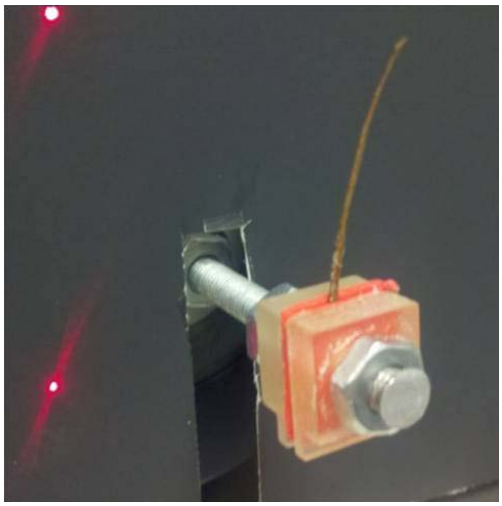

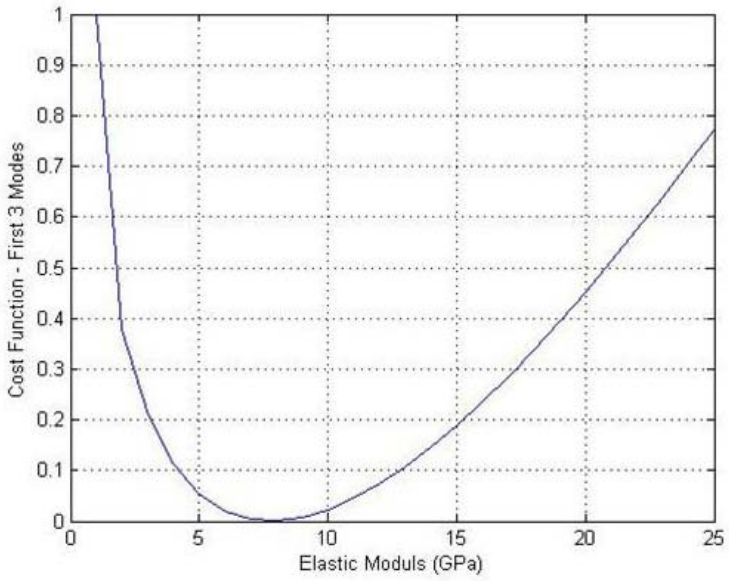

Figure 1.8: Experimental Modal Analysis: Setup and Results [2].

Using a simplified finite element analysis (FEA) model of the vein and optimization techniques, a value for E of the FEA model was optimized so that the the first modal response frequency observed in the vibrometer test were matched in the FEA model. This methodology has been used previously to determine various composite material's properties successfully [12].

$$J = \sum_{n=1}^{n_{modes}} \left[\left(\frac{\omega_{x,n}}{\omega_{f,n}}\right) - 1\right]^2 \ldots \quad (1.1)$$

Equation 1.1, depicts the simple cost function used to tune the fundamental frequency of the model to the experiment. By iterating on the elastic modulus variable of the FEA model, the minimization of J is easily realized as depicted in Equation 1.1. Using this method, E of the veins was determined to be 6.8 GPa [2].

O'Hara used a Wyko NT900 Optical Profiler that was able to determine to a sub-nanometer accuracy of the shape and thickness for the membrane [2]. O'Hara also implemented instrumented indentation of the membrane, a common practice for determining the mechanical properties of thin films and small structural features [2]. Figure 1.9 describes the nanoindentation process used by O'Hara. Using twenty-five specimens and taking multiple measurements for each specimen, O'Hara determined the the elastic modulus of the membrane was 3.12 GPa [2].

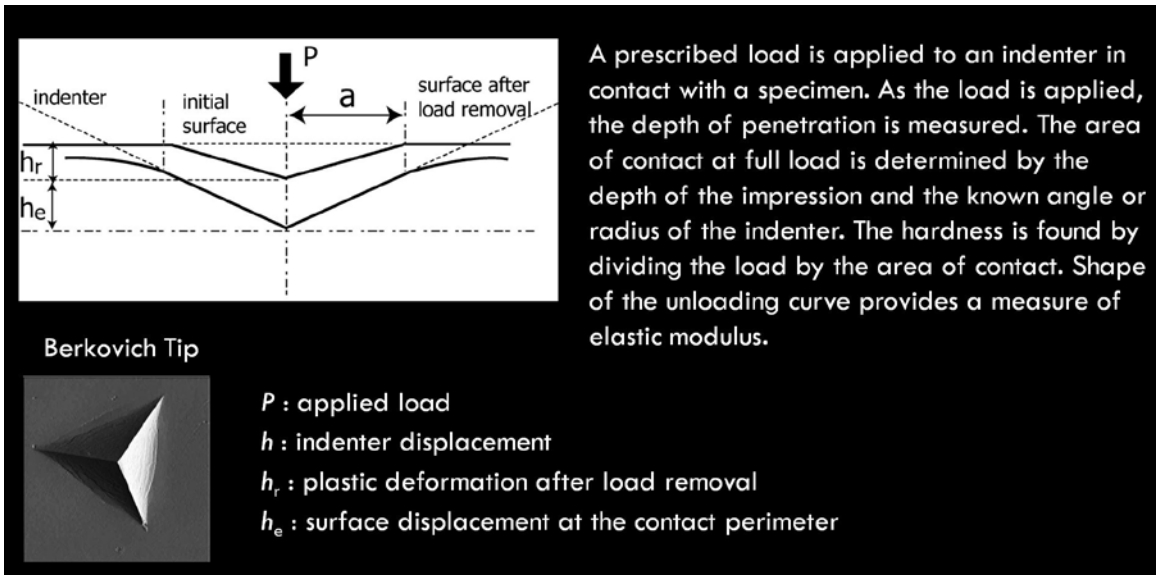

Figure 1.9: The Nanoindentation Process [2].

1.6. Manufactured Engineered Wing Materials

The development of FWMAV requires that the wings be able to produce significant lift with the least amount of energy input. This necessitates a wing that can serve multiple functions, be easily controlled, and have a low mass. A manufactured

wing based off the biological wing needs to be able to match the physical characteristics of the biological wing, as well as be repeatably manufactured. Keeping this in mind, several different types of materials were looked at when selecting materials to be used in the design of the manufactured MAV wing. Two different functions for the materials were examined, use in the vein structure and use in the membrane of the manufactured wing. Since the wing would be primarily experiencing bending in flight, the goal in selecting a material was that the flexural stiffness of the engineered wing would match the flexural stiffness of the bio wing, equation 1.2.

$$E_{bio}I_{bio} = E_{eng}I_{eng} \tag{1.2}$$

Ultimately, despite looking at several other materials, it was determined that the only material that is readily availible, capable of achieving this task, and has a low enough mass to be used as the vein structure for the engineered wing is a unidirectional carbon fiber composite. Kapton was chosen to represent the membrane based on its strengh and low density.

1.6.1. Introduction to Unidirectional Carbon Fiber Laminates

When performing the structural analysis of the engineered wing, it is of the utmost importance to understand the material properties of the unidirectional carbon fiber composite that make up the vein structure of the model. This section will serve to introduce the reader to the basics of such composites. Unidirectional carbon fiber composites are the most common example of continuous fiber composites, composites in which the fiber is continuous throughout the length of the entire specimen. Unidirectional carbon fibers are continuous fiber composites where all the fibers are aligned in one direction, hence the name unidirectional.

The nature of the fibers makes such unidirectional carbon fiber composites anisotropic. The orientation of the unidirectional fibers plays a significant part in the material properties of the material. The orientation of a fiber is the angle, θ, in which that fiber forms with the global axis coordinate system. Figure 1.10 serves to graphically define the lamina coordinate systems (numbered) and the global laminate coordinate system (lettered).

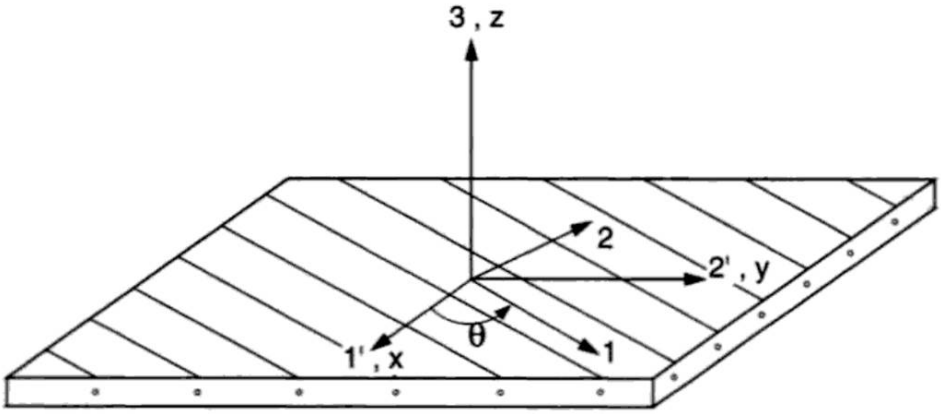

Figure 1.10: The Principal Directions of the Lamina (1,2,3), and the Reference System of the Laminate, (x,y,z) [13].

For construction purposes, the unidirectional fibers are set in a matrix, usually epoxy, and formed into thin sheets called lamina, or plies (See Figure 1.11) [14].

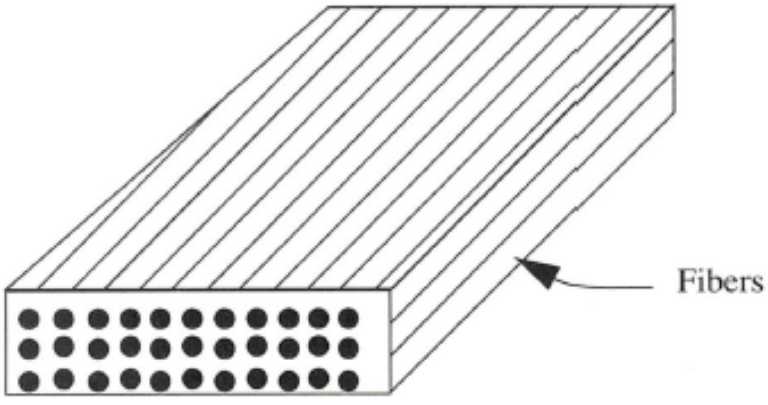

Figure 1.11: Unidirectional Lamina [14].

Laminates are made by stacking the lamina, or plies, of the unidirectional fiber at various fiber orientations, (See Figure 1.12). Laminates are beneficial in that they can be arranged in a near infinite number of orientations and ply numbers so that the composite's material properties can be tailored to specific design (See Chapter 2).

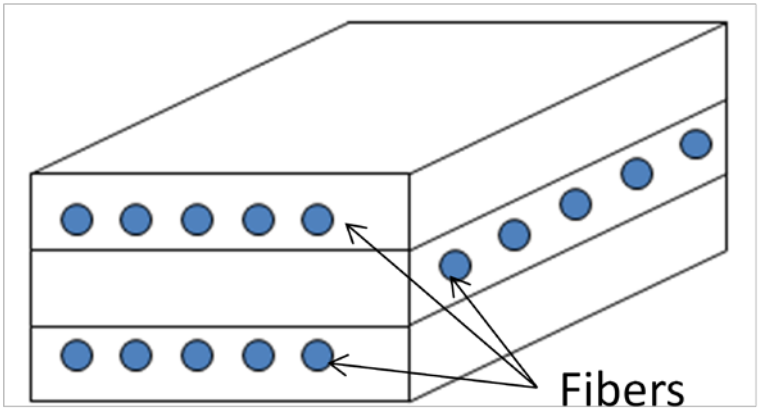

Figure 1.12: Unidirectional Lamina Stacked in order to form a Laminate.

1.6.2. Unidirectional High Modulus Thin Ply Laminates as MAV Wing Structure

Materials such as steel, titanium and plastic polymers were found to be either too heavy or too weak. This showed the necessity for a material with a high specific modulus, E/ρ. Composites composed of carbon fiber and epoxy resin seemed like a natural choice. Not only do they possess a high specific modulus, but they also offer the ability to tailor the number of plies as well as the fiber orientation of those individual plies. This allows for more control over how the material will respond under loading conditions, allowing for a fiber orientation and ply number that could best suit the loading conditions applied. Because of the unidirectional carbon-fiber composite is not isotropic, it caused some significant difficulties when performing the analysis. The issues associated with the carbon fiber and modeling will be explained in subsequent chapters.

Unidirectional high modulus carbon fiber composites have already proven to be useful on MAVS. The Harvard Micro Robotics Research Laboratory has used a pitch based carbon fiber (XN-50A) with a cyancate ester resin (RS-3C) produced by Tencate on their MAV design [15]. The pitched based fibers of the selected composite have a high strength and modulus compared to other types of available composites (See Figure 1.13 [16]). This makes them desirable because less material can be used to achieve the same strength within the model, but at a lower mass. The material was set up in a [0/90/0] orientation, allowing the composite to have stiffness in both the spanwise and chordwise directions of the wing, however difficulties were found in the manufacturing process that were not presented in the literature. These issues will be discussed in subsequent chapters.

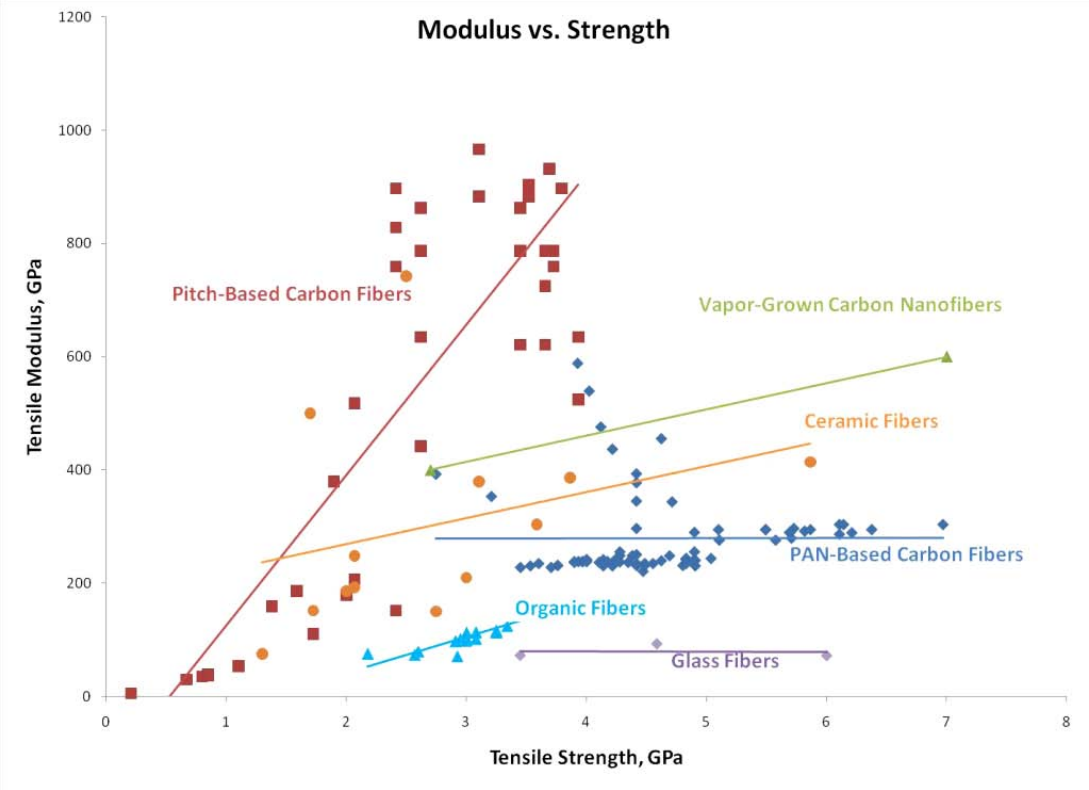

Figure 1.13: Composite Fiber Types

Since the carbon fiber used by Harvard team was unavailable, O'Hara selected YSH-70A fiber for use as the vein structure in the engineered wing, material properties shown below in table 3.

Table 1.3: YSH-70A High Modulus Fiber Properties

Fiber	*Tensile Modulus*	*Tensile Strength*	*Density*	*Fiber Dia*	*Yield*
YSH-70A	720 GPa	3.6 GPa	2.14 g/cm3	7μm	125 g/1000 m

Previous work has shown that the inertial properties and flexural stiffness of the wing play an important part in the dynamic and structural response. It is important to understand how the carbon fiber vein structure would affect an engineered wing. Since the carbon fiber material itself can have variations in the ply orientation angle and the number of plies, it is important that any analysis of the structure consider this. It is also important to note that since the composite is anisotropic, the geometry will affect the material properties at different points along the structure.

1.7. Finite Element Approach

Many consider FEA to be one of the most important structural innovations in recent history. It allows for user inputs of geometry and mass to perform complex structural analysis much quicker than would be possible by hand. It seems only natural that the finite element approach should be used in the analysis of an engineered MAV wing. As Travis Sims [17] has shown with his work, FEA can be a powerful tool to solve a problem, but it can also lead to more questions.

1.7.1. A Modal Frequency Approach

Like Norris, Sims understood the importance of the structure of a wing. Sims objective was to create a model of the Manduca Sexta's forewing grounded in

experimental vibration testing, See Figure 1.14 [17] [7]. In his work, as with all FEA models, there are two competing requirements: maximizing geometric simplifications to ensure tractability, and minimize unnecessary deviations from the physical structure. Sim developed the geometry of his model using CT imaging. Since the real material properties of the bio wing were unknown, Sims' generated material properties so that his model would match the observed modal frequency results exhibited by a liberated hawkmoth wing [17].

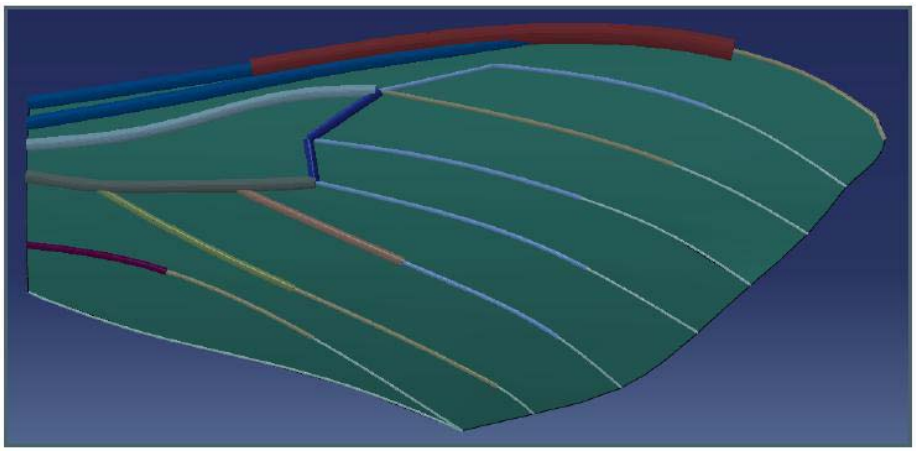

Figure 1.14: Finite Element Model of Manduca Sexta Forewing [17].

Sims' model yielded similar results to those seen by Norris in his modal analysis except for the third mode, See Table 1.4 [17]. While Sims does not offer a clear explanation for this, he notes that the mode shapes of the first three modes examined in the model were the same as for the biological wing.

Table 1.4: Natural Frequency Results Generated by Travis Sims [17].

Mode	*Experimental, Hz*	*FE Model, Hz*	*Minimum Difference*
1	86 +/- 2	84.6	0.0%
2	106 +/- 2	106.1	0.0%
3	155 +/- 2	317.7	102.4%

The work done by Sims showed that material properties were not the only important aspect in matching a wing, as had been previously suggested by Combes and Daniels [18]. Sims came up with the following areas of interest that should be looked at when determining the characteristics of a bio wing [17].

1. The material properties.
2. The geometry/shape of the wings, specifically the venation pattern and vein structure.
3. The natural unique camber of the wing.

In an effort to improve his model, Sims added some camber to his wing by applying the wing outline to a constant camber cylinder. While groundbreaking, this camber does not represent the actual camber found on the wing. However, from Sims' results, one can see the importance that camber will have on the wing (See Figure 1.15).

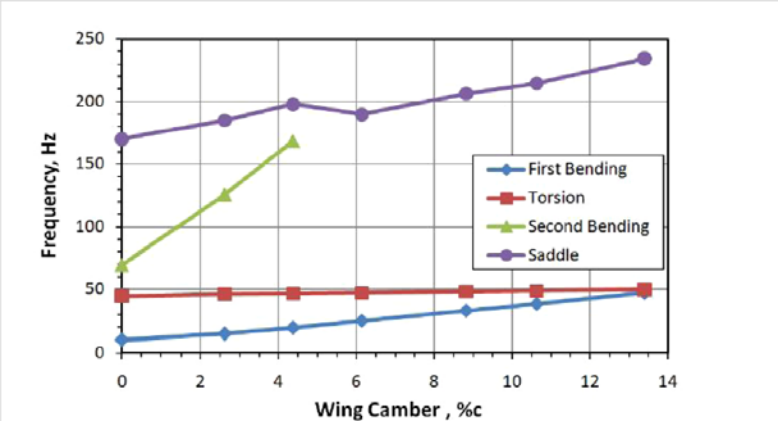

Figure 1.15: Effect of camber on ω_n for the Manduca Sexta Forewing [17].

The hawkmoth is not the only insect currently being analyzed as a potential for a bio-inspired MAV. Marrocco, Venkataraman and Demasi have investigated the use of a dragonfly's wing and have developed a finite element model [19]. For their model, they assumed a planar shape and used material properties for steel to represent the veins and aluminum for the membrane since material properties of the dragonfly were unavailable.

They were however able to import a complex geometry of the wing, and vary the thickness of the wing across its span and chord length (See Figure 1.16).

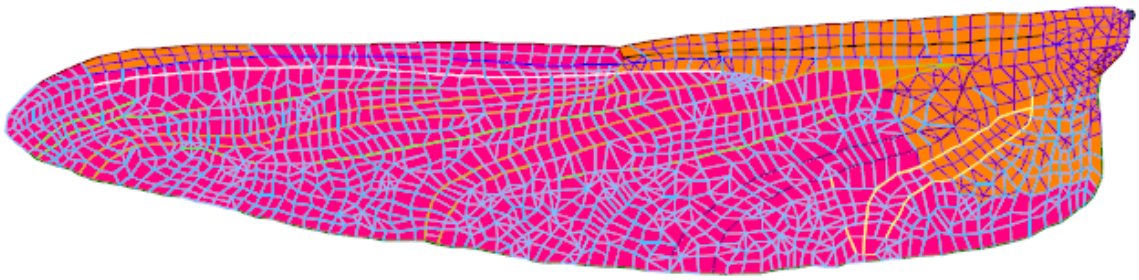

Figure 1.16: FEA Model of Marrocco et al Dragonfly Hindwing [19].

Performing a modal frequency analysis, Marrocco et al were able to see the effects the veins played in the modal shapes of the wing. A second set of runs were done to compare the effects of mass on the model (See Figure 1.17). While this information provides an important insight into the dragonfly, the steel and aluminum wing is not intended to mimic the dragonfly's wing, or an engineered wing based on the dragonfly. It was merely to investigate the mode shapes of the wing.

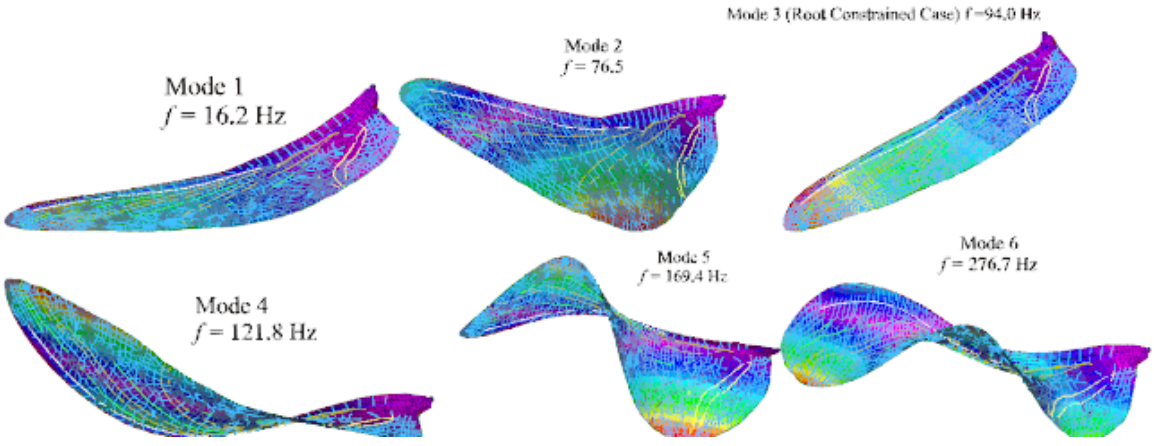

Figure 1.17: Modal Frequency Analysis of Engineered Dragonfly Wing [19].

Further literature review on structural analysis of FMAV wings shows a significant lack of results. Analysis on manufactured MAV wings is still in its infancy. One recent examples that could be found included work done by Malik and Qureshi [20]. While the work proved to be insightful, the structures analyzed did not have the geometric or material complexity of the MAV wing that is the subject of this thesis. Malik and Qureshi used both MATLAB and ANSYS for their analysis. Their model has a solid leading edge beam with a trailing membrane, see Figure 1.18. This figure shows Malik and Qureshi's model in ANSYS (top) and MATLAB (bottom) undeformed (left), and the first modal shape [20]. The frequency for the first mode was less than 2 Hz. It should be noted that this is significantly lower than the frequency in which most insects flap [6].

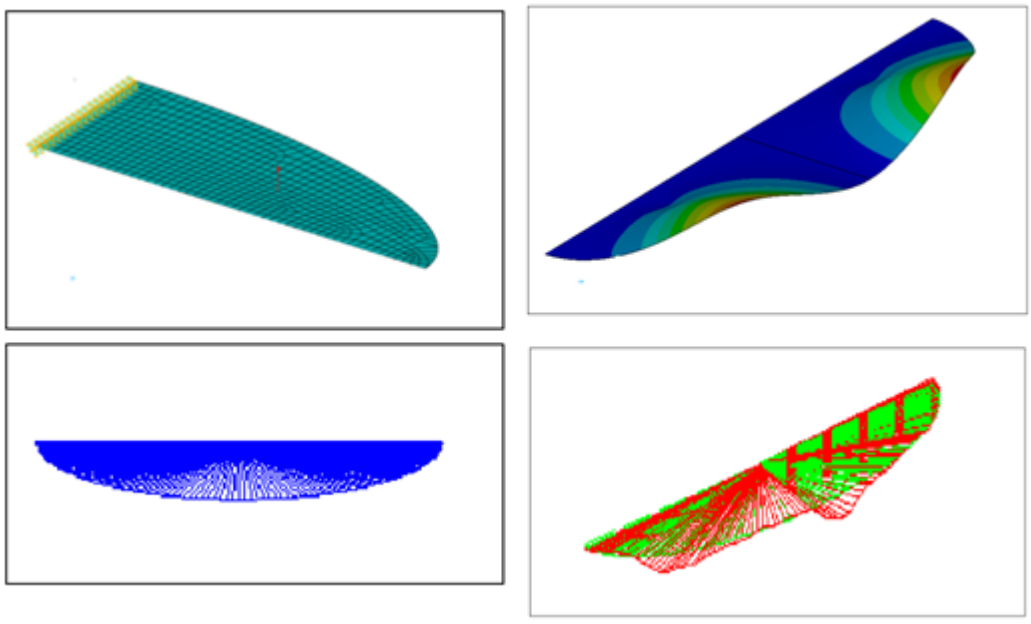

Figure 1.18: ANSYS and MATLAB Models of Flapping Wings by Malik and Qureshi [20].

Sims' areas of interest, along with the mass properties deemed to be important by O'Hara and Marrocco et al, show that designing a MAV wing structure is not an easy task, especially considering the uncertainty of some of the biological wing characteristics. It is easy to see then, how a better understanding of an engineered wing would be beneficial. An analysis of O'Hara's engineered MAV wing will allow for better understanding of the engineered structure and how it varies from its biological counterpart.

1.7.2. A Flexural Stiffness Approach

Both Sims and Norris were influenced by the works of Combes and Daniels, both biologists at the University of Washington. Combes and Daniel observed that the large-scale deformations observed during the flight of insects were controlled by the architecture of the wing [18]. This work represents one of the few works that showed investigations into the structural aspects of the wings.

The parameter that Combes' and Daniels' decided was important to investigate was flexural stiffness. They define it as "the composite measure of the overall bending stiffness of a wing; it is the product of the material stiffness (E, which describes the stiffness of the wing material itself) and the second moment of area (I, which described the stiffness generated by the cross sectional geometry of the wing)" [18]. The mathematical equation for a beam is shown below in Equation 1.3.

$$EI = \frac{FL^3}{3\delta} \tag{1.3}$$

Here the parameter [L] is the effective beam length, [δ] is the wing displacement at the given position of force application, and [F] is the applied force. For their case,

Combes and Daniel used the following equation, Equation 1.4, to solve for the second moment of area. In this case [*w*] is the width, and [*t*] is the thickness of the wing.

$$I = \frac{wt^3}{12} \tag{1.4}$$

Combes and Daniel set up a way to test this parameter based on experimental and FEA results (like Sims) which is represented in Figure 1.19. The figure shows the wing displacement tests used to measure the flexural stiffness of the wing. Figure 1.20 shows the finite element model representative of Combes' and Daniels' flexural stiffness experiments. A similar method will be employed in this thesis for analysis of the engineered wing.

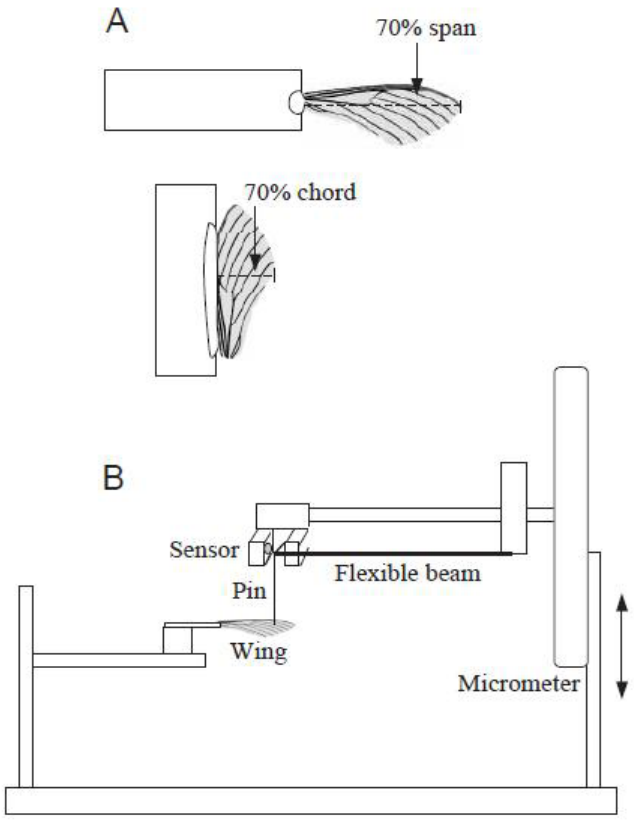

Figure 1.19: Combes' and Daniel's Initial Flexural Stiffness Investigations [18].

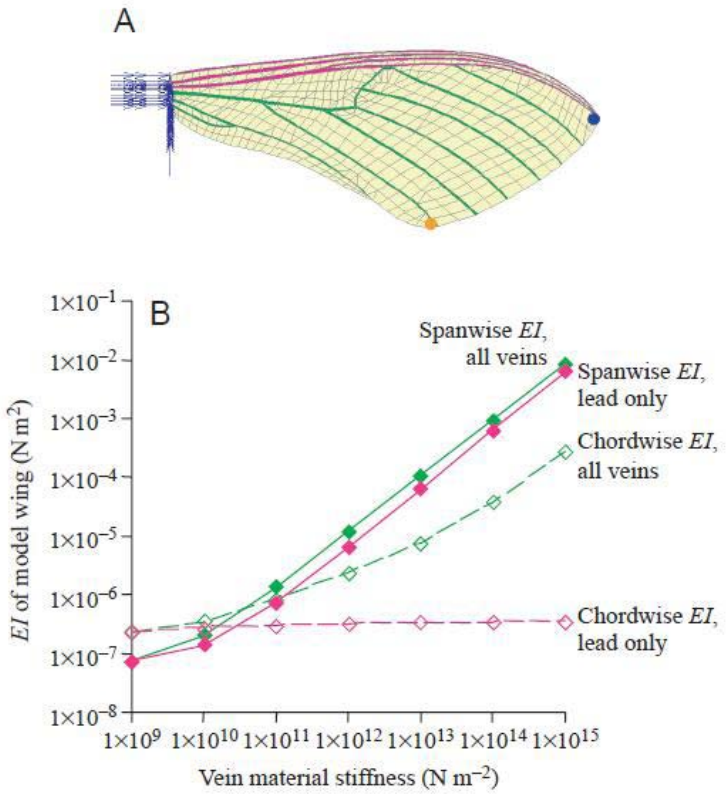

Figure 1.20: The FEA Model with Results Developed by Combes and Daniels

Through their investigation, Combes' and Daniels' were able to measure the stiffness of the wing, and it is from this experiment that they were able to measure the chordwise and spanwise stiffness of several different wings. Looking to standardize the size of the specimens tested, several different species wings were tested. Plotting the spanwise and chordwise flexural stiffness versus the wing span and chord length respectively for these tests, Combes' and Daniels came up with the conclusion that size scaling was the dominant factor in determining overall flexural stiffness [18]. It is important then, that when manufacturing a FMAV for the wing to follow similar spanwise and chordwise characteristics to those found by Combes' and Daniels', Figure 1.21.

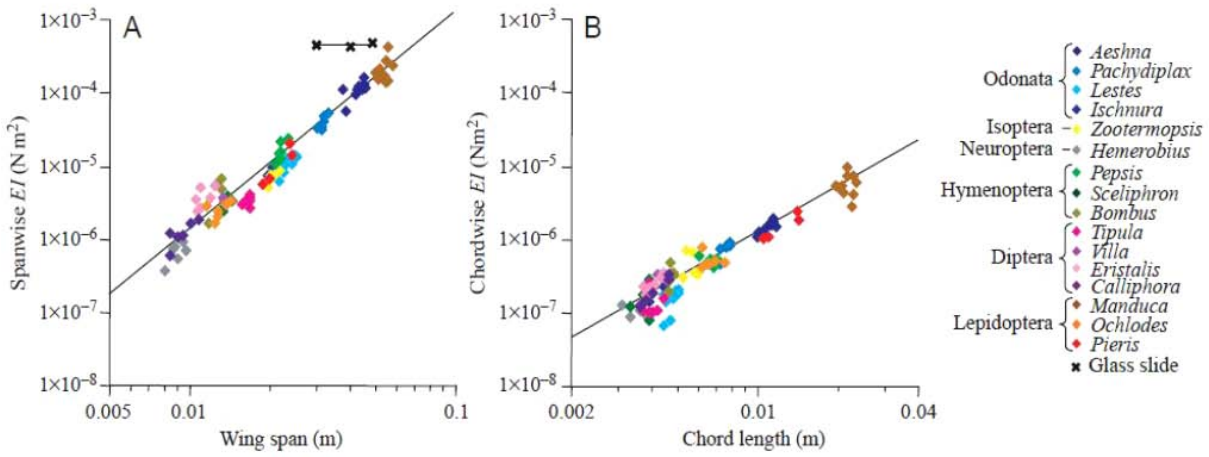

Figure 1.21: Results from Combes' and Daniels' Measurement of Flexural Stiffness [18].

Combes' and Daniels' approach to analyzing wings has shown some common characteristics are shared amongst different species. Their FEA model like Sims original, did not characterize the camber of the wing. While flexural stiffness measurements should provide yet another tool to compare the FEA model against the engineered wing, a more complex model than is needed to handle the frequency modal analysis as well as point loads measuring flexural stiffness. This is important to consider when developing an FEA model for the engineered wing.

1.8. Objective and Document Ovierview

Looking at what work has been done, it can be seen that the area of MAV research still has a long way to go. The objective of this research is to perform a structural analysis on an engineered Manduca Sexta forewing with a composite vein structure. The composite material was examined to determine issues associated with the use of an anisotropic material in MAV wing contraction. Also, as part of the analysis an FEA model was created that had the ability to do the following:

1. Accurately predict mode shapes and frequencies of a modal frequency analysis.
2. Accurately model displacements due to point loads.
3. Be easily modified to incorporate any future design changes.

The following chapters will discuss how this process was carried out, as well as any issues encountered and possible solutions. Chapter II will detail some of the theory used in this project in dealing with the carbon fiber composite material, and the use of finite element method. Chapter III will explain the construction of the composite material and the engineered wing, and go over the analysis of the composite material. Chapter IV will go over how the FEA model of the engineered wing was developed, as well as experimentation done to validate the model. Chapter V will display the results of the FEA, as well as provide a discussion on those results. Finally, Chapter VI will provide conclusions and a summary of the work done in this thesis.

II. Carbon Fiber Composite Construction and Theory

This chapter serves to demonstrate an understanding of the mathematics involved in the analysis performed for this project. The two main areas of focus include the material properties of carbon fiber composite material, which forms the vein structure of the wing (See Figure 2.1), and an understanding of FEA frequency analysis, and how the composite was modeled so that such an analysis could be performed. Figure 2.1 is a diagram depicting the wing structure analyzed and manufactured. The reader should notice how the individual vein shapes cut through the associated composite ply orientations. It is important to understand how this was handled, and this chapter will go over some of the techniques used.

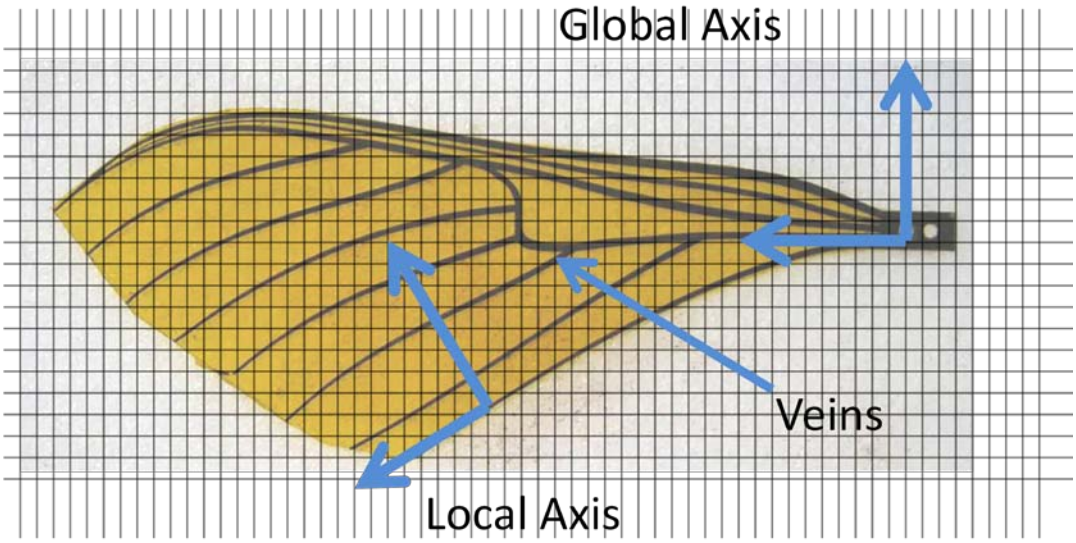

Figure 2.1: The Manufactured Wing with Lines Representing the 0° and 90° Layout of the Carbon Fibers.

2.1. Unidirectional Carbon Fiber Material Construction

This section will serve to define the material properties of the YSH-70-A/RS-3C carbon fiber composite used in the vein structure of the wing, show how the material was

constructed, as well as go over the theory behind calculations that were used in the analysis of the composite itself and in the analysis of the manufactured wing.

The lamina material properties are provided by the manufacturer as well as confirmed by experimental methods, however the laminate needed to be constructed and its properties calculated. The laminate properties varied from the lamina properties due the variation of the ply orientation of the fibers. In the case of the engineered wing, a 3-ply lamina was arranged in a [0/90/0] orientation, as shown in Figure 2.2.

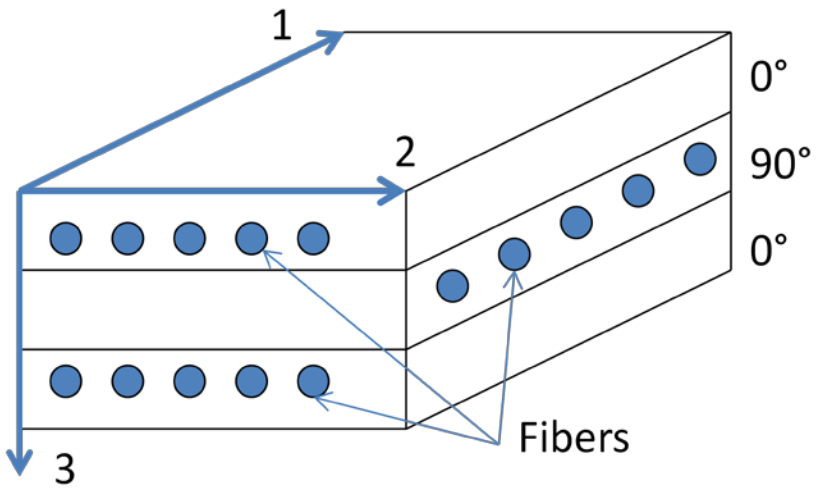

Figure 2.2:Diagram of the [0/90/0] Composite Laminate.

Two main sets of calculations were performed during the analysis of the composite, the lamina transformation equations, which account for the change in material properties of the lamina based upon the fiber orientation angle, and the Halpin-Tsai equations, which account for changes in the material properties due to short fibers. Short fibers occur when the length of the fiber is approximately less than 100 times the diameter of the fiber, and have a force component acting along the length of the fiber.

Such fibers occur in the manufactured wing due to the curvature of the vein structure cut from the single sheet of the [0/90/0] composite as shown in Figure 2.3.

2.1.1. Laminate and Wing Construction at AFIT

Part of the analysis was determining how it was constructed. The laminate used in the fabrication of the engineered wing was constructed at AFIT. This was specifically done from an economical efficiency point of view. The pre-preg, lamina where the fibers are already impregnated in a partially cured matrix, was used by several groups of students, all constructing small samples of the composite at various times, in various ply orientations and various numbers of plies. It was deemed impractical to have every student group purchase small samples of cured carbon fiber for every application. Since 3-ply laminate is not common, this kept different groups of students from having to special order their composite which can be very expensive for the small amount of carbon-fiber used. It also had the advantage of allowing AFIT students to lay-up and cure their laminate within a day as opposed to having to order, and wait an unknown amount of time for it to be shipped.

The composite arrives at AFIT in rolls of pre-preg. Since the pre-preg must be stored below 32°F in order to prevent the matrix from curing prematurely, the roll of pre-preg is cut with a straight edge and razor blade into 8” x 11” sheets (See Figure 2.3) so that they are able to be stored in a common household freezer at AFIT until needed. These sheets will make up the individual lamina of the composite. Note: The roll pictured on top in Figure 2.3 is not the actual carbon fiber pre-preg used at AFIT because the composite has already been cut up. The actual pre-preg is pictured on the bottom, and

is sandwiched between thin sheets of wax paper on one side and a thin film of plastic on the other side.

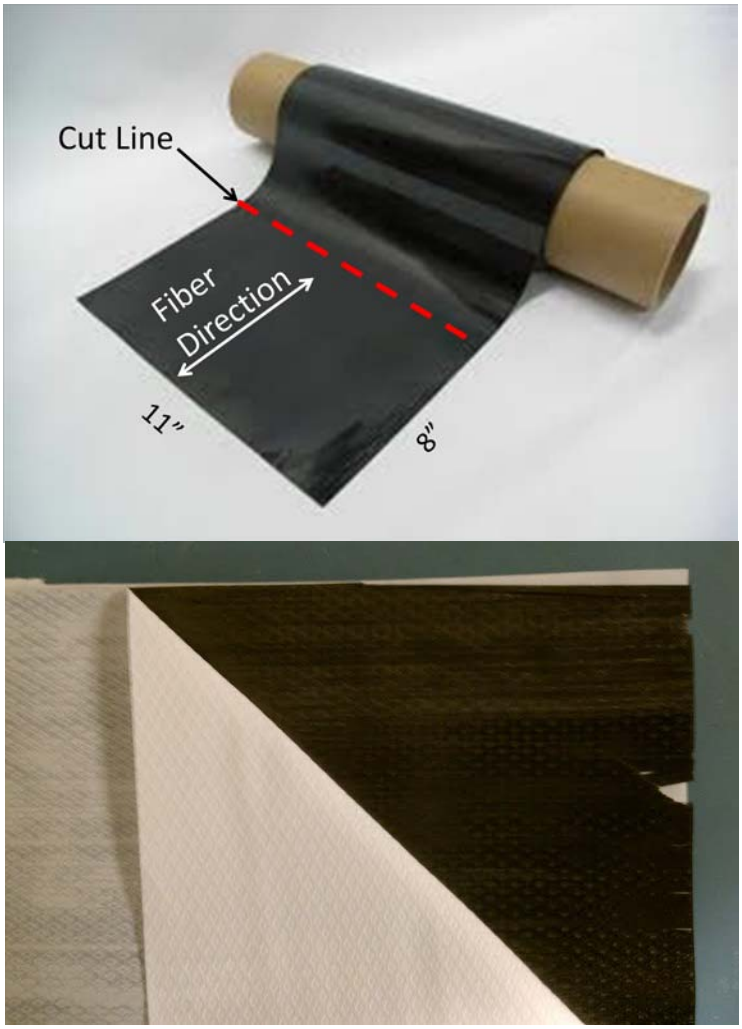

Figure 2.3: A Diagram of the Roll of Pre-preg Carbon Fiber Composite (Top), and Actual Composite Sheet with Protective Film (Bottom).

Once the plies are ready to be stacked, the protective plastic film and wax paper sheets are removed from each ply. These plies, with the help of a straight edge, are stacked one on top of another in the desired [0/90/0] orientation.

This new uncured laminate is then prepared to be placed in the heat press. The uncured laminate is placed in between Teflon, metal plates, and cardboard plates as

shown in Figure 2.4. The heat transfer paper and particleboard used are to ensure that the force from the heat press is evenly distributed to the composite, and the steel and metal plates allow for the composite to remain flat. The non-porous *TEFLON* ensures that the composite does not adhere to the metal plates during or after the curing process, and the porous *TEFLON* allows for excess matrix material to bleed out without adhering to anything.

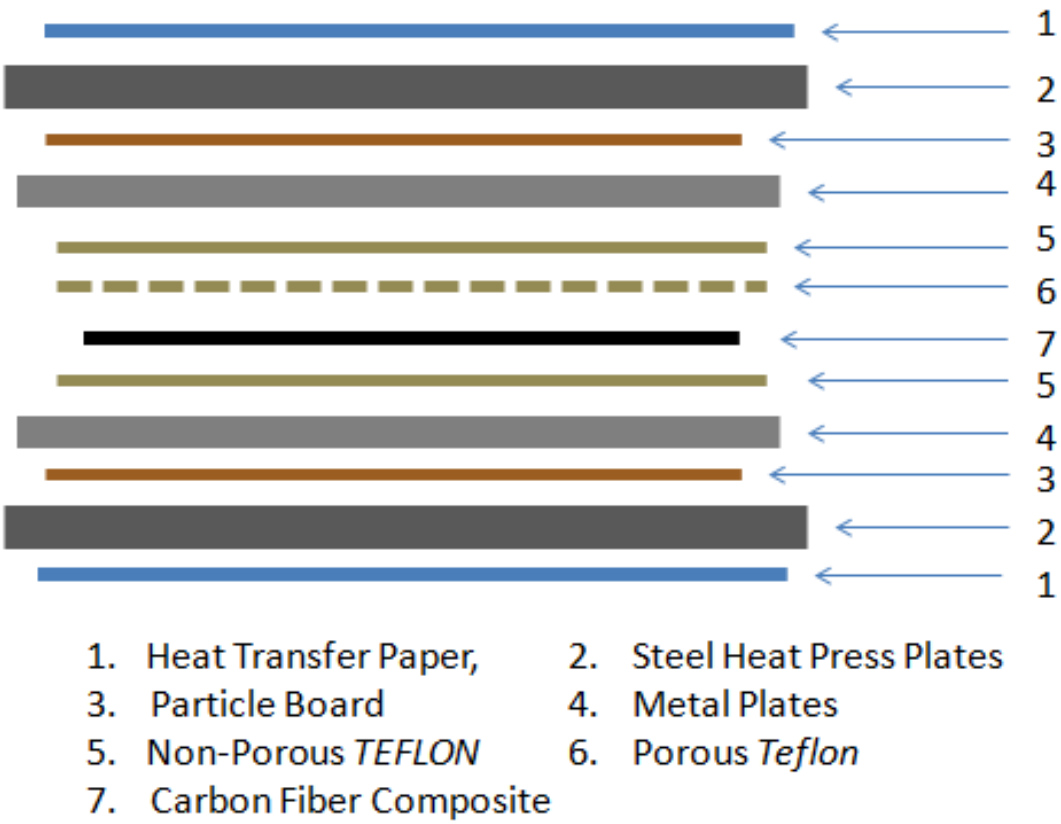

Figure 2.4: Set-up of the Material for the Heat Press.

The pre-preg stack is then placed into a LPKF Multipress S, Figure 2.5, a heat press that is capable of providing both pressure and heat required to cure the pre-preg material. The material was pressed initially for 10 minutes at 30°C and 30N/cm^2, then for 120 minutes at 192°C and 100 N/cm^2. Pressure was removed and the composite was

allowed to cool at room temperature for several hours before being removed from the oven, Figure 2.5. This process cures the laminate so that it is then ready to be used.

Figure 2.5: LPKF MultiPress S.

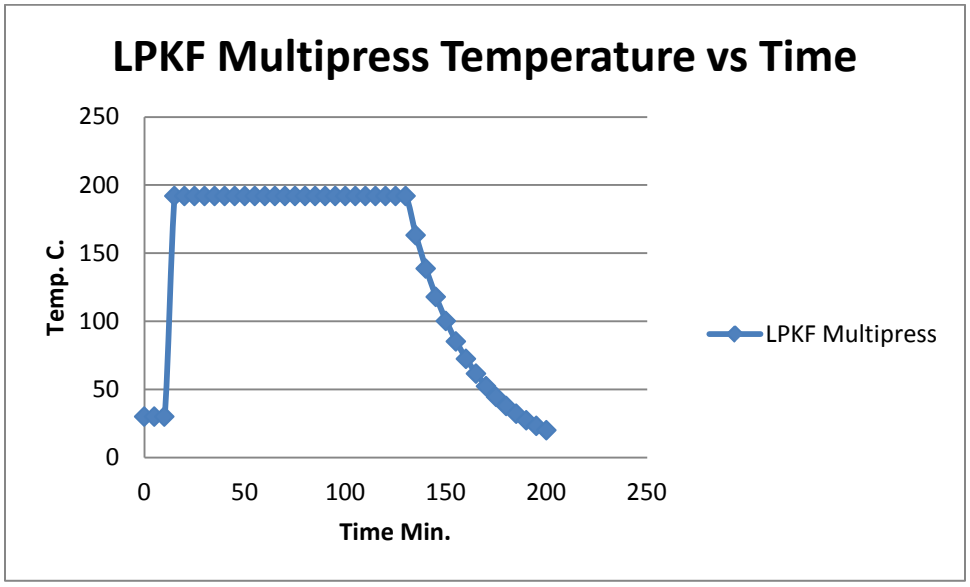

Figure 2.6: LPKF Multipress Temperature and Time for Composite Curing Cycle.

Once the carbon fiber had been cured, the composite is ready to be cut into either the wing or other test specimens. Due to the small nature of the veins or the specimens, a very precise method is required for manufacturing. This was done using a laser cutter,

and was performed at several locations, the Sensors Directorate at WPAFB, or Mount Laser and Photonics Center (MLPC), in Miamisburg, OH, Figure 2.7. While the locations and the lasers used for the cutting were different, the general process is the same.

The single sheet of carbon fiber is placed into the laser cutting area. A straight edge is used as a guide to line up the carbon fiber sheet within the laser itself by ensuring that one edge of the sheet is placed up against the straight edge. The carbon is held in place by a vacuum being pulled from below the flat cutting surface of the laser. A .dxf file is created previously in a computer automated design (CAD) program that represents the path that the laser will follow to cut. This file is imported into the computer that controls the laser. The settings of the laser should be arranged so that the laser is able to cut through the carbon fiber, but also so that the carbon fiber does not become burnt during the process. This is important because as the composite burns, the integrity of the material is compromised. Once these settings have been determined, the composite is then cut. For the case of this project, several sample parts were made and examined by MLPC in order to ensure the effectiveness of the cut, and the effects of the cut on the composite material. This ensured that as the material was cut with the laser, no adverse affects to the material occurred, such as overly heated edges, which could cause the material to burn and degrade the material properties.

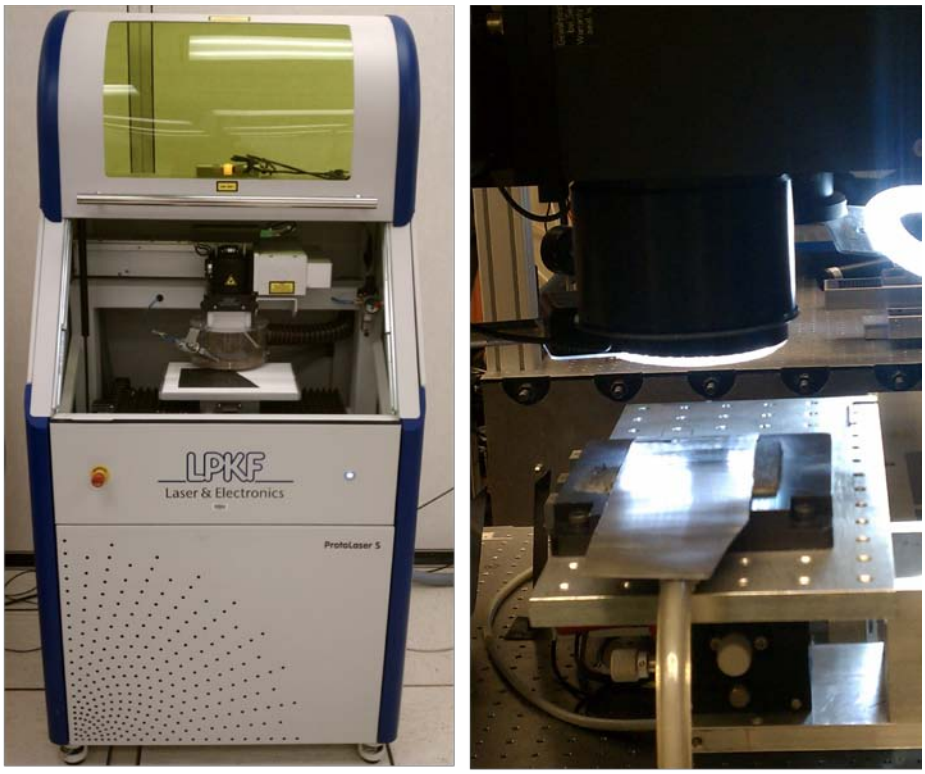

a) LPKF Laser at WPAFB b) Laser at MLPC

Figure 2.7: Laser Cutters used a) LPKF PhotoLaser S at WFAFB, and b) In-House Laser at MLPC.

Finally the Kapton membrane is applied to the wing. This is done using 3M 45 spray on adhesive that is sprayed into a small container, which is then applied via a paint brush by hand to each of the carbon fiber veins in the wing. The membrane is then placed onto the vein structure, and the adhesive is allowed to dry. Once the adhesive dries, excess membrane is trimmed away, and the wing is then ready for use, Figure 2.8.

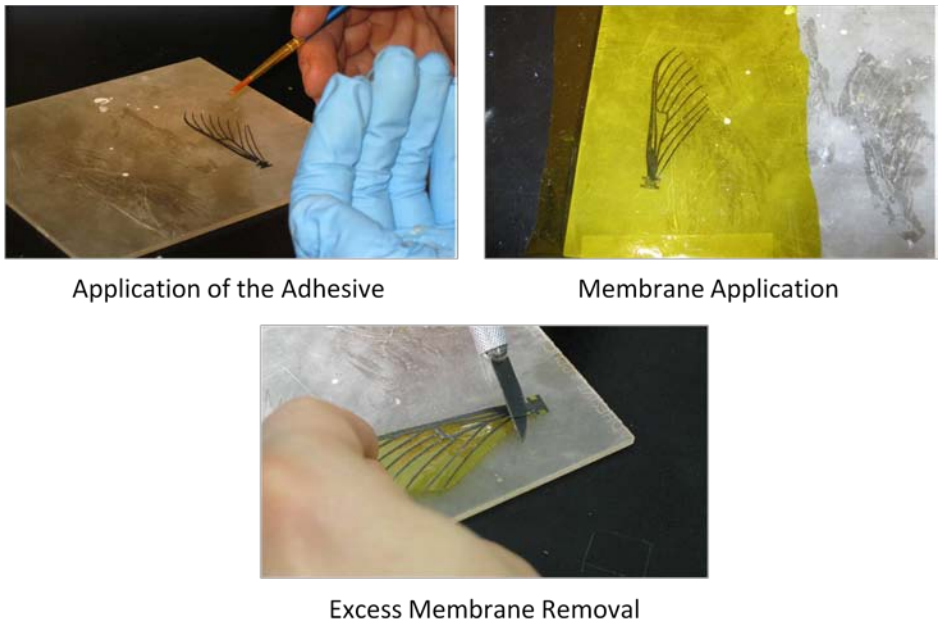

Figure 2.8: Application of the Kapton Membrane.

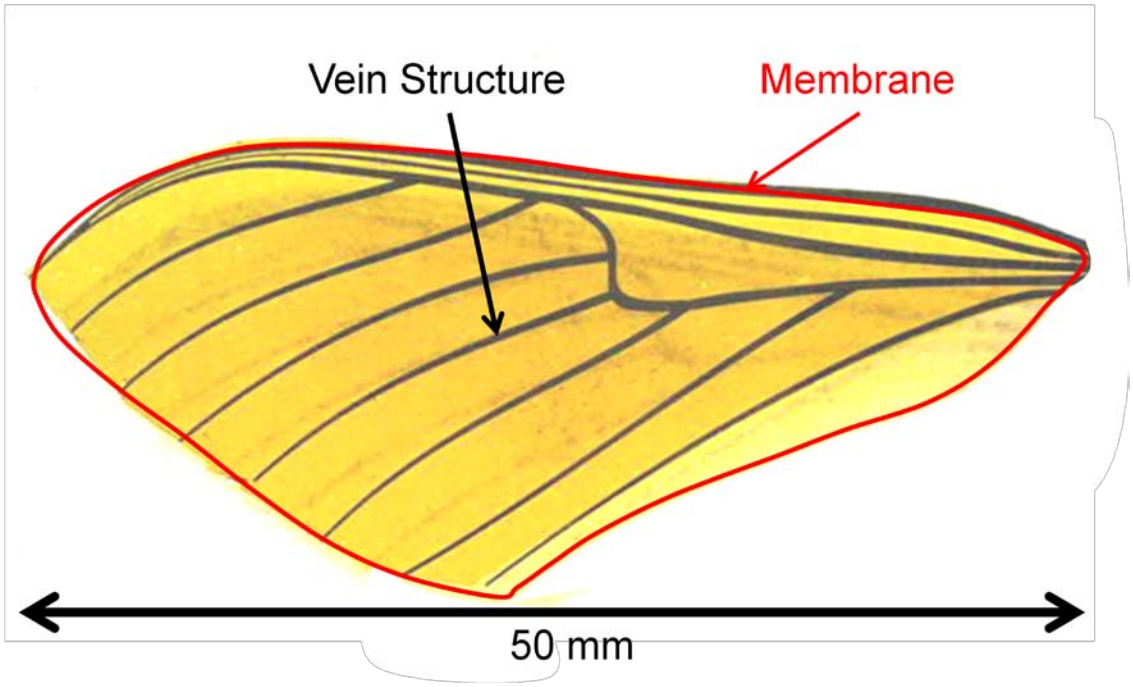

Figure 2.9: Completed FMAV Wing.

2.2. YSH-70-A/RS-3C

This section will serve to establish the baseline material properties of the YSH-70-A/RS-3C carbon fiber composite used in the vein structure of the wing. The baseline

material properties were provided by the manufacturer, Appendix A, and had been confirmed by O'Hara, who had previously tested 20-ply specimens of the composite using ASTM D 3039 and ASTM D 3518 standards. These tests were done in coordination with the University of Dayton Research Institute and Air Force Research Laboratory Materials Directorate on ply orientations of 0, 90 and +/- 45 degrees test specimens [2]. The tests would allow for the calculations of the moduli in the principal and secondary axes, as well as the shear direction. Table 2.1 shows the resulting lamina material properties as determined by the tests, and is compared with the properties given by the manufacturer [2].

Table 2.1: Material Properties developed by O'Hara and Manufacturer [2].

YSH-70-A/RS-3C Lamina Material Properties			
	20 Ply	**Manufacturer**	**% Difference**
$\mathbf{E_1}$	4.15 E+11 Pa	4.20 E+11 Pa	*1.20*
$\mathbf{E_2}$	5.52 E+09 Pa	5.51 E+09 Pa	*0.18*
$\mathbf{v_{12}}$	3.00 E-01	2.80 E-01	*7.14*
$\mathbf{G_{12}}$	4.85 E+09 Pa	4.83 E+09 Pa	0.41

While there is a slight difference in material properties based on the 20 ply compared to the manufacturers specifications, such a small error is common between test specimens and the material properties. Figure 2.10 [1] shows the stress-strain curve for the 5 samples of the 20-ply test performed by O'Hara. These results were averaged to arrive at the given modulus.

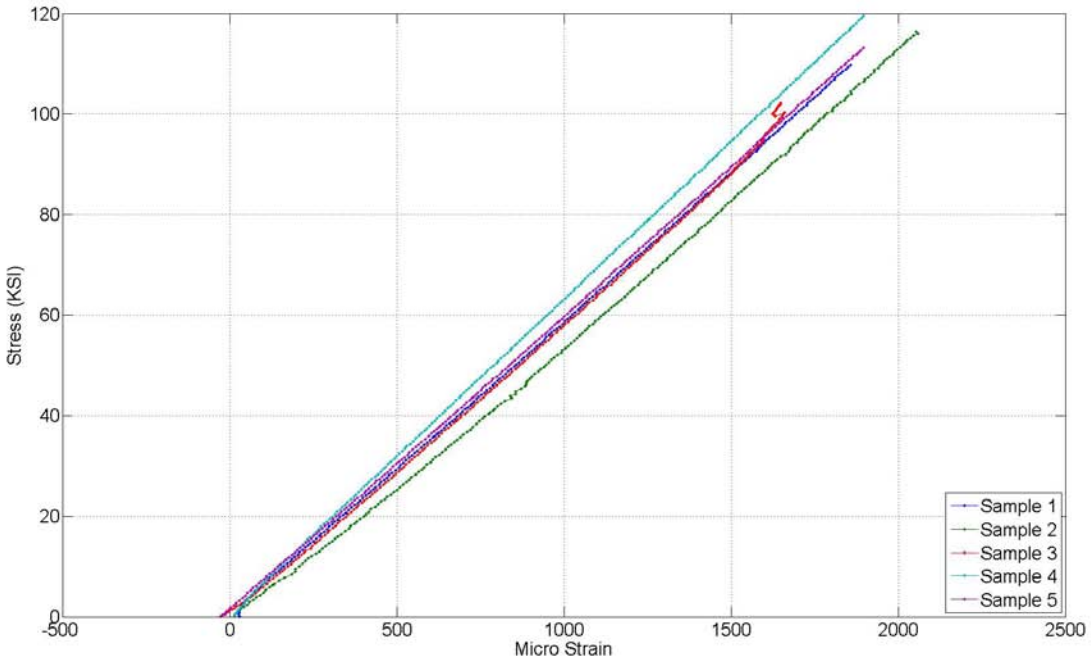

Figure 2.10: 20-Ply Tensile Test Stress-Strain Curve

The results from these tests confirm that the base material properties provided by the manufacturer were mostly correct. Therefore, it was the manufacterer's properties listed in Table 2.1 above that were used in further analysis.

2.3. Lamina Engineering Constants

In order to perform the transformation analysis required to follow the veins curvature as previously mentioned, an angular reorientation had to be created using the geometry shown in Figure 2.9. These transformations account for the fact that the laminate was constructed in a [0/90/0] orientation, and are used to solve for the material properties of the lamina for instances when the segments considered are not orientated to 0°.

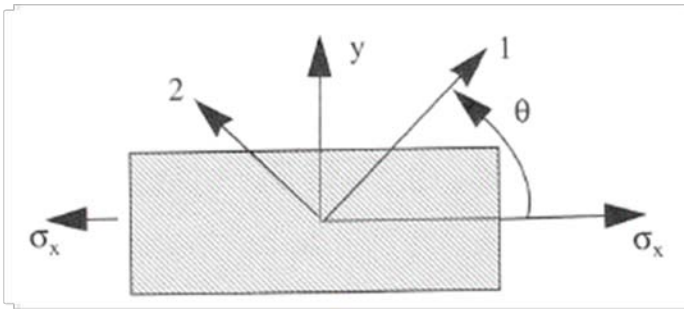

Figure 2.11: Off Axis Lamina Under Tensile Stress, with Global (x,y) and Material (1,2) Axes

The material properties in the local coordinate system (x,y,z) are as follows for the case of a beam:

$$E_x = \frac{E_1}{\left[m^4 + n^4 \frac{E_1}{E_2}\right]} \qquad (2.1)$$

Where E_x is the elastic modulus in the x axis, E_1 is the elastic modulus of the composite at 0°, E_2 is the modulus of the composite at 90° orientation, m is the cosine of the ply orientation, and n is the sine of the ply orientation. It is important to recognize the effect that the ply angle has on this equation.

To illustrate the effects that the ply orientation has on material properties of the lamina, the Modulus in Tension is plotted against the lamina orientation for YSH-70A/RS-3C, (See Figure 2.12).

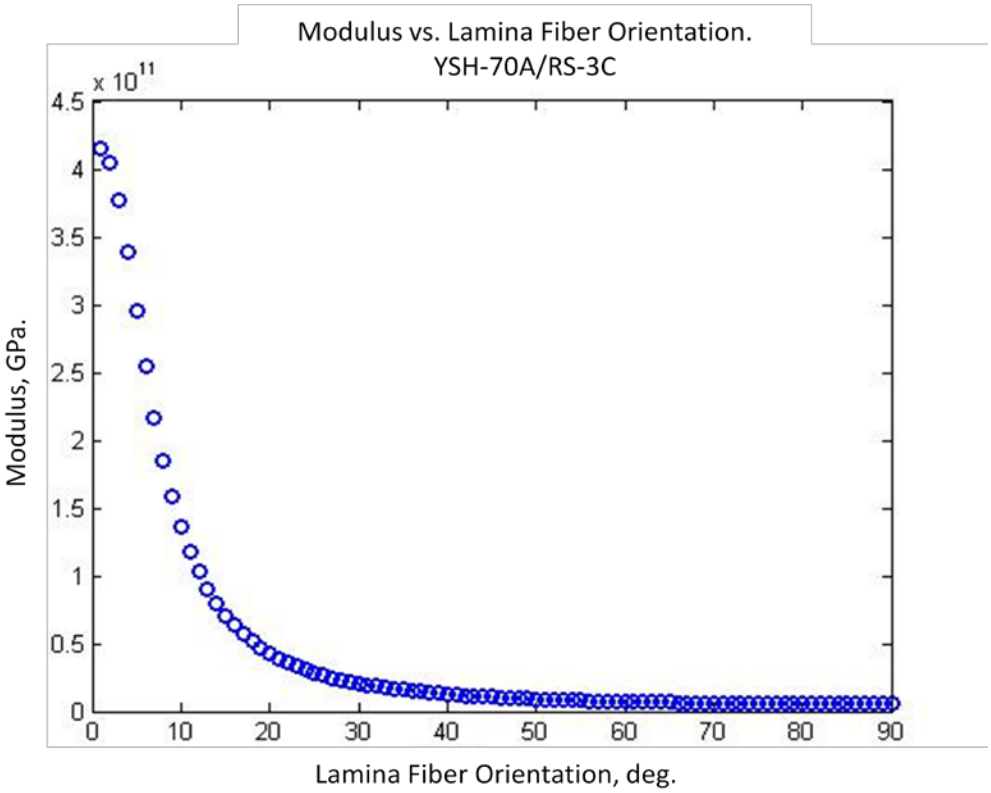

Figure 2.12: The Effects of Tension Modulus vs. Lamina Orientation Angle of the Fiber for YSH-70-A/RS-3C.

It can be seen that there is a drastic decline in modulus of the material as the ply orientation deviates from 0°. This is of extreme importance, especially for the use of a thin 3-ply laminate. Considerable amounts of time were spent in understanding the effects of this while performing the analysis as will be shown later in this chapter.

2.4. Halpin-Tsai (Short Fibers)

Since the vein structure being fabricated for the engineered wing is very narrow and cut across the individual fibers, short fibers that may have occurred were accounted for by use of the Halpin-Tsai Equations, Equation 2.5 [21]. Short fibers are defined as fibers where the length of the fiber is not significantly larger than the diameter of the

fiber. While there is no defined length to diameter ratio for a fiber to be defined as "short", the accepted ratio is typically around 100 [21].

$$\frac{\overline{P}}{P_m} = \frac{1 + \zeta\eta\phi}{1 - \zeta\eta\phi} \tag{2.5}$$

The engineering constants, E_f and E_m, were directly substituted for P_m and P_f in Equation 2.5. Where E_f is the modulus of the fiber, E_m is the modulus of the matrix, obtained from the manufacturer, Appendix A. For the case of circular fibers, which were present in the wing, the following factors were inserted into Equation 2.5. Equations 2.6 and 2.7 show these factors, where l is the length of the fiber in the 1-direction, t is the thickness of the tape and w is the width of the fiber in the 2-direction.

$$\begin{aligned} \zeta_{E_{11}} &= 2(l/t) \\ \zeta_{E_{22}} &= 2(w/t) \\ \zeta_{G_{12}} &= 1 \end{aligned} \tag{2.6}$$

$$\eta = \frac{\frac{E_f}{E_m} - 1}{\frac{E_f}{E_m} + \zeta} \tag{2.7}$$

For the case of circular fibers, w=t. It should be noted that for cases where the length of fiber is sufficiently long, no significant difference in material properties is occurred through the use of the Halpin-Tsai equation. Using these equations, the material properties were solved for the lamina.

2.5. Finite Element Analysis

A significant amount of the analysis of the engineered wing was performed using FEA. An FEA model was constructed by developing a MATLAB program that is capable of generating an input file to be submitted to ABAQUS, a finite element model solver. This technique was used in order to more easily capture the complex nature of the wing. Frequency modal analysis of the wing was performed, as well as point load tests on the wing. The following sections go through the theory and processes required to perform the analysis and experimentation.

2.5.1. Finite Element Frequency Analysis Theory

When performing the frequency analysis of the wing, it is important to understand the fundamental concept behind what is being done within the finite element analysis program. While the basic theory behind finite element analysis when dealing with static loading is readily available, the theory behind using FEA for frequency analysis is not as readily available. Therefore, only the basics behind the frequency analysis will be covered in this section.

The modal frequencies of structure are based on the structures stiffness and mass properties. In the finite element model, the mass and stiffness are represented at a finite set of second order differential equations in the time domain, [t] (equations of motion, Equation 2.8) as follows:

$$K \cdot U + M \cdot d^2U/dt^2 = 0 \tag{2.8}$$

Where [K] represents the stiffness matrix of the finite element model, [U] represents the vector of nodal displacements, with six degrees of freedom (three rotation, and three

translation). [M] represents the finite element mass matrix. The nodal displacement vector is set to the equation below:

$$U = \Phi e^{i\omega t} \tag{2.9}$$

Substituting the equation of motion (Equation 2.10), obtains the following eigenvalue problem.

$$[K - \omega^2 \cdot M]\Phi = 0 \tag{2.10}$$

[Φ] is the resulting mode shape (eigenvector), and [ω] is the associated frequency (eigenvalue). ABAQUS was used to calculate and display the mode shape and associated frequency. It is important to note that the associated modal shape and frequency is also associated with the boundary condition, which may not be evidently clear from the equations above. The boundary condition for this project was clamped, prohibiting displacement in all six degrees of freedom. Mathematically, this would be evident in the vector of nodal displacement, [U], where the values for the clamped nodes would be set at zero.

2.5.2. Effective Moment of Inertia

Since beam elements were used in this project, properly modeling the nature of the composite is important since the material does not have constant material properties through the entire cross section. The effective moment of inertia allows for one material property to represent the element while changing the dimensions of the element's beam profile to maintain its physical characteristics. In order to capture this, the effective modulus of the beam cross section is taken for each beam element used to model the composite vein in the model.

For the given section of the vein, the average angle is calculated and the ply orientations for each element are determined. Using the code in Appendix B, the material properties for each lamina are determined. Since only one set of material properties from the beam needs to be used, the material properties from the lamina with the highest axial modulus was chosen to represent the entire beam with the exception of the density, which will be explained in Section 2.5.3. Using the material properties from the ply with the highest axial modulus for the element allows for maximum width of the beam profile in the model to be viewed within the model as the same physical width of the carbon-fiber at the same point on physical specimen. Since there is a large difference in the stiffness of the material based on fiber direction, this prevents the maximum width of the beam element profile from becoming too large so that when the beam profile is displayed in ABAQUS one can easily see a shape similar to the actual wing and not a vastly distorted image.

A ratio of the axial moduli of the other two plies to the maximum modulus determines the reduction of area needed by those plies to retain the physical characteristics of the beam. Equation 2.11 shows the equation used to perform the transformation.

$$N_x = \frac{E_{x\_ply}}{E_{x\_max}} \tag{2.11}$$

Where E_{x_ply} is the elastic modulus of the lamina in the local x direction. E_{x_max} is the maximum elastic modulus of the lamina in the local x direction for the laminate. N_x is the axial modulus ratio of the x^{th} ply.

The axial modulus ratio is used to change the area of the ply so that when the singular material property is applied, the beam section maintains the same axial modulus. In order to keep the effective moment of inertia the same for the element, the distance of the ply from the neutral axis needs to be kept constant, therefore when changing the area of the height and location of the ply was held constant and only the width was modified. The effective width of each of the two other plies was simply the width of the beam section multiplied by their individual axial modulus ratios, Equation 2.12.

$$W_{new} = N_x \; x \; W_{orig} \tag{2.12}$$

Where W_{new_ply} is the new effective width for the lamina in the model's cross section, and W_{orig} is the original cross section width of the lamina in the model.

Implementing the effective moment of inertia calculation changes the beam elements profile from a rectangular shape to a shape similar to an I-beam for most elements. Figure 2.13 shows a representation of a section of the three ply carbon-fiber material and the new beam section that would result based on the effective moment of inertia calculations.

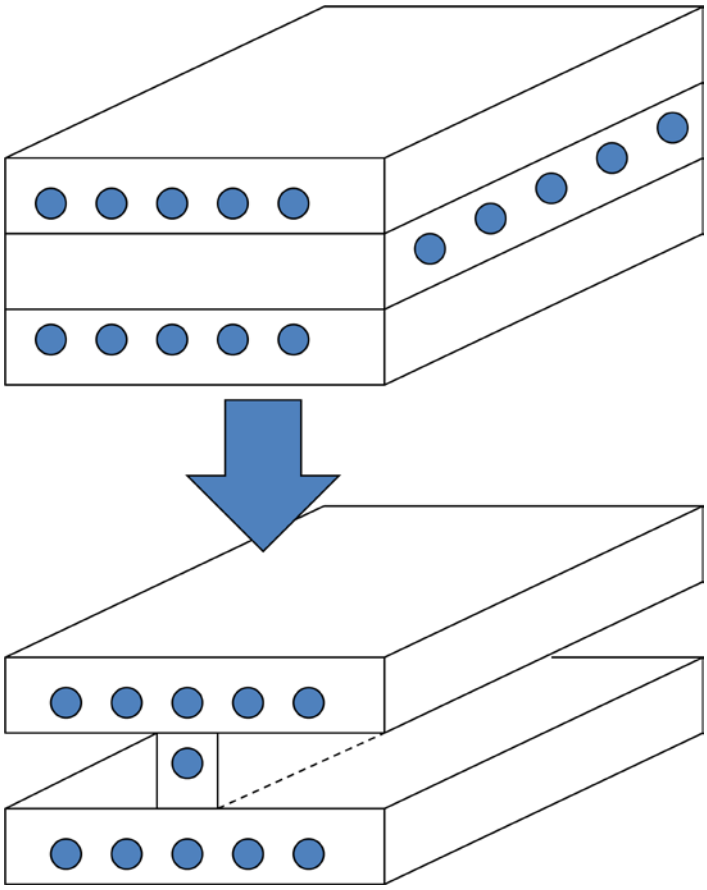

Figure 2.13: Diagram Showing the Effect on the Beam Cross Section after the Effective Moment of Inertia Calculations is Applied.

2.5.3. Effective Density

While the stiffness of the element represents the physical characteristics of the carbon fiber, the mass of the element is changed due to the change in area if the density is kept the same. In order to account for this, the density of the material for the element is changed so that the mass of the element is the same as it was prior to the change in area taking place. This is a simple calculation based on the ratios of the cross sectional area of the new beam section compared to the physical cross sectional area of the wing at that point, Equation 2.13

$$\rho_{new} = \rho_{orig}\, x\, \frac{A_{orig}}{A_{new}} \tag{2.13}$$

Where ρ_{new} is the new density for the element, ρ_{orig} is the original density of the composite, A_{orig} is the average physical cross section of the manufactured wing at the same location as the element, and A_{new} is the new cross section of the beam element after the effect moment of Inertia calculations have been performed.

III. Carbon Fiber Composite Analysis and Results

This chapter will serve to describe the work done to analyze the material properties of the carbon fiber composite used for the vein structure of the engineered wing. Due to the requirement for a low mass, the composite was chosen to serve as the vein structure due to its high strength and low density. Previous work done at Harvard showed that the composite was a viable alternative to metals or polymers, and suggested that a [0/90/0] orientation was useful in that it gave the composite the ability to be stiff in the spanwise and chordwise direction [15]. However, some of the issues encountered in this project were not documented in the literature. It was important to understand how these issues affected the material properties of the composite, and ultimately in the engineered wings themselves.

One can observe that, as shown in Figure 3.1, the actual orientation of the fiber in a particular vein is predicated upon the veins curvature at a coordinated point. This make the through thickness material properties per segment anisotropic. Thus, it became necessary to not only develop a method to handle this orientation requirement, but to make sure that any material property was correctly defined. This chapter serves to evaluate the unidirectional carbon fiber composite used in the manufacturing of the engineered MAV wing. The vein structure of the wing was cut out of a single sheet of composite material made of three plies of unidirectional carbon fiber stacked in a [0/90/0] orientation as shown, Figure 3.1. Evidence suggested some issues with the carbon fiber composite material properties, and an effort was made to understand and eventually characterize material variations before beginning the analysis of the wing.

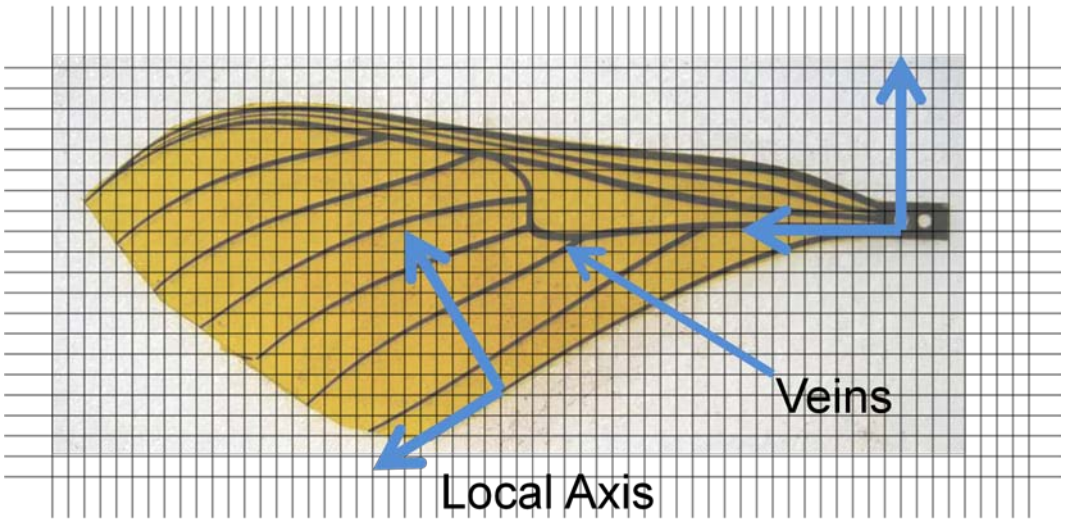

Figure 3.1: The Manufactured Wing with Lines Representing the 0° and 90° Layout of the Carbon Fibers.

3.1. Laminate Material Modal Frequency Experimentation

Prior to the analysis of the engineered wing, there were several questions raised about the validity of the unidirectional carbon fiber composite material properties used in the creation of the engineered MAV wing stemming from the results of the previous tensile tests, and the lack of literature on the use of 3-ply specimens. Since the carbon fiber composite is used to construct the veins of the engineered wing, Figure 3.1, and provide most of the structure's mass and stiffness, it was important to examine any of these concerns. Therefore, an analysis of the carbon fiber composite was performed in conjunction with the analysis performed on the engineered wing.

3.1.1. Laminate Material Sample Testing

Wishing to use a non-destructive method, a modal frequency test was performed on carbon fiber composite specimens that were 40 mm long by 5 mm wide in order to examine the material properties and determine the validity of the given material properties, since only three plies would be used to construct the laminate. These

specimens were three-ply laminates with fibers at a [0/90/0] orientation. The specimens are significantly smaller than the 120 mm by 25 mm specimens tested by O'Hara when selecting the carbon fiber composite for the wing [2], and closer to the size of the veins that are present on the engineered wing.

For the modal frequency test, the specimens were clamped at the base, and vibrated with airborne excitation in a pseudo random manner, Figure 3.2. This modal frequency test is the same method that was used to determine the characteristcs of the vein material properties, and was also used by DeLeon (See Section 1.5, and Equation 2 for more details) [1].

Figure 3.2: 40mm x 5 mm Beam with Airborne Excitation.

In order to increase the reflectivity of the specimen so that they could better reflect a signal back to the laser vibrometer, the beams were marked with a white PENTEL 100W S paint pen in the manner described by DeLeon [1]. Ten specimens were tested to determine the frequency of the first mode of the beam specimens. Results of the test are shown below in Table 3.1.

Table 3.1: Frequency and Mass Experimental Results.

YSH-70-A/RS-3C [0/90/0] Specimens		
Sample	Mode 1 (Hz)	Mass (mg)
1	150	22.8
2	140.6	23.5
3	140.24	22.8
4	135.2	22.7
5	148.4	23.4
6	146.1	23
7	150.8	23
8	151.6	23.7
9	137.5	23.2
10	148.5	24
Average	***144.894***	***23.21***
Standard Variation	*5.9601911*	*0.43063261*

A FEA model was constructed, seen in Section 3.2., and compared against the average of these experimental results.

3.2. FEA Beam Model

An FEA model of the carbon fiber test specimens was constructed using ABAQUS. Two models were made, one using 10 quadratic (B32) beam elements 21 nodes, Figure 3.3, and the other using 64 composite shell elements (SQR4), 264 nodes, Figure 3.4. Both models used the material properties found in Section 2.2, with the necessary calculations and changes made to the beam element, Chapter 2. Note the

I-beam shape of the beam element model due to the composite structure. The base of the beams were clamped, 0 degrees of freedom (DOF), while all other nodes were given 6 DOF. Modal frequency analyses of the beam elements were performed.

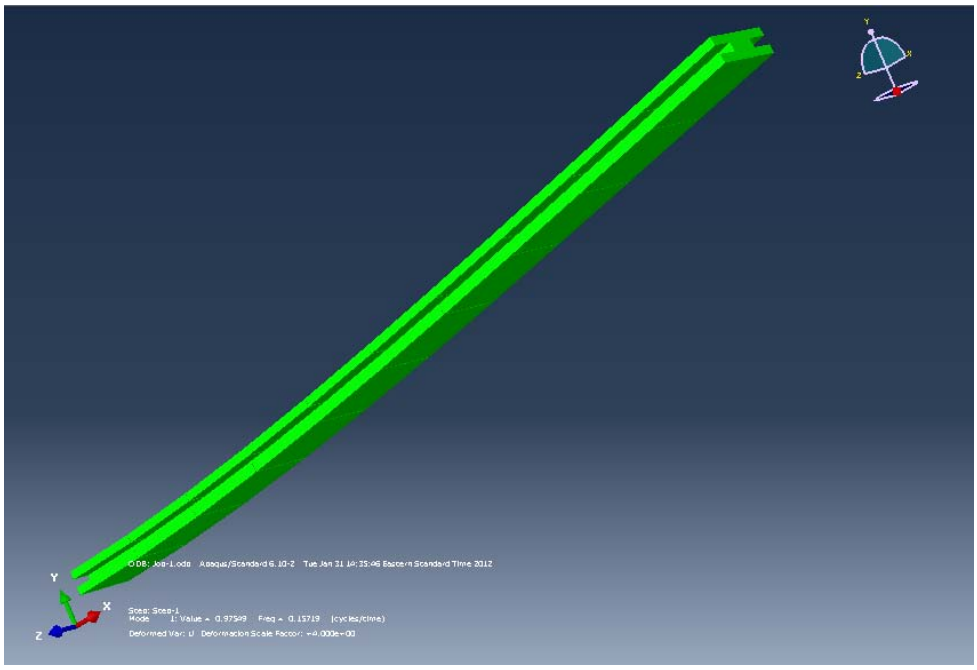

Figure 3.3: Beam Element Finite Element Model of Test Specimens.

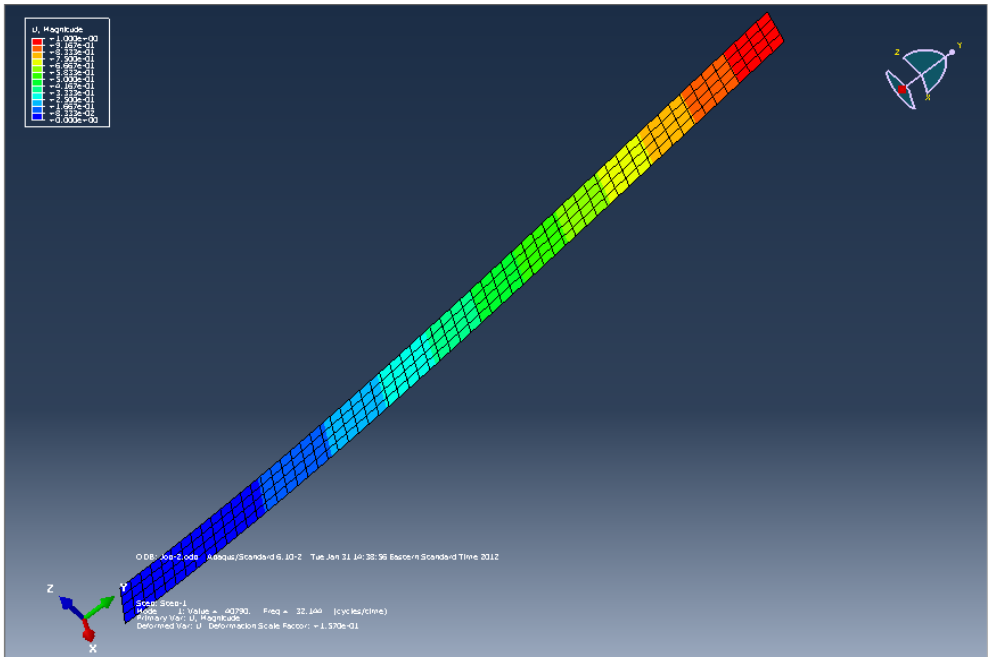

Figure 3.4: Composite Shell Element model of Test Specimens.

The result of the modal analysis of both beams was for a first bending frequency of 219.5 Hz, Table 3.2. This was significantly lower than the experimental data obtained in Section 3.1.1. Therefore, the composite material warranted further investigation since the same material and manufacturing process was being used in the engineered wing. It was important to understand what was causing such a significant deviation in the expected modal frequency in order to perform an accurate analysis of the wing.

Table 3.2: Comparison of Experimental Data to FEA Reasults.

Comparison of Beam Specimen Results		
	1st Mode (Hz)	**% Difference to FEA**
Experimental	144.89 (avg)	34.0%
Beam FEA	219.5	-
Composite Shell	219.5	-

3.2.1. Modifiable FEA Beam Model

Since there was a significant difference between the experimental and analytical results, a MATLAB code was developed, Appendix C. This code imports pre-determined nodes and elements based on the input file (.inp) of the wire element developed above Appendix D. The code changes the thickness of the specimen, the ply orientation of lamina, and the angle at which the beam was cut in comparison to [0/90/0] orientation of the composite material. These changes are written into a new input file that is solved using ABAQUS. The code then also has the ability to read the data file (.dat) from ABAQUS, which contains the modal frequencies of the model, and store the modal frequencies in MATLAB where they can easily be compared.

This code allowed rapid changes to be made to the model, therefore allowing a better understanding of the effects of the thickness of the specimen, the ply orientation of lamina, and the angle at which the beam was cut in comparison to [0/90/0] orientation of

the composite material. This code was used to vary each of these inputs to allow a better understanding of how they affected the modal frequency of the test specimens.

3.3. Carbon Fiber Analysis

Several options were explored to determine the source of error in the laminate specimens:

1. Incorrect material properties provided by the manufacturer.
2. Incorrect dimensions due to low number of plies in the laminate, and small dimensions of the specimens.
3. Errors in the manufacturing of the laminate resulting in errors in ply orientation.

Each of these was examined in order to determine a root cause of the material property deviation.

The first thing examined were the given material properties of the composite. O'Hara had previously tested twenty-ply specimens of the composite using ASTM D 3039 and ASTM D 3518 standards shown in Table 2.1.

3.3.1. Laminate Material Dimensions

Since it was determined that the material properties of the composite matched closely those given by the manufacturer, the next thing that was examined was the dimensions of the test specimens. Incorrect dimensions could cause error in the equations used to determine the expected analytical modal frequency of the test. Using Fowler Precision calipers with a tolerance of +/- 5 microns, every specimen was checked. Variation observed in the width and length of the beam observed was within the tolerance of the calipers used, and therefore was not investigated further.

The thicknesses of the beams were also measured. It was found that the thickness of the specimen varied between 135 and 160 microns, and had an average thickness of 145 microns. This was different from the expected 150 microns, and has some effect in the modal frequency. A finite element model described in Section 3.2.1 was created to determine how much of an effect this would have on the first modal frequency. Using MATLAB Code, Appendix C, the thickness of the beam was varied from 135 to 160 microns, resulting in 6 runs of the beam model. The results of the test are shown below in Figure 3.5.

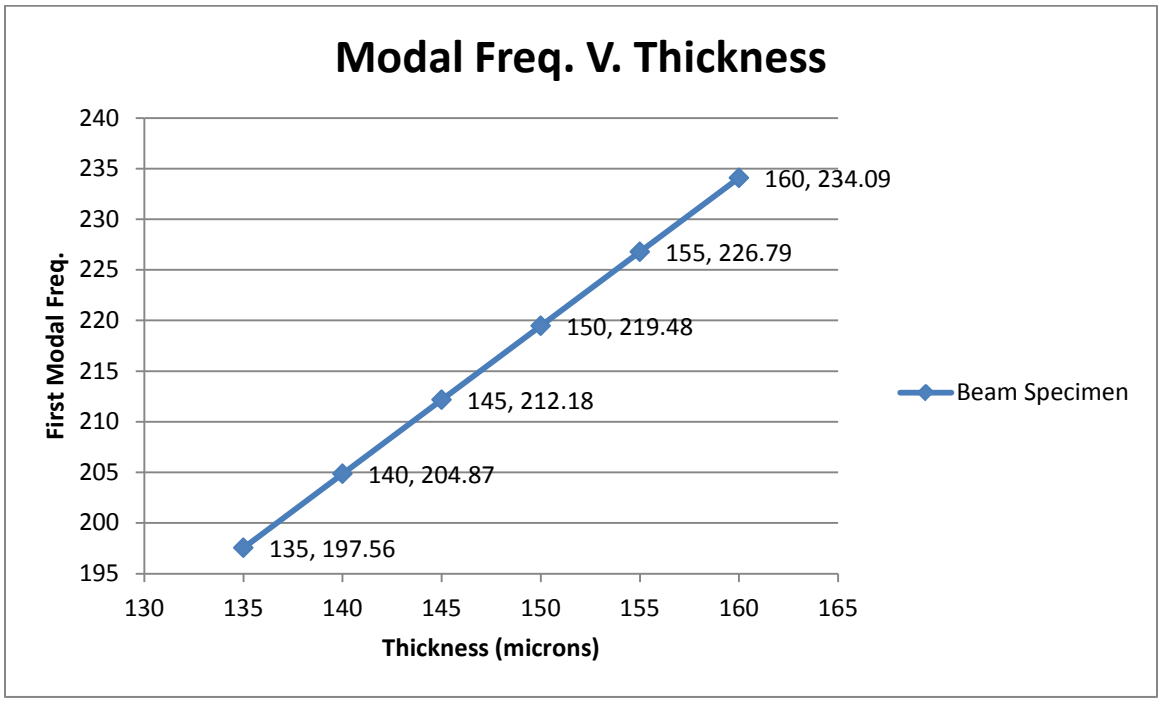

Figure 3.5: Variation of Beam Thickness and Effects on First Modal Frequency.

. The results of the test shows that the frequency of the specimen is thickness dependent, varying between 197.56 and 234.09 Hz. While this is a significant change, it does not explain the 144.89 Hz response seen during the experimentation. Further

investigation was done looking at the ply orientation and errors that could have been caused during manufacturing.

3.3.2. Lamina Ply Orientation & Manufacturing Errors

Errors in manufacturing were then examined. Based on the calculation in Section 2.2, it was determined that a small variance in the ply orientation could cause significant variations on the material properties. The alignment of the fibers was then examined to see if such a variation existed. Multiple test specimens measuring 40mm long by 1mm wide were constructed out of the same [0/90/0] carbon fiber composite as the engineered wing and the material sample specimens, See Figure 3.6. From these specimens, it was hoped to determine if there was any variation seen between the orientation of the fibers and along the straight edge of the test specimen. Any such variation would indicate that either the ply orientation of the top ply was not at a 0° orientation, the angle at which the laser was cutting was not parallel to the orientation of the fibers, or both.

Figure 3.6: Test Specimen for Ply-Orientation Test.

These test specimens were then examined using a Zeiss Discovery V.12 optical microscope, (Figure 3.7). This microscope has up to 150x magnification, allowing the

individual fibers to be seen on the composite test specimens. Each of the test specimens were examined under the microscope, with digital images being captured for each specimen, (See Figure 3.8). The fiber orientations of the test specimens were then measured using a developed MATLAB code, (See Appendix E).

Figure 3.7: Zeiss Discovery V.12 Optical Zoom Microscope.

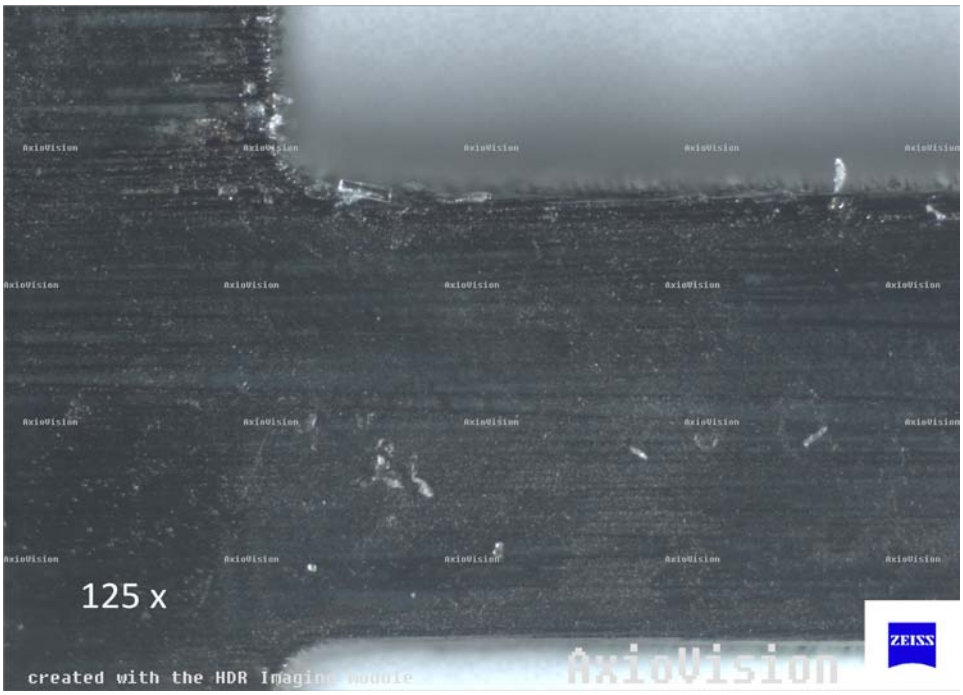

Figure 3.8: Image of Test Specimen used to Evaluate Angle of Fibers within the Composite.

The developed MATLAB code is designed to open an image of the test specimen in MATLAB. Once in MATLAB, the user selects two points on the straight cut edge of the test specimen. This edge was selected because it should run parallel to orientation of the fibers on both the top and bottom plies of the test specimen. The code then forms a line between the two points to use as a reference axis. The user then selects two points on ten separate fibers on the test specimen. Again, the code forms a line between the two points selected on each of the fibers. After the points on all ten fibers have been selected, the code calculates the average angle between the lines formed from the selected individual fibers, and the reference axis. This process was repeated several times for each test specimen to ensure that any error in selecting the fibers would be averaged out.

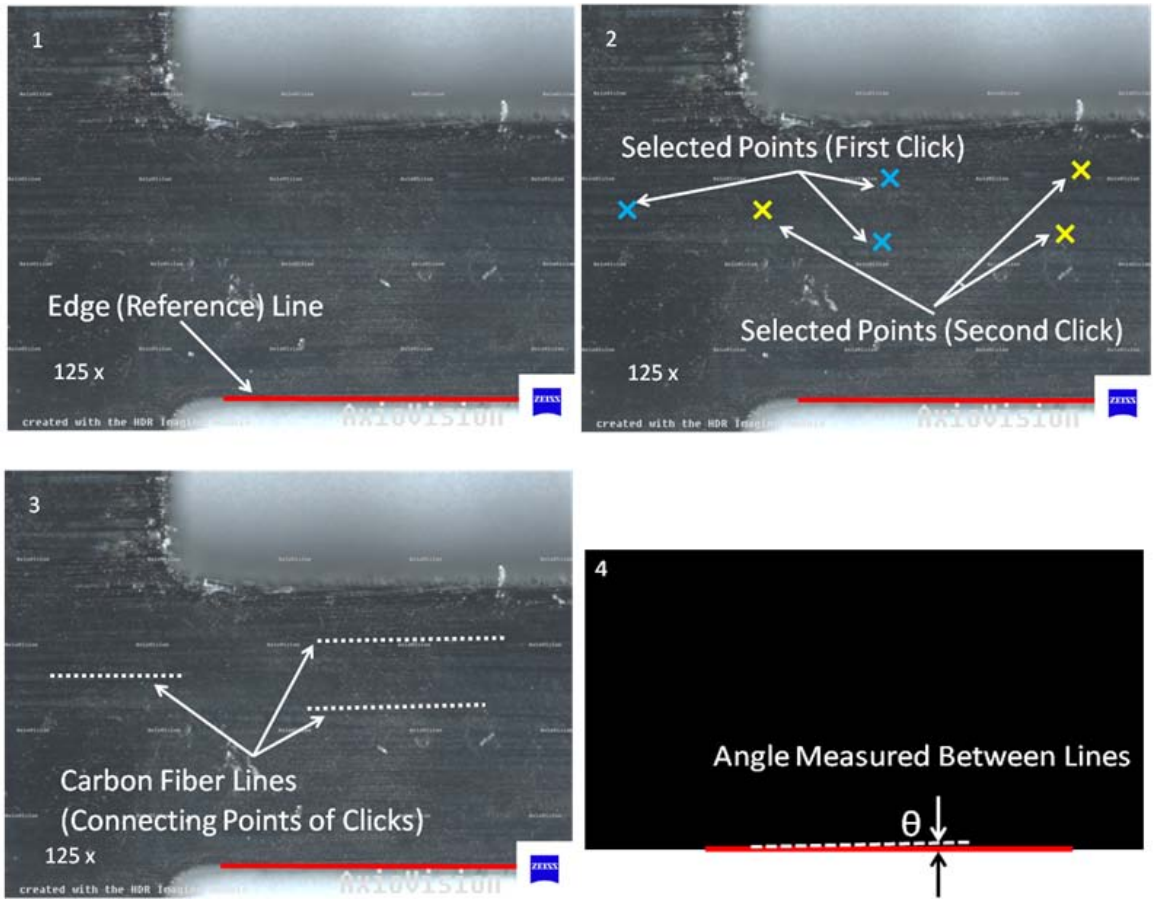

Figure 3.9: MATLAB Code Process for Measuring Carbon Fiber Angle.

If the fibers were aligned in the [0/90/0] manner as prescribed in manufacturing, the fibers should all be parallel to the edge of the test specimen. However, this test showed that this was not the case for any of the specimens. All of the test specimens exhibited fibers that formed a small angle relative to the reference axis. In other words, the angle of the fibers were not at [0/90/0] degrees, but rather had some degree of variation in the fiber orientation. Results from the test are shown below in Table 3.3.

Table 3.3: Results from Optical Microscpe Test.

Optical Microscope Fiber Measurements	
Test Specimen	**Average Angle**
1	2.55°
2	3.49°
3	4.22°
4	3.08°
5	2.94°
6	2.33°
7	1.94°
8	1.65°
9	2.27°
10	2.75°
Average:	***2.494°***

It became quickly apparent that the deviation in ply orientation was the result of either the hand lay-up of the laminate, or the placement of the laminate into the laser cutter. Since previous testing was only able to measure the angle of the outer two layers relative to the cut of the specimen, more testing was done to confirm the sources of error.

Wishing to quantify if a variation in the ply angle was present, two other sample carbon fiber specimen tests were performed. The objective of the tests was to determine the variation in the orientation of the carbon-fiber lay-up for the [0/90/0] laminate, as well as determine the ability of the hand lay-up technique to correctly achieve the desired ply orientation.

Two tests were devised in order to achieve this goal. Both test specimens were sheets of 8” x 11” carbon fiber. The composite was constructed in the same manner the composite used in the previous tests, however a few things were changed. For the first test, instead of all three plies of the laminate being identical sizes, the two pre-preg sheets formed the middle 90° layer and the top 0° layer were trimmed to be slightly smaller. The pre-preg used for the top layer was trimmed slightly smaller than the pre-preg used for the middle ply. As the laminas were stacked, two edges of the lamina were aligned on top of the previous ply. This meant that at the edge of the laminate sheet, all three plies were visible, as can be seen in Figure 3.10.

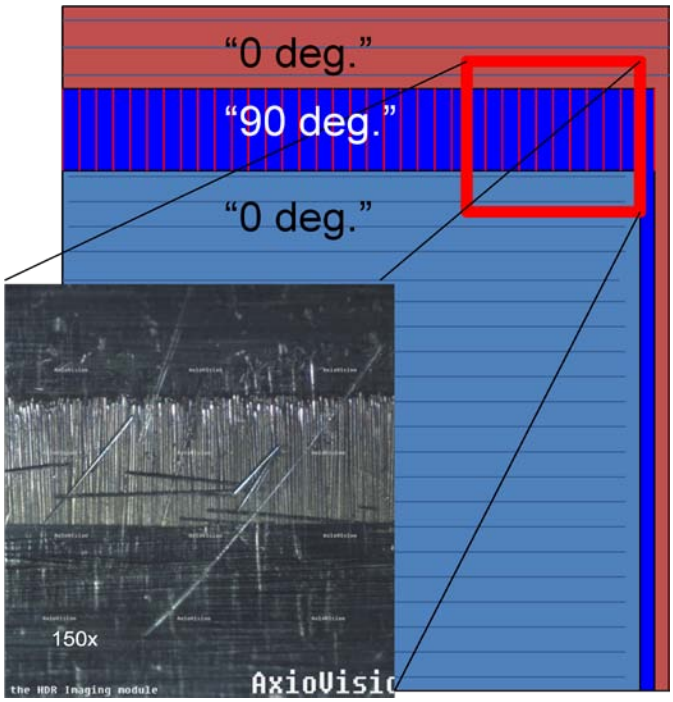

Figure 3.10: 3-Ply Test Stack-up Exposing All Three Plies.

Figure 3.11: 3-Ply Test Specimen Optical Microscope Digital Image.

Using the same developed MATLAB code as the previous test, the angle between the plies was measured. For this test, the bottom ply was established as the reference axis. This allowed the angle of the other fibers to be measured relative to that bottom ply. Figure 3.11 shows an image taken by the optical microscope of the test specimen and used to measure the angle of the fibers.

Another test was performed using a two-ply 0/0 laminate to again verify the results. The 0/0 laminate for this test was used because it would be easier to visually see the error. Again, the top ply was trimmed to be slightly smaller than the bottom ply. Figure 3.12 shows a diagram of the test specimen. Figure 3.12 shows images from the optical microscope. The same develop MATLAB code was used in both cases to evaluate the image.

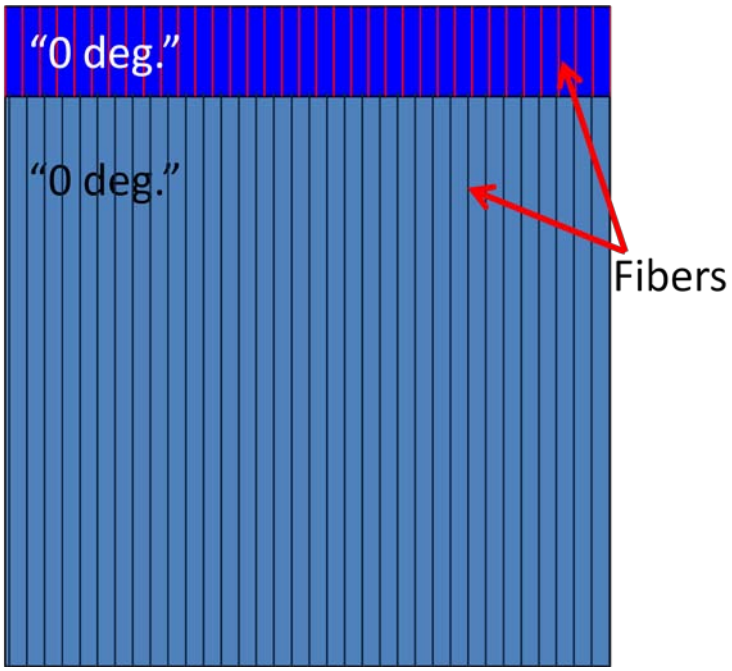

Figure 3.12: Diagram of Test Specimen Showing Fiber Alignment.

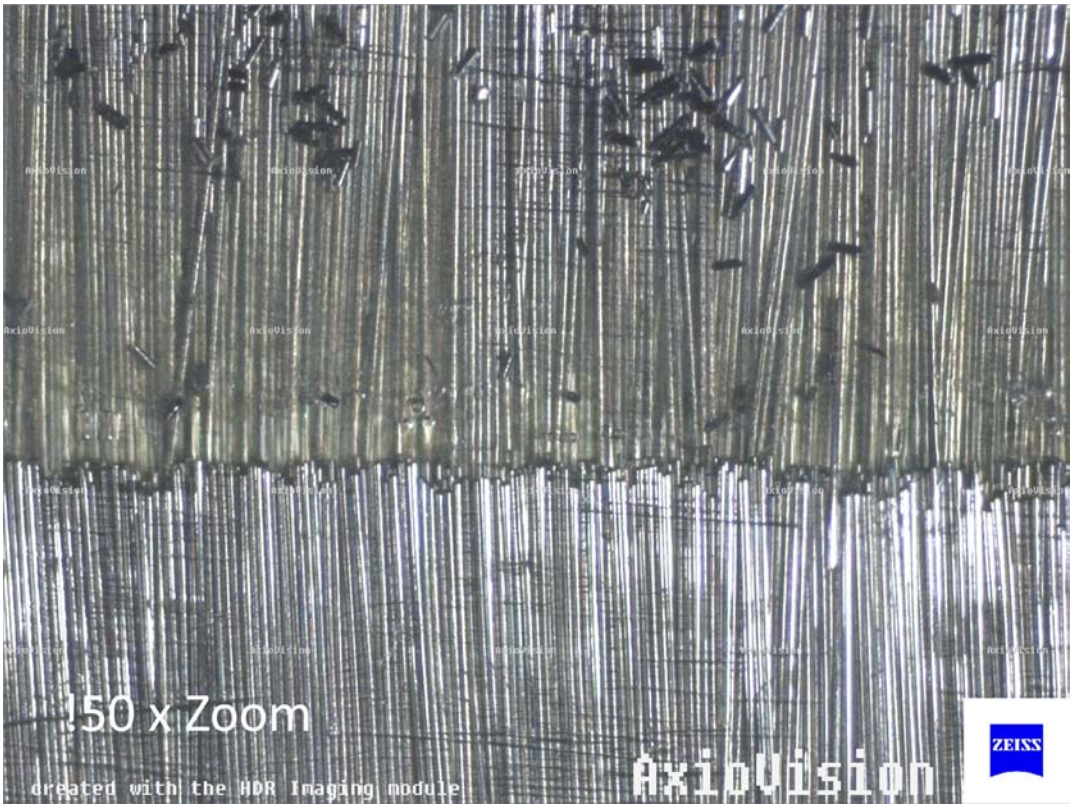

Figure 3.13: Optical Image of the 2-Ply Unidirectional Test Specimen

The results from both tests showed that the same approximate 2° variations in ply angle were present in this test as in original test. Based on how quickly the modulus of the lamina properties decrease as the angle of the ply goes away from 0°, the error in the ply orientation was primarily responsible for the low first modal frequency observed in Section 3.1.1.

3.4. Sources of Error

While it is important to understand the effects of the idiosyncrasies in the ply orientation, it is also important to understand how they became present. This section will serve in an attempt to explain why these occur.

The variation in thickness of the ply orientation can be considered an effect of normal material variation. As the pre-preg is stacked, there is some bleed off of the matrix epoxy as it is cured in the heat press. Since the laminate contains only three plies, even a small amount of matrix lost correlates to a larger percentage of the material lost. While a 5-micron loss of material would not be as noticeable in a laminate with significantly larger number of plies, the thin ply nature of the laminate used makes it a more significant factor.

While the thickness variation can be considered part of normal material variation, the ply orientation cannot. One would expect that the ply orientation of the fibers should vary slightly due to the nature of the hand lay-up. However, the fact that it was consistently off needed to be examined.

One of the things assumed about the carbon-fiber pre-preg sheets was that they were rectangular. This was based on the fact that the roll of pre-preg has a constant width, and all cuts were made parallel to the edge of the pre-preg roll. However, it was

found that the edges of the pre-preg sheets used in the lay-up of the composite do not always remain straight during construction, Figure 3.14. This was found to be a result of the material moving and being deformed or damaged as the plastic protective sheet was removed on the pre-preg.

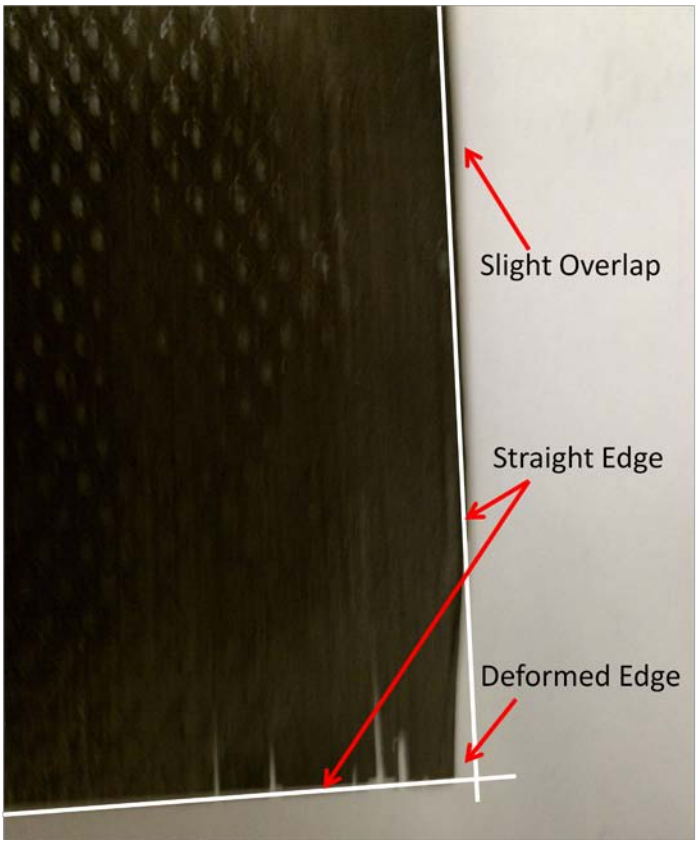

Figure 3.14: Image showing Deformation in Pre-Preg During Manufacturing.

Since the edges of the composite were no longer straight, the use of a straight edge no longer ensured that the angle of the fibers was aligned with the prescribed fiber orientation, Figure 3.15

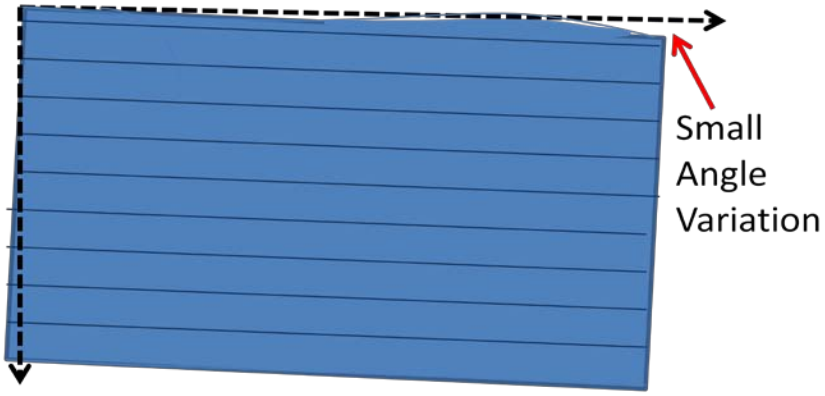

Figure 3.15: Small Angle Variation in Ply Due to Deformed Edge of Pre-Preg.

Such a deformation would not only have an effect as the pre-preg plies were stacked, but also as laminate was placed into the laser cutter. Any variation in the angle in which the composite was placed into the laser cutter would have an effect on the ply orientation by essentially "adding" the misaligned angle to the ply orientation of each layer of the composite, Figure 3.16. This angle, α, either can be caused by human error, or the deformed edge of the composite discussed above.

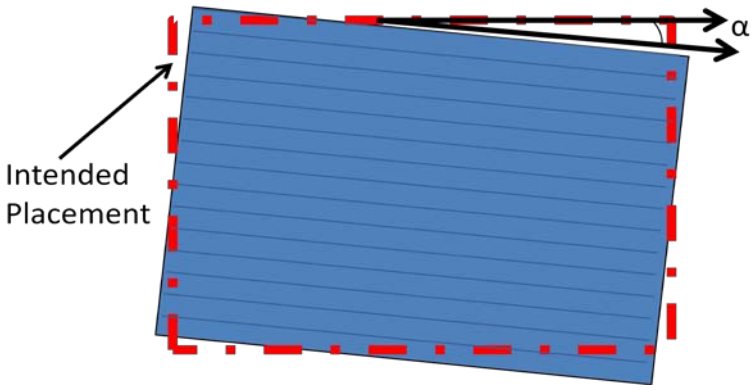

Figure 3.16: Error in the Placement of the Composite in the Laser Cutter.

3.5. Monte Carlo Validation

This following section shows an analytical validation of the experimental results. These results are important to show the range at which the variability found in the experiments can have on the effect of the material properties and modal frequency of carbon fiber specimens.

A Monte Carlo solution to determine how much variation in ply angle (theta) and laser cutter angle (alpha), and thickness would account for the differences seen in the experimental and analytical results. A Monte Carlo solution uses random variables, in this case using a Gaussian distribution of random variables, to vary results. The Gaussian distribution was used based on the measurements taken of the various variables. The Monte Carlo approach is used because it allows a quantification of the variable results seen, as well as to show the probability of results occurring.

Using the same FEA model developed in Section 3.2.1, the thickness of the specimen (Mean = 145 microns, & 1Std), the ply orientation (Mean = 2.5 deg, & 1 Std) and the cut angle (Mean = 2.5 deg, & 1 Std) were varied randomly using a Gaussian distribution. This solution was done using ABAQUS as a solver and developed MATLAB code, Appendix F, to set up and record the results of the Monte Carlo solution. The results of the analysis are shown in Figure 3.17, showing the first modal frequency for each of the runs in the Monte Carlo solution.

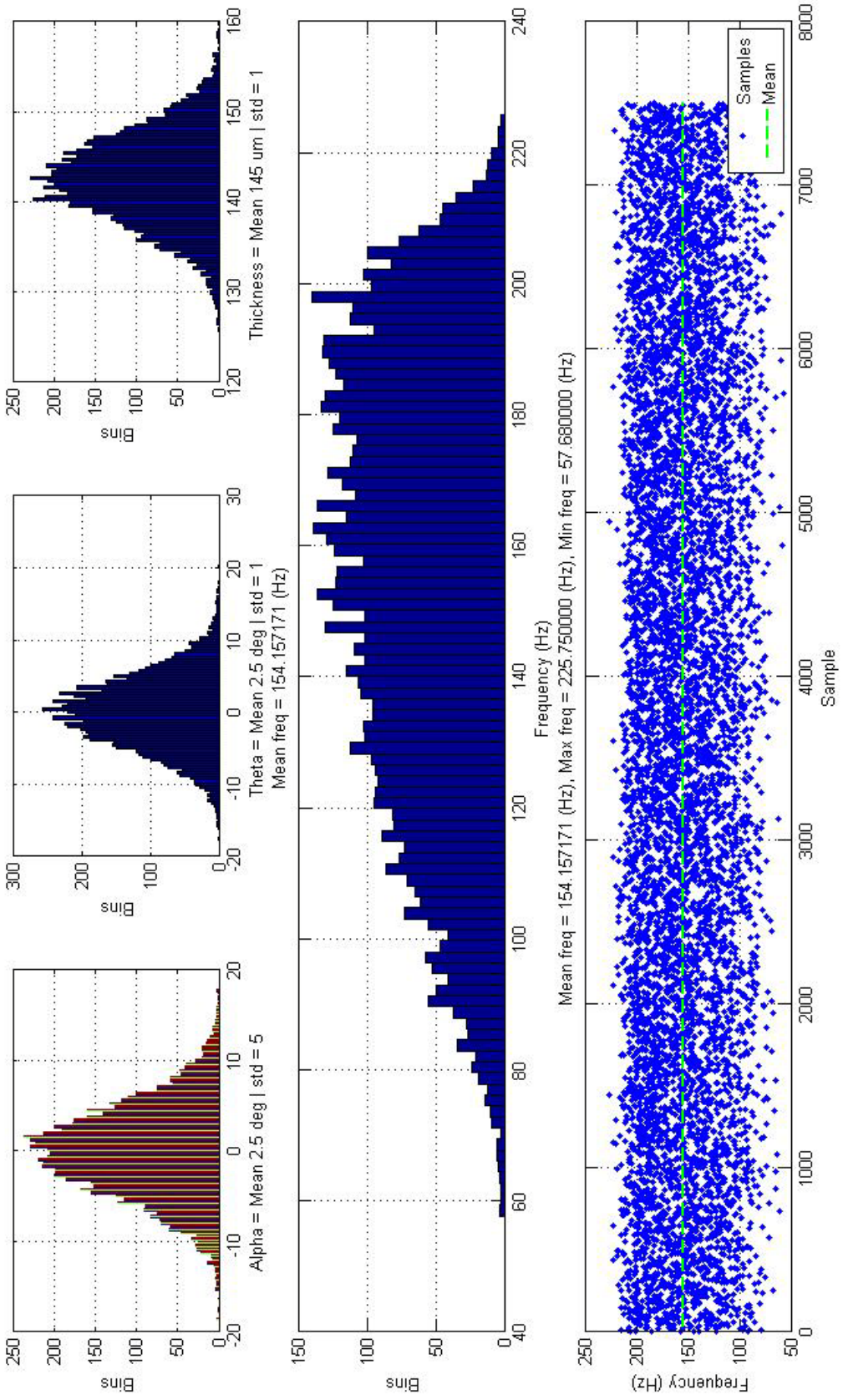

Figure 3.17: Results of Monte Carlo Solution.

Based on this approach, it can be seen that from the observed idiosyncrasies in the material, the low first modal frequency results from the laser testing can be explained. Taking into account all the idiosyncrasies, an average first modal response of the specimens tested in Section 3.1.1 is 154.16 Hz according to the Monte Carlo solution. Based on the distribution, the 144.89 Hz average can be explained as a highly probable, albeit slightly below average, solution.

3.6. Laminate Material Property Analysis Conclusions

Based on the experimentation results and the Monte Carlo analysis, it can be seen that the deviation in ply orientation, whether caused by hand lay-up or angle in which the carbon fiber was placed into the laser cutter, and the slightly smaller thickness were responsible for the results of the lower first mode frequency in the experimentation. This could lead the veins of the engineered wing to be less stiff than their design point, and should be taken into account when performing the analysis of the engineered wing. This also underscores the importance to have the FEA model easily changed so that the variability seen with the composite can be incorporated when comparing the results.

IV. Manufactured Wing Experimentation and Analysis Properties

The goal of this project was to analyze the manufactured engineered wing developed by O'Hara, Figure 4.1. The veins of the wing were constructed according to the method described in Section 2.1.1. The veins of the wing are cut out of a single sheet of [0/90/0] three-ply unidirectional carbon-fiber composite, based on the geometry of the Manduca Sexta, with a Kapton membrane.

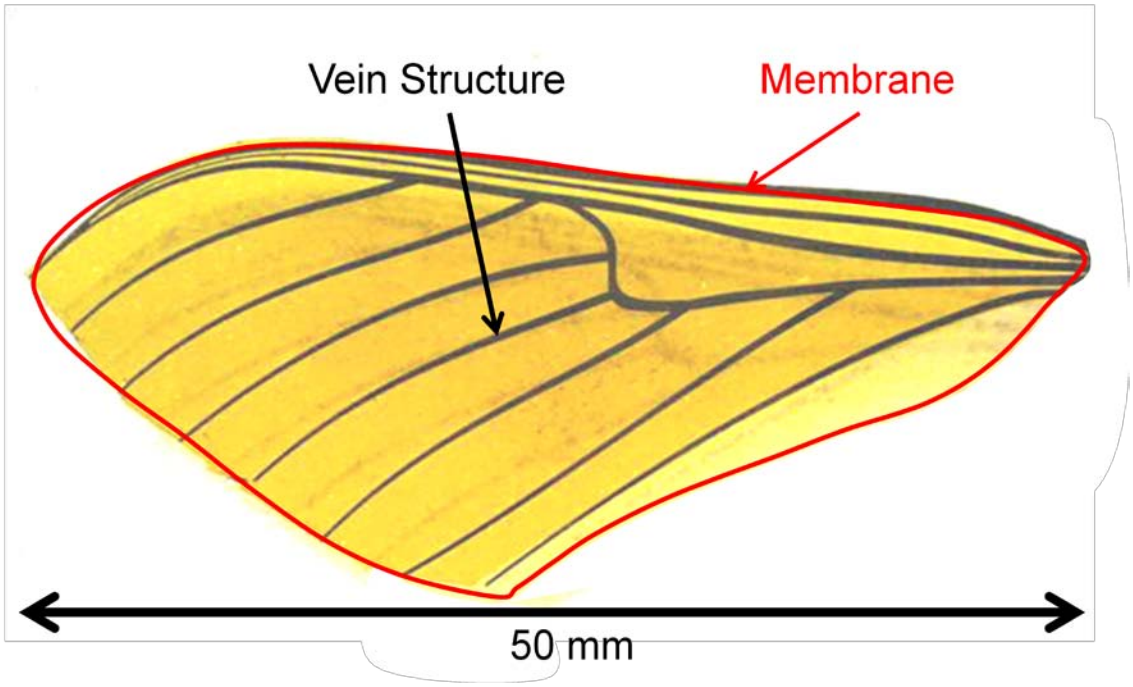

Figure 4.1: Completed Bio-Inspired Wing.

The model was created in order to take into account the effects of the carbon fiber composite's idiosyncrasies, allowing for the idiosyncrasies to be varied within the model, similar to the beam analysis performed in Section 3.5. Both analytical and experimental methods were used in order to evaluate the wing. The mode shapes and frequencies were used to compare the FEA model with the engineered wing. Norris determined that the ratio of the modal response of the wing was important in characterizing the wing's

stiffness [6]. Therefore, it was important the FEA model matched the modal frequency of the engineered wing. This chapter will cover the set up of the experimentation, the FEA model used in the analysis..

4.1. Engineered Wing Modal Frequency

DeLeon measured the modal shapes and frequencies of the engineered wing [2]. It is these experimental values for which the model was set up and compared against. For his experiment, the base of the wing was clamped, Figure 4.2, and attached to a Brüel & Kjœr Mini Shaker 4810 that would impart the vibrations into the wing.

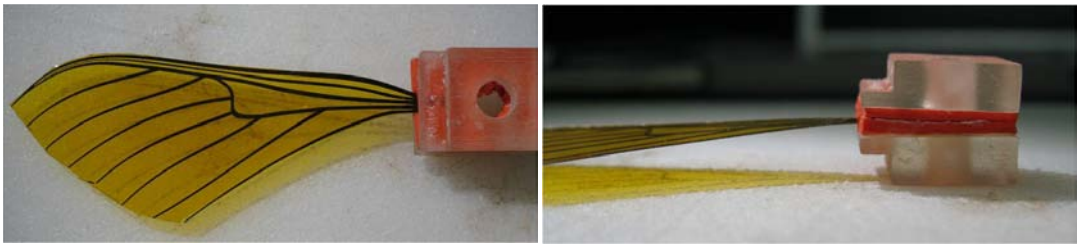

Figure 4.2: Clamped Wing.

The wing was placed into the vacuum chamber at AFIT, Figure 4.3, and attached to the shaker. A pseudo vacuum (less than 1% atmospheric pressure) was pulled, and the wing was shaken using a pseudo random input. The dynamic response of the wing was measured using a Polytec SLV. The SLV uses a laser to take precise distance measurements, and is capable of taking measurements along several points along the wing. When comparing these measurements to a reference point on the clamp of the wing and the pseudo random input of the vibrometer, the SLV is able to determine the modal frequencies and corresponding mode shapes.

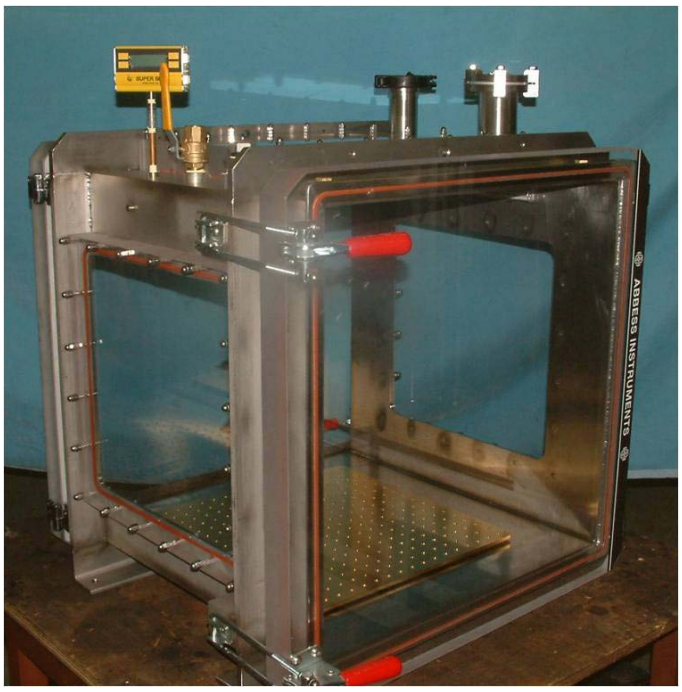

Figure 4.3: Vacuum Chamber used at AFIT.

Based on this experiment, DeLeon determined that the first and second modal frequencies of the engineered wing are 58.1 Hz and 80.3 Hz respectively. These values match the *flap*, and *feather* mode shapes determined by Norris, Figure 4.4. [6].

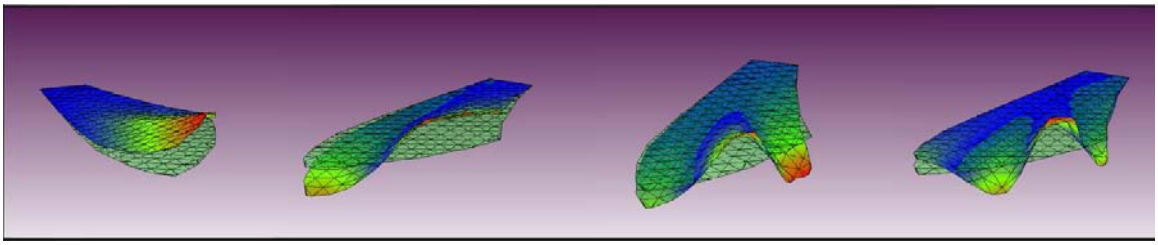

Figure 4.4: Mode Shapes of the Manduca Sexta Wing, *flap*, *feather*, *saddle*, and *bisaddle.*

4.2. Wing Model MATLAB Code

One of the main purposes of this project was to create an FEA model of the engineered wing. This model will allow for any changes in material or dimensional properties of the wing to be evaluated prior to physical fabrication, saving both time and money in the creation of a viable FMAV. Due to the complex nature caused by the orientation of the fibers, and the curvature of the veins, Figure 4.5, the model was developed using a developed MATLAB code to generate an FEA input file that could be solved in ABAQUS. This developed code made it easier to assign individual elements on the vein correct material properties based on the curvature.

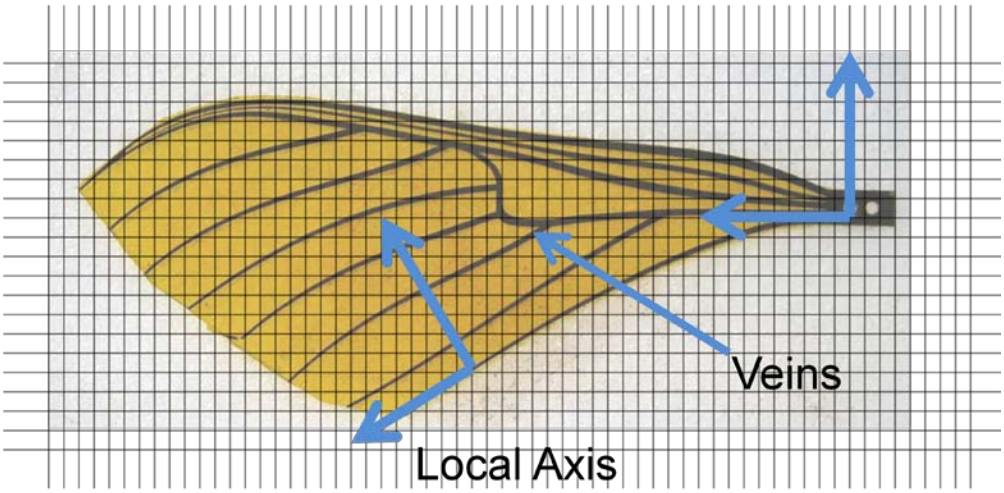

Figure 4.5: Diagram Showing Fiber Orientation over the Vein Curvature.

This model will also serve to evaluate the effects of the carbon fiber manufacturing idiosyncrasies, and how they affect the modal frequencies of the engineered wing. Therefore, a code that varied the idiosyncrasies seen within the carbon fiber composite was set up and an analysis was performed on the wing model. In order for this approach to be utilized, the model needs to be easily modified to account for the varying composite material properties. Therefore, a MATLAB code was developed,

Appendix G, so that multiple input files can be created to reflect such varying manufactured variations. These input files were solved using ABAQUS, with the results of the code being read by the developed MATLAB code to collect data for analysis. This section will serve to explain the creation and capabilities of the code used to generate the FEA models. The flowchart below, Figure 4.6, shows the general process performed in the creation and analysis of the FEA model.

Furthermore, since the experimental modal results of the engineered wing did not match the results of the biological wing, the model was made to be easily modified. This would allow for future work done on the design of the engineered wing to be easily incorporated into the model. The model has the ability for the composite ply orientation, thickness of the plies, number of plies and width of the veins to easily be changed. Also, since the geometry is based on a separate file, the geometry of the wing can easily be changed in order to incorporate camber or other changes of geometry compared with using ABAQUS' CAD program. This will be important for future work done on the wing.

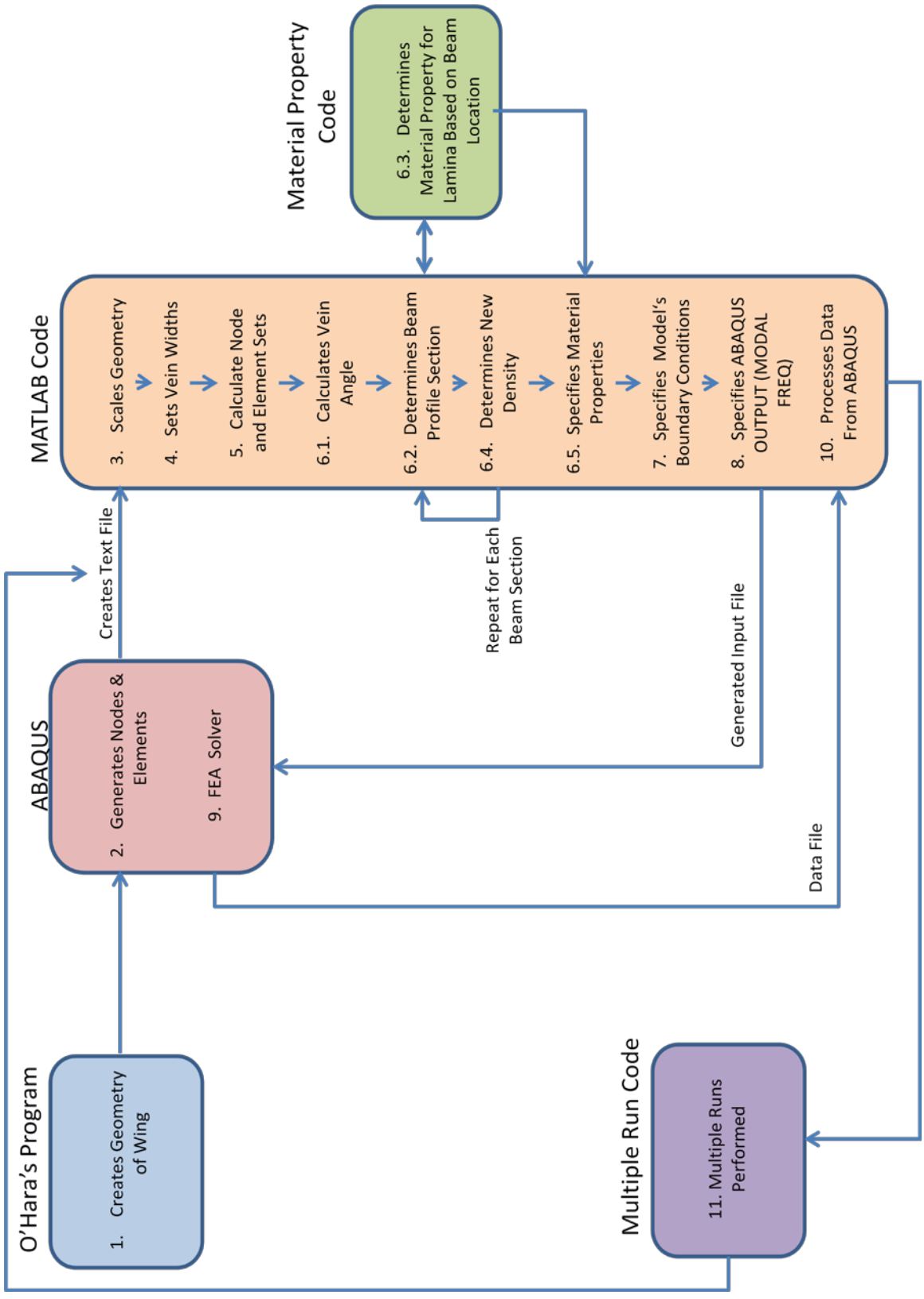

Figure 4.6: Flowchart showing the Process of Generating the Wing FEA Model.

4.2.1. Creating the Geometry of the Wing

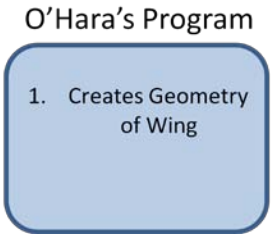

The geometry of the wing was created in MATLAB using a code developed by O'Hara [1]. The code bases the geometry of the wing on an image taken vertically above a Manduca Sexta wing laid on a flat surface. The user then defines the points along the individual veins, which are then splined to form a curve that matches the geometry of the vein, Figure 4.7, shown in blue.

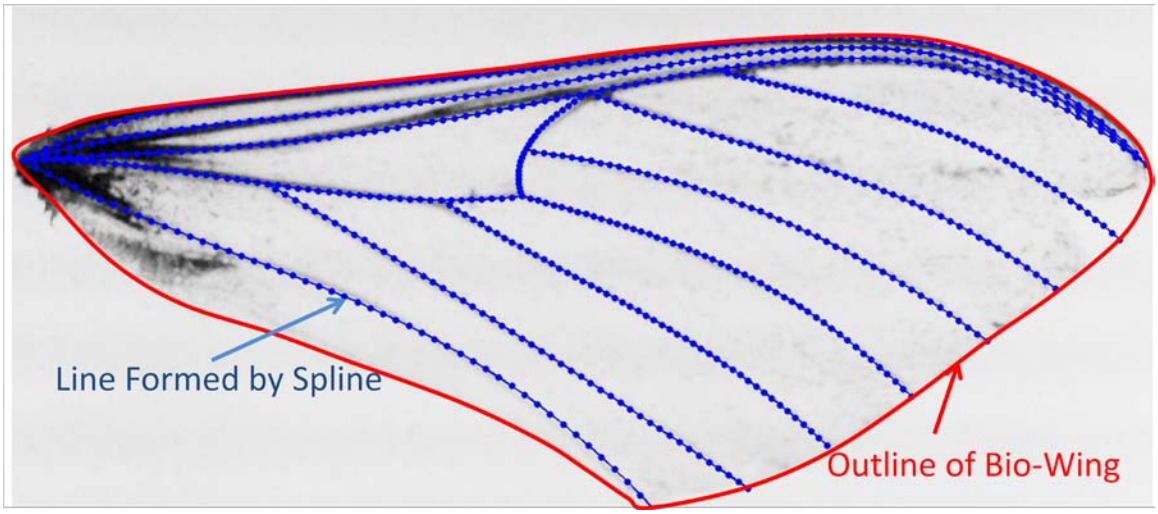

Figure 4.7: Bio-wing with Selected Points, Creating the Basis for the Vein and Membrane Nodes for the Engineered Wing Model.

Points along the edge of the membrane are then selected, Figure 4.7 (shown in red). The program then creates another splined line along the outline of the membrane. Using the points created along the lines for the veins, and the membrane, various sections of membrane were created that could easily be transformed by ABAQUS into nodes and

elements, Figure 4.8. The generation of the nodes and elements will be explained in Section 4.2.2. The geometry was visually compared to the engineered wing before proceeding with the analysis in order to ensure the dimensions matched.

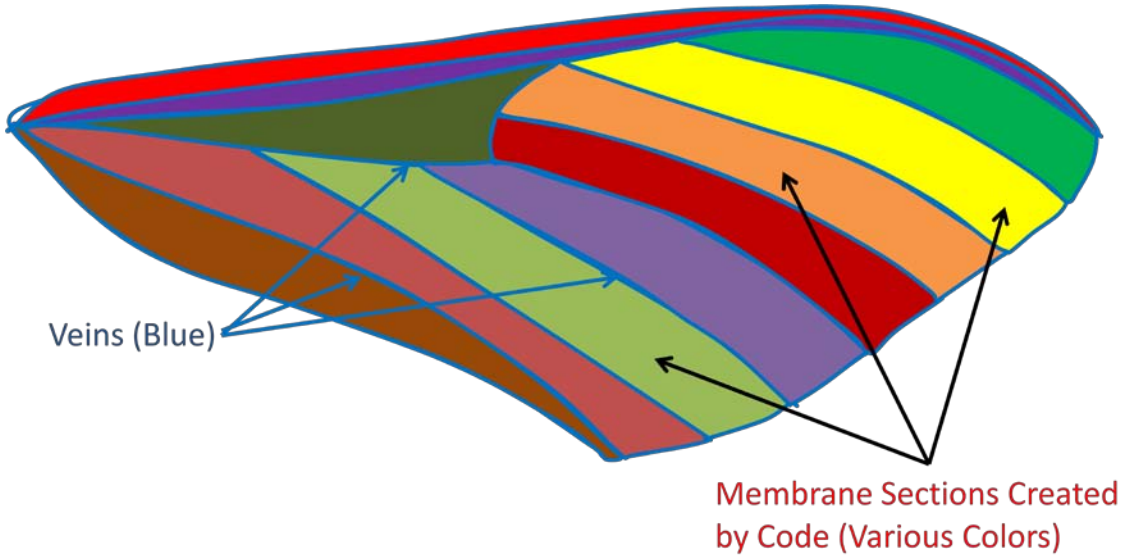

Figure 4.8: Diagram showing membrane sections of the wing.

4.2.2. Generate Nodes & Elements

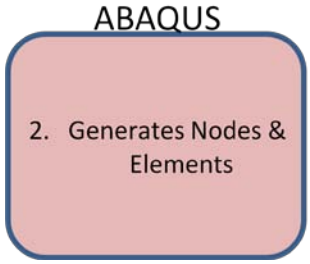

The lines representing the veins and membrane are then imported into ABAQUS, using a Python script. This automatically creates points with X and Y coordinates along the path of the lines created with O'Hara's program, with the Z coordinates all being zero due to the fact that the wing is made using a flat plate. These points will serve as the location for the nodes within the model. A total of 22,248 nodes were created for the

model. Common nodes were created along the veins which were used for both the veins and the membrane. This was done to mimic the fact that the membrane was physically attached to the veins using adhesive.

Elements are used to tie the nodes of the model together. The type of element used affects how the stiffness matrix, K, of the model is set up. For this project, quadratic beam elements, B32, were used for the veins, and eight node shell, S8R, and six-node shell, STRI65, elements were used for the membrane.

The B32 element is a 3-node quadratic, 1-D beam element in space, Figure 4.9 [22]. The element uses parabolic interpolation, with 6 DOF, 3 translation, about the X,Y and Z axis, and 3 rotation, about the X,Y,Z axis. This Timoshenko beam element was chosen based on its ability to predict bending displacements compared to other beam elements [22].

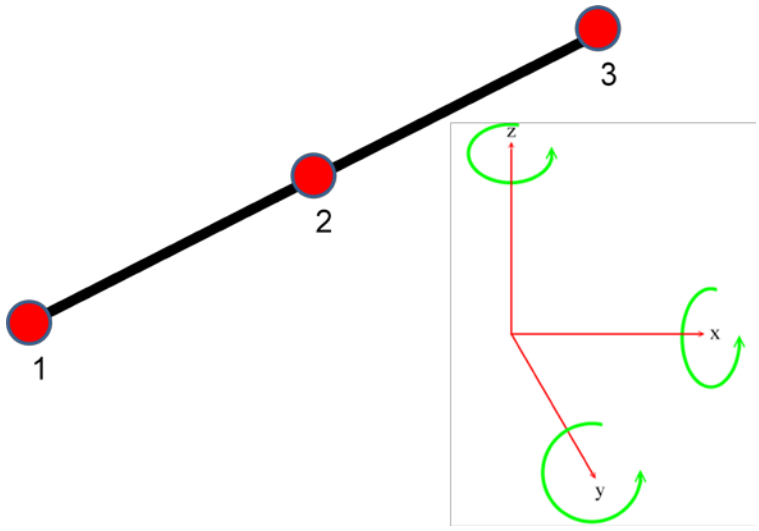

Figure 4.9: B32 Element, Showing 6 DOF.

The S8R shell element is an 8-node doubly curved shell element with reduced integration, Figure 4.10. The element also has 6 DOF per node (3 translation, 3 rotation).

This element was chosen based on previous experience of its ability to model the membrane material. The S8R element does not have the ability to deviate too much from its square shape [23], and for certain cases, which will be explained later, triangular elements were used.

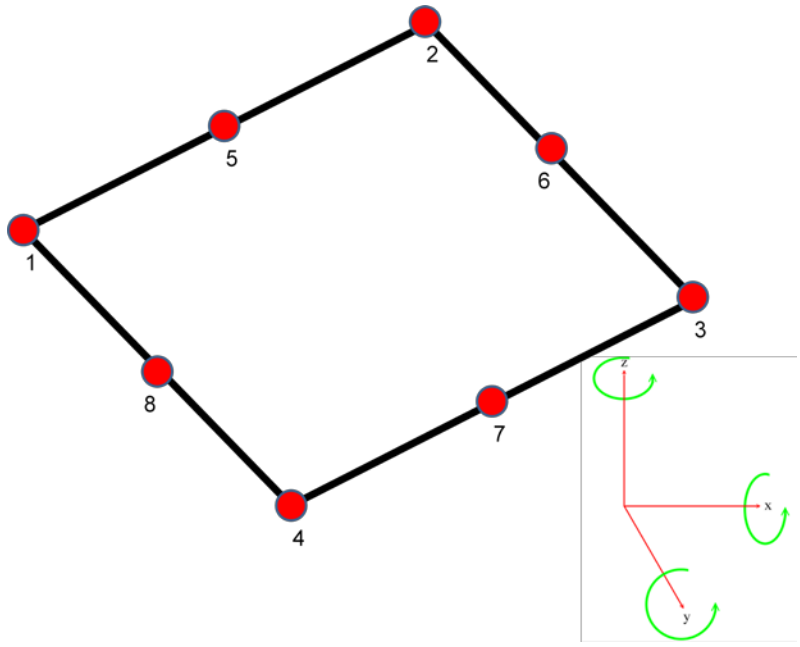

Figure 4.10: S8R Element, Showing 6 DOF.

The final element chosen was the STRI65 element. The STRI65 element is a 6-node element, with 6 degrees of freedom when attached to 6 DOF nodes on certain elements (such as S8R), and 5 DOF in free space, or at boundary conditions, Figure 4.11 [23]. Since all the STRI65 elements in the model are attached to S8R elements, 6DOF exist. Unlike the S8R element, this element does not have the ability to change thickness, and therefore should only be used for thin membranes. Since the membrane of the wing is thin, 20 microns, relative to the chordwise direction, 50,000 microns (50mm), this was an acceptable limitation. This element was also chosen based on its ability to better model certain areas within the geometry due to angle constraints.

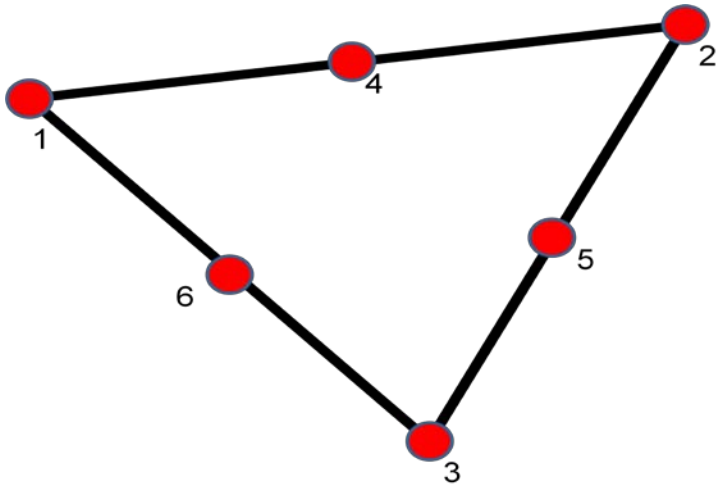

Figure 4.11: STRI65 Element.

The elements were assigned to the nodes using a build in ABAQUS feature, where the user would select the geometry, either the veins or the membrane, and assign either the beam or the plate elements. ABAQUS used both triangular and quadrahedral elements for the membrane due to the angle restraints placed on the quadrahedral shell elements. Figure 4.12 shows shell elements where the quadrilateral formed by the nodes has interior angles that are within acceptable limits, and exceed acceptable limits (greater than 145°, less than 45°) where a triangular element would be used instead.

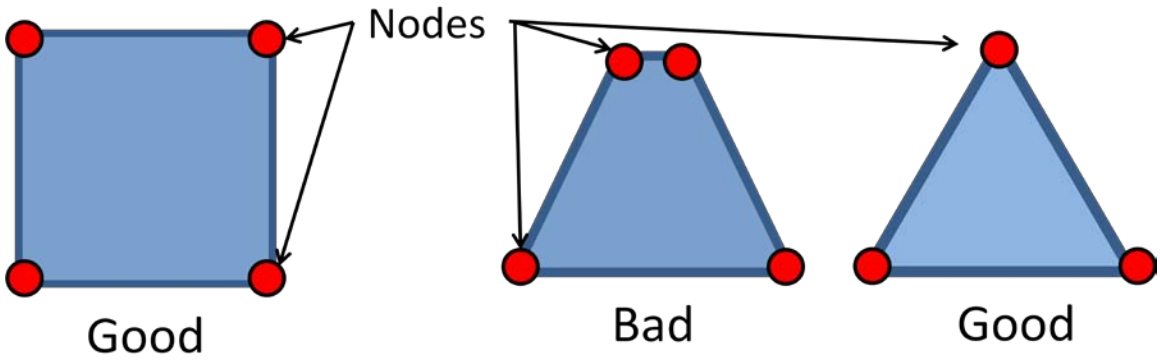

Figure 4.12: S8R and STRI65 Elements..

The vein structure of the wing was modeled using quadratic beam elements, (B32 elements in ABAQUS). These elements represented the thin, slender shape of the veins as was evident from the material property evaluation in Chapter III. They also had the advantage over the use of shell elements in that they could be easily modified. Unlike shell elements, the width of veins could be changed easily without worrying about the geometric considerations of the four-node elements, such as the angle formed between each node to form the element, Figure 4.13. This figure shows shell elements where the quadrilateral formed by the nodes has interior angles that are within acceptable limits, and exceed acceptable limits (greater than 135°, or less than 45°).

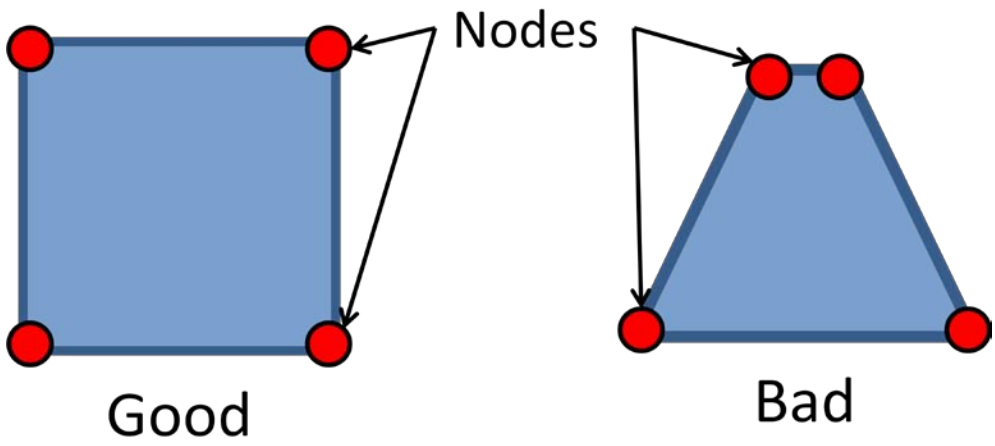

Figure 4.13: Figure Showing both Good and Bad Placement of Nodes for Shell Elements.

If the geometry of the wing were to be changed for future iterations, then the shell elements would have to be checked to ensure that they all fall within acceptable limitations. This is something that would not have to be done to the beam elements due to the fact that the nodes are placed in a straight line for each element. The width of the element is assigned via a beam section profile. The profile section affects the stiffness matrix of the model, however unlike the shell element, the geometric coordinates of the

nodes and elements in the model will not change, Figure 4.14. While it would be possible to check the placement of the nodes in the shell element prior, it would be time intensive and provide no significant advantage versus using beam elements that have already proven their effectiveness.

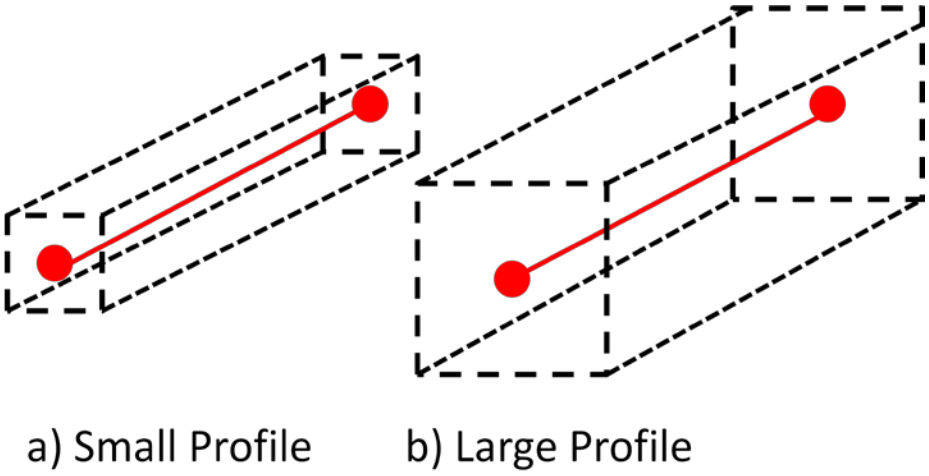

Figure 4.14: Element with Two Different Profiles. Notice Actual Element and Nodes Remain Unchanged.

1,093 B32 elements were created. This large number of nodes was necessary in order to ensure that angle between each beam element was small. This was done in order to better capture the curved geometry of the wing, as well as the material properties, which as shown previously are highly sensitive to changes in ply orientation. 1.093 is the minimum number of elements that will keep the angle between each beam element less than one degree, except for where the Arculus and Cubitus veins meet (see Section 4.2.4.).

7,183 S8R elements and 175 STRI65 elements were used. The high number was necessary to ensure that the membrane could be fixed to the veins in the model, i.e. have common nodes for the beam and the membrane. Figure 4.15 shows a complete image of the wing showing the elements used.

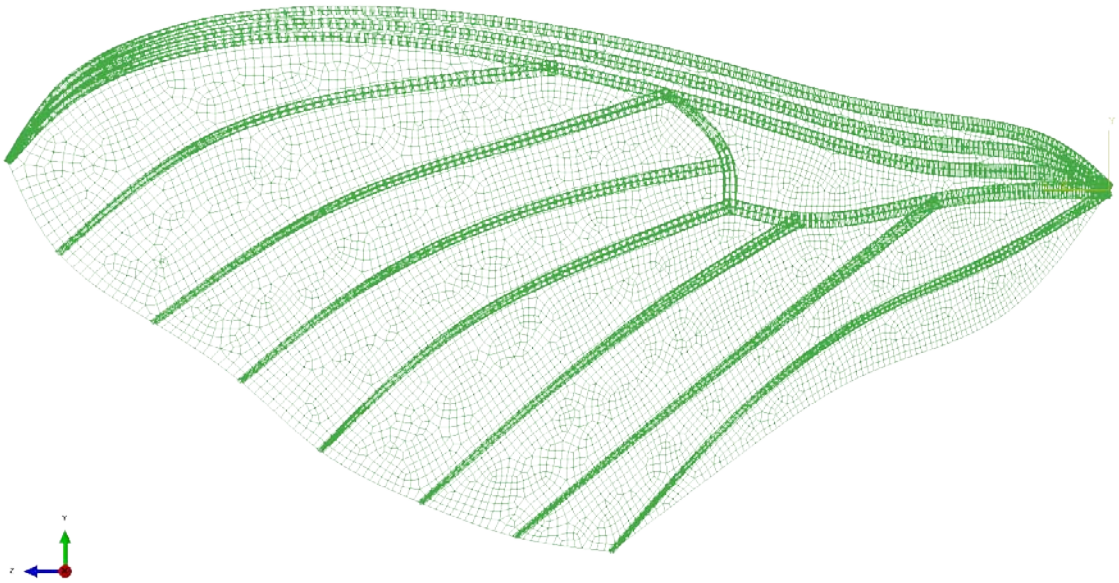

Figure 4.15: Wing Model Showing Elements.

4.2.3. Scale Geometry

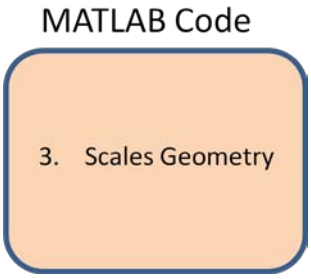

Since the geometry in O'Hara's program is outputted in inches, the scale of the geometry needs to be changed. This is done with the wing model MATLAB code. The code determines the length of the wing based on the X,Y, and Z coordinates, and then scales the model to the desired size, in this case 50mm. This is important because incorrect geometry can have a significant effect on the modal frequency analysis.

In addition, for the sake of simplicity, the model was shifted so that every node has a positive X coordinate. This was done in order to simplify calculations done later in

the program dealing with the beam vein element orientation angles and material properties.

4.2.4. Vein Width

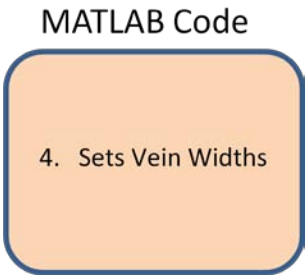

The widths of the individual veins of the manufactured wing were varied linearly from root to tip of the individual vein. This was done as an approximation based on the actual Manduca Sexta wing in order to match the material properties. Figure 4.16 shows the venation patter of the Manduca Sexta wing. This can be compared to the geometry selected for the engineered wing, Figure 4.17, shown in blue. In order to simplify the geometry in the engineered wing, the veins R1, R2, R3 and R4, and A1 were modeled as one vein.

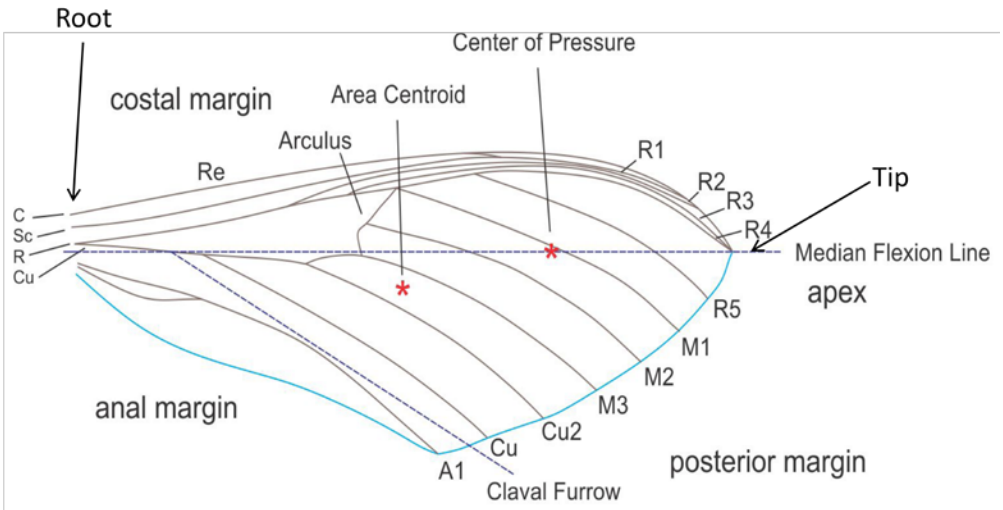

Figure 4.16: Venation Pattern of the Manduca Sexta.

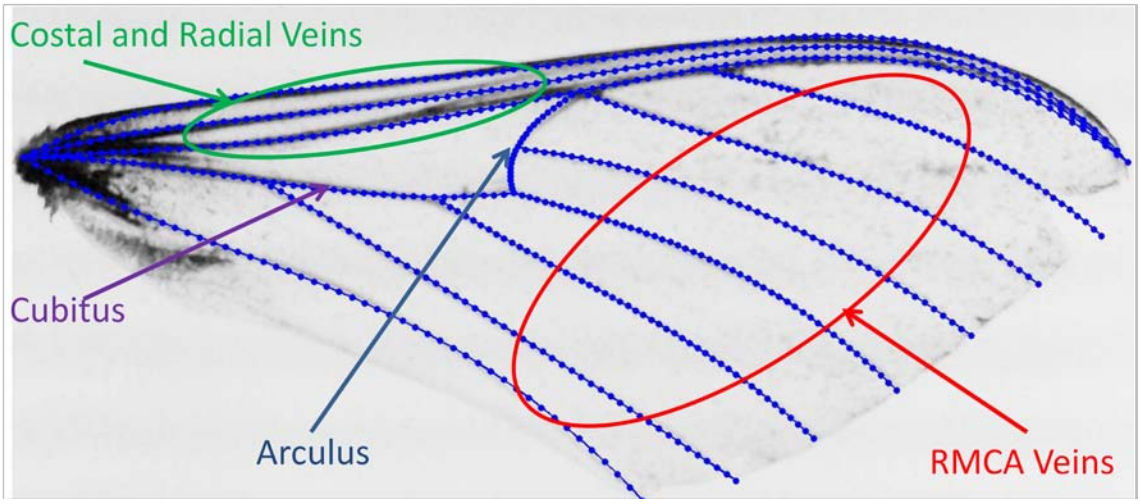

Figure 4.17: Venation Pattern of the Engineered Wing.

The dimensions of the veins were based on the engineered wing. In the sizing of the engineered wing, the width of the veins were varied linearly from the root of the vein to the tip. For manufacturing simplicity, the Costal and Radial veins on the leading edge

of the wing were combined into three veins, and given the same root and tip dimensions, Figure 4.17. Also, the Anal vein, the Medial veins, and two of the Cubitus veins were grouped (Figure 4.17) and given the same dimensions at the root and tip of the veins. The Cubitus vein along the Medial Flexion Line (Figure 4.16 and Figure 4.17), and the Arculus were given unique dimensions.

Each B32 element in the above stated sets of veins was assigned the same width for the root and tip. Since each beam element must maintain a constant width, the value for the width of the beam element was determined based on the location of the mid-node. This resulted in a gradually decreasing beam cross section, Figure 4.18.

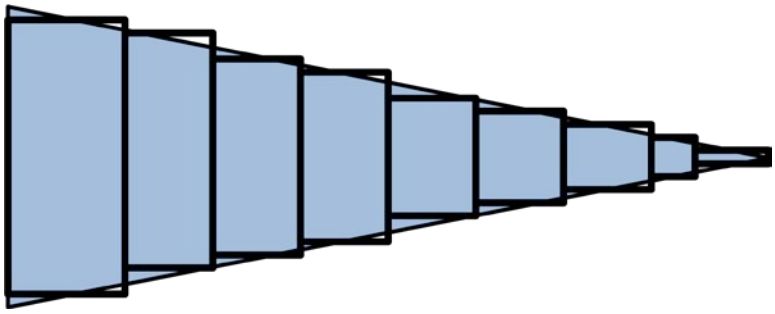

Figure 4.18: Beam Element Width for a Tapered Beam.

4.2.5. Node and Element Sets

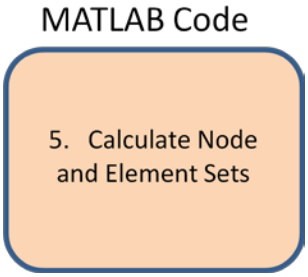

Node sets are sets of nodes that either are assigned a boundary condition, or are assigned to elements that are part of the same element set. Element sets are sets of elements that share that same material property and section property. All nodes and

elements in the model must be assigned to a node set and an element set in order to be considered in the stiffness matrix when solving the model. It is important to note that this is not where any properties are assigned to the nodes or elements, rather the nodes and elements are just being sorted into groups to be assigned those properties later in the code.

Assigning the nodes and elements to the various node and element sets was done in the wing model MATLAB code. In the case of this model, the nodes that make up each beam element need to be placed in their individual node set. This is because as the curvature of the beam changes, so do the material properties, and beam profile, See Section 4.2.7. This resulted in 1,093 different node sets being created to account for the beam elements. Three more sets were created, one for the S8R elements, one for the STRI65 elements, and another for the boundary condition. This resulted in a total of 1,096 node sets. Only 1,095 element sets were created due to the fact that the boundary condition is only applied to nodes, and not element. Therefore, there was no need to create an element set for the boundary conditions.

4.2.6. Determine Material and Profile Properties

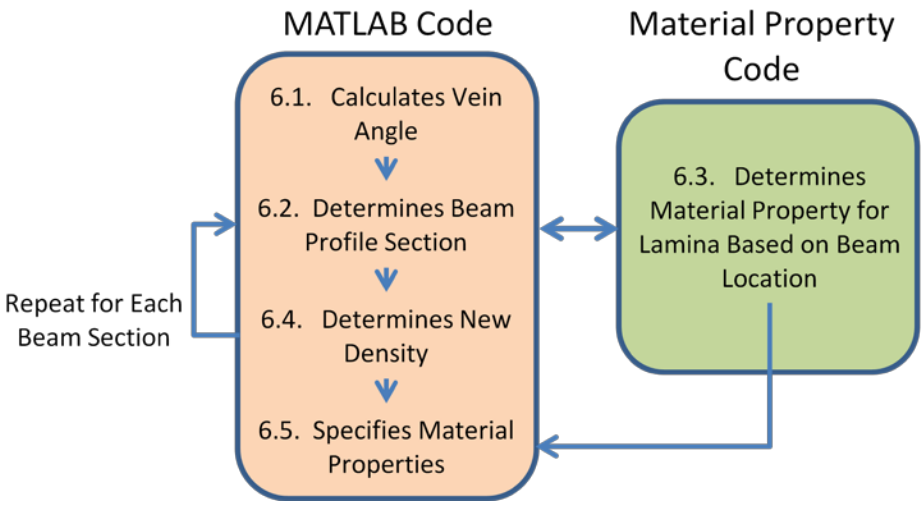

The material properties, and profile section of the elements of the model play an important part in determining the stiffness of the model. These properties need to be defined for every element in the model in order to form the stiffness matrix, K. Since the Kapton membrane is an isotropic material, all the shell elements representing the membrane can share the same material property and profile section. However, due to the changing local axis of the material due to the curvature of the veins, Figure 4.19, each B32 element required its own unique material property and beam section based on the ply orientation at the local axis. This section will discuss the process used to determine and assign the section properties and material properties for each set of elements created in the previous section.

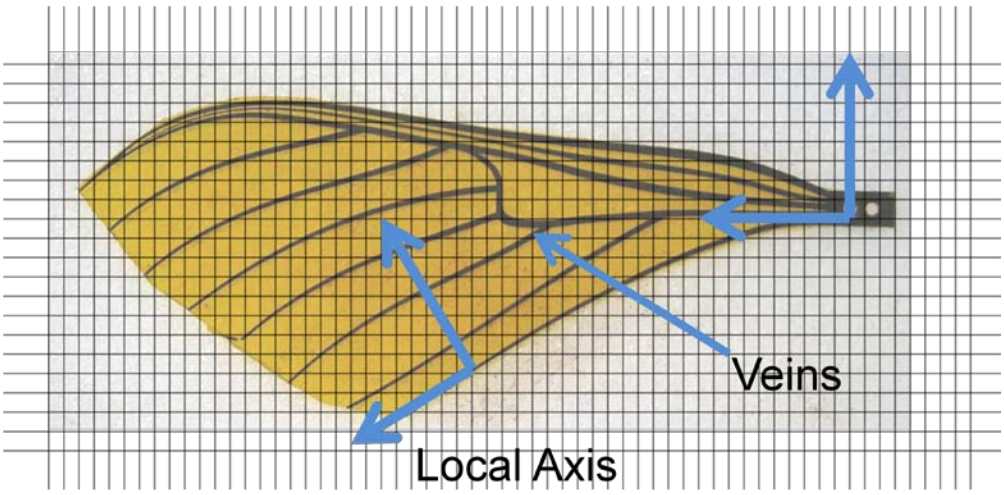

Figure 4.19: The Engineered Wing Showing the Directions of the Composite Fibers.

Kapton's properties, Table 4.1, were applied to all shell S8R and STRI65 elements using a single set of material properties.

Table 4.1: Kapton's Material Properties

Material Properties, Kapton	
Modulus	2.5 G Pa
Density	1.42 g/cc
Poisson's Ratio	0.3
Thickness	20 microns

The application of the beam, B32 elements properties required more effort due to the anisotropic nature of the material. Since the material property varied based on the ply angle, the local axis needed to be determined. Therefore, based on the coordinate location of the two end nodes in each element, the angle, which the element made in relation to the global axis, was determined in the MATLAB code using trigonometry. This was done in order to create a homogeneous beam, which could more easily be modified than the ABAQUS composite shell element, especially when changing the

physical width of the veins. This avoided problems with shell element nodal angles as described in Section 4.2.2.

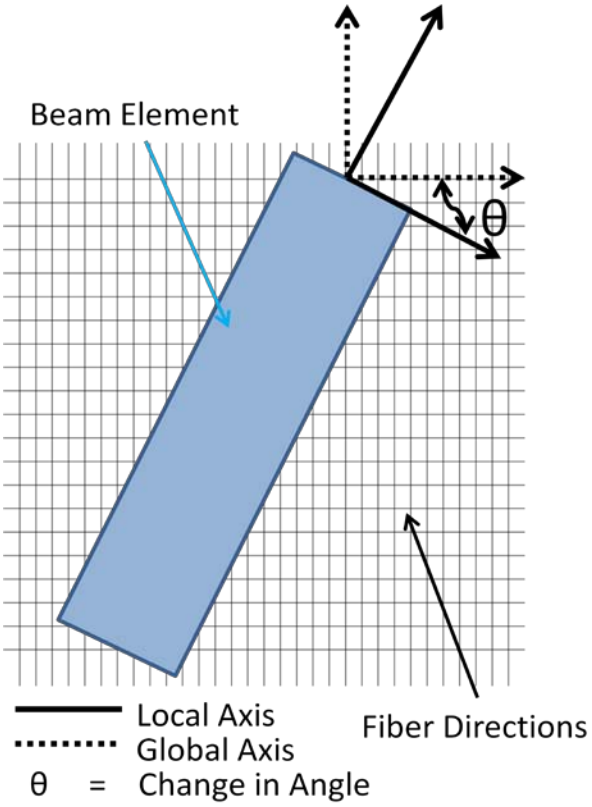

Figure 4.20: Difference betweeen the Global and Local Axis for the Beam Element.

Once the angle for each element has been determined, the local axis for the material can be determined. This is done by subtracting the difference between the angle formed between the local and the global axis. This was done for each ply angle in the [0/90/0] composite and resulted in the ply orientation angle for each lamina. This information was necessary in order to determine the material properties of the composite for the element.

After the local ply orientation for the element was determine, the local material properties were determined, based on Equation 2.1 in Section 2.3, using a material

property MATLAB function, Appendix B. This code determined the local lamina properties, which would be used during the generation of the beam profile cross section.

In order to account for the differences in the modulus for the individual lamina, the effective moment of inertia of the element needed to be determined. The MATLAB code then performed the effective moment of inertia calculations described in Section 2.5.2., Figure 4.21. The width of the vein was determined based on the input given in Section 4.2.4. In order to keep the vein visualization in ABAQUS consistent with the physical widths of the veins at each element location, the largest modulus, E_x, calculated amongst the three plies was used to determine the effective width of the other two plies.

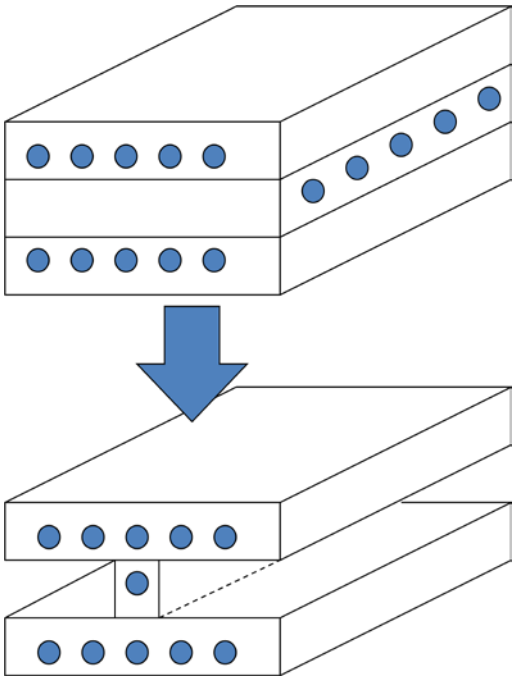

Figure 4.21: Effective Moment of Inertia Transformation for the Vein B32 Profile.

This method of transformation was only applicable as long as effective width of the top on bottom lamina was greater than ½ the effective width of the middle lamina, See Figure 4.22. ABAQUS was unable to perform the calculations on profile sections

that exceeded this criterion because it is incapable of solving means where the moment of inertia in the 2 direction is larger than the moment of inertia in the 1 direction.

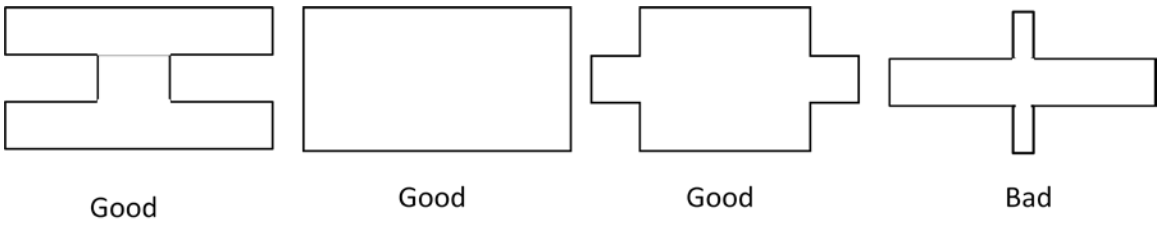

Figure 4. 22: Effective Moment of Inertia Profile Sections.

Six elements in the original model failed this criterion, all of which were in the Arculus where the angle of the beam element approaches 90° from the global coordinates. In order to deal with these six elements, a check was put in the code that would transform bad elements into rectangular beams with the same profile cross sectional area, Figure 4.23. Since this was only done in for six of the 1,093 beam elements, the effect in the modal frequency was assumed to be negligible.

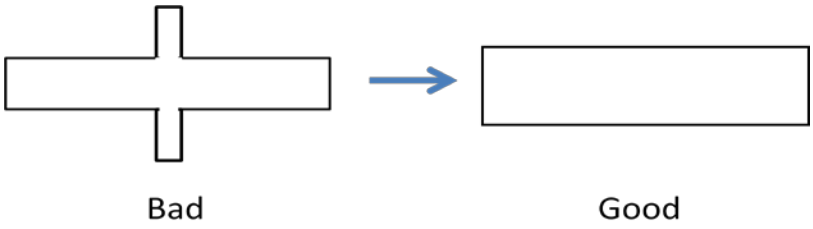

Figure 4.23: Changing of Cross Sectional Profile for Beam Profiles at Angles Close to 90°.

As the profiles were formed, the material properties of the largest modulus, were recorded and placed into the input file as material properties. A total of 1,093 material properties were calculated, one for each beam element. These properties were recorded with the material property for the Kapton in the generated input file. Figure 4.24 shows an up-close view of a vein and the vein profile used in the wing.

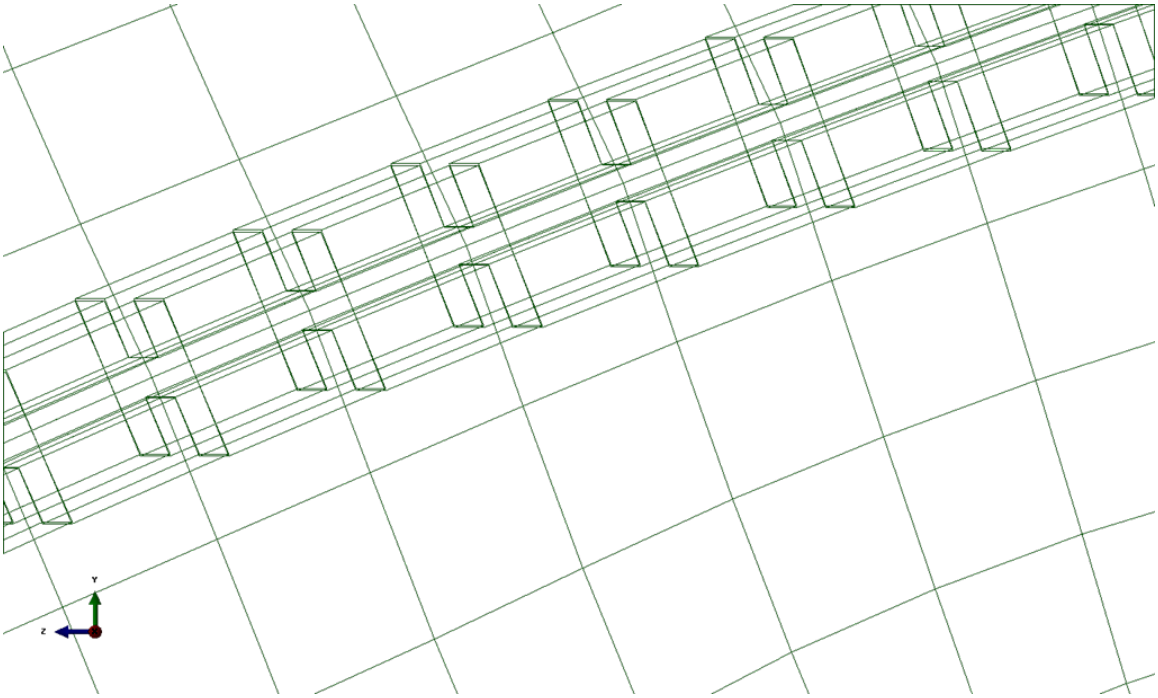

Figure 4.24: Wing Model Elements Zoom-in View, Showing Elements and Beam Profile.

4.2.7. Boundary Conditions

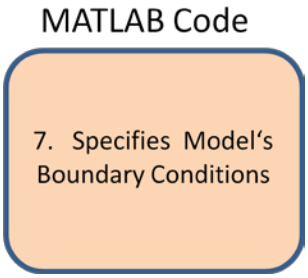

A boundary condition in finite element method is used to limit the degrees of freedom of each node. In the case of the project, the boundary condition present was the clamped base of the wing, Figure 4.25. For this, a node set was creating that included 6 nodes at the base of the model that were limited to 0 degrees of freedom, i.e. no translation or rotation. Figure 4.26 shows the location of the clamped nodes on the FEA model.

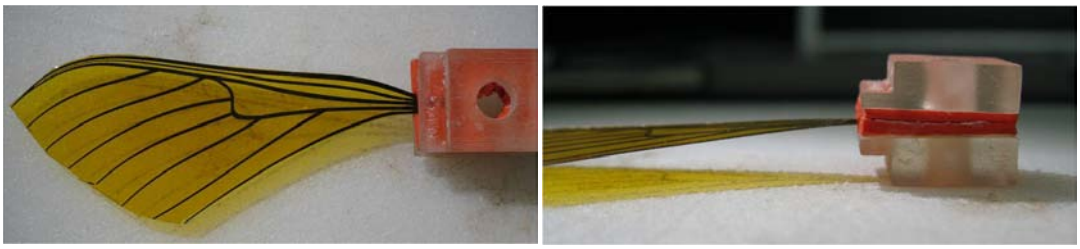

Figure 4.25: Clamped Base of the wing.

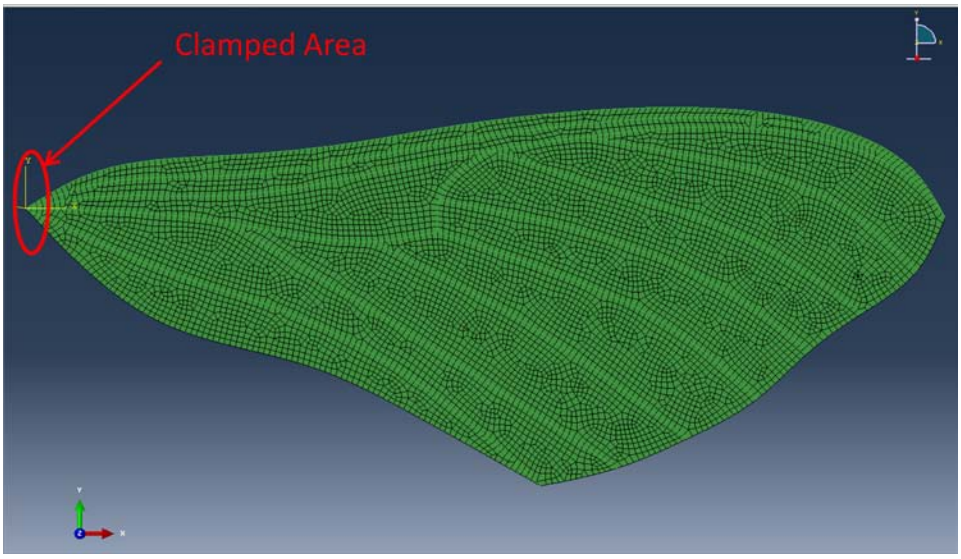

Figure 4.26: Wing Model Showing Clamped Area.

4.2.8. Output Requests

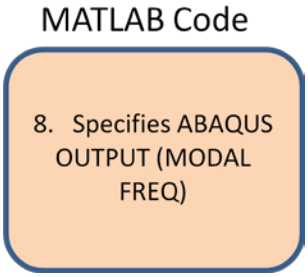

A step module in ABAQUS define the type of analysis that will be performed on the model. A step also defines any loads and boundary conditions that will be performed in the analysis. For the case of this project, the clamped boundary condition described in Section 4.2.7. was applied. A step was created in order to solve the modal frequency of

the model. The first 10 modes of the model were solved for in the solution. No loads were applied due to the nature of modal frequency analysis.

4.2.9. Processing Data

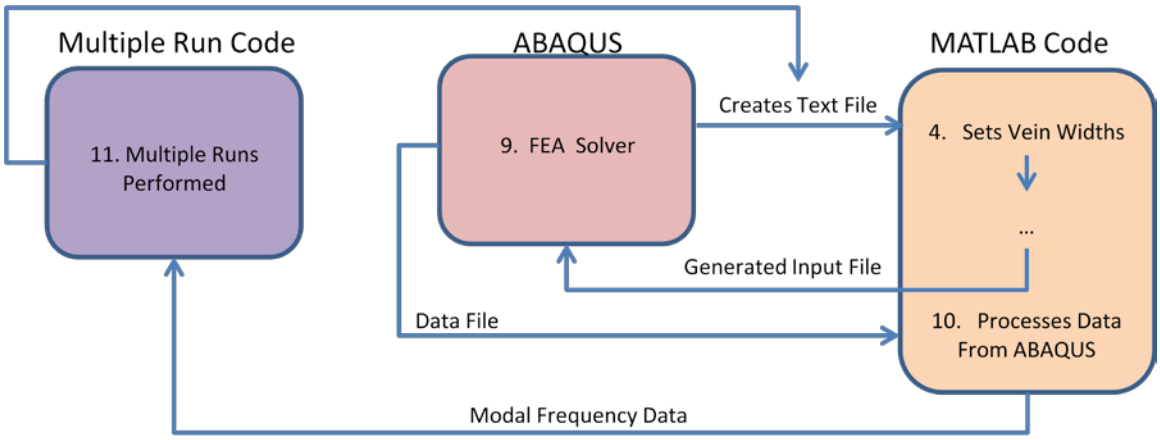

Once this step is complete, the creation of the model is complete, and it is ready to be solved. The MATLAB code develops an input file, Appendix H, based on the conditions specified in this chapter. Figure 4.27 shows a completed model of the wing with the elements shown. The beam profiles are displayed and shown in green, with the membrane being displayed in white. The input file needed to be solved using a finite element solver, and multiple runs needed to be conducted to determine the effect of the carbon fiber idiosyncrasies on the modal frequencies of the wing will be discussed.

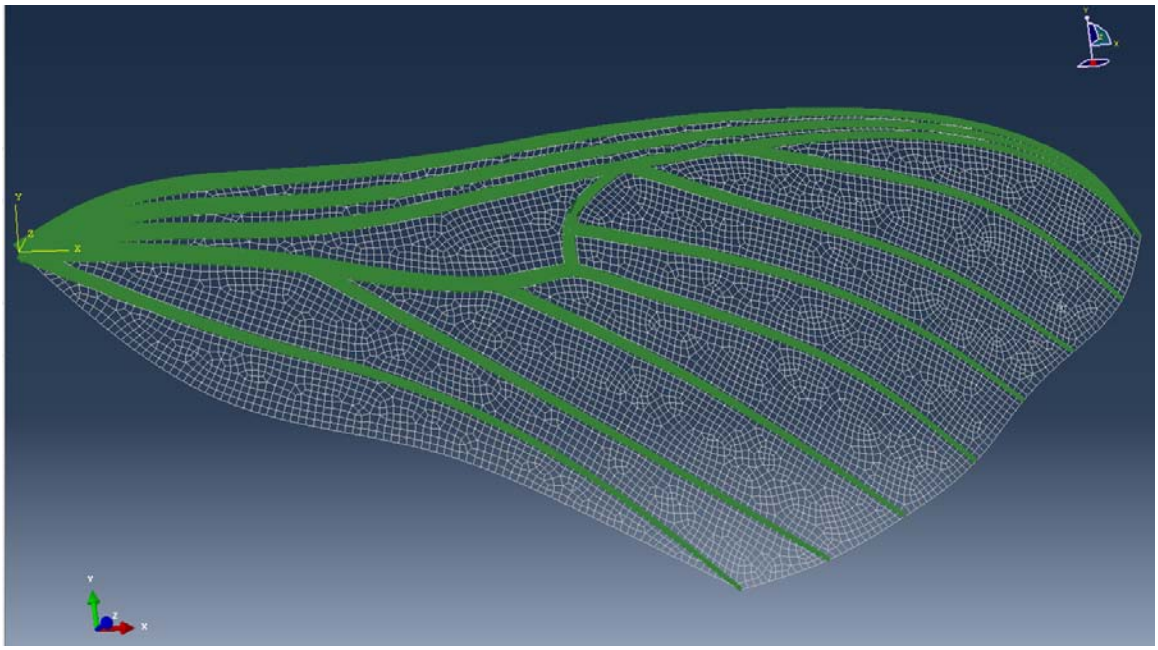

Figure 4.27: Final Model of the Wing with Beam Elements Highlighted(Green).

ABAQUS was used in order to solve the developed model. This was done automatically using MATLAB commands, without manually importing the file into ABAQUS CAE itself:

(`eval(['dos(''abq6111 job=' Input_File ' interactive'')']))`. (Note, the .inp file must be stored in the open MATLAB directory).

ABAQUS creates a data file with the outputs, eigenvalues and eigenvectors, specified in Section 4.2.8. The data file is a text file, and is read by the MATLAB code, which stores the values for the first two modes, which were visually determined to be the *flap* and *feather* modes, in a matrix to be graphed and analyzed.

The Multiple Run Code code was developed, Appendix I, in order to submit variable runs to ABAUS in order to determine the effects of the carbon fiber idiosyncrasies on the wing. As with the beam, it varied the thickness, the ply orientation and the cut angle of the vein structure of the wing. However, due to the time constraints

and the significantly longer run time for the wing analysis as opposed to the beam, a full Monte Carlo solution was deemed unrealistic, as it would have taken months to complete the number of runs required for a full solution. Instead, the effects of the individual variables, thickness, laser cut angle, and ply orientation were varied to determine the probable range of modal frequencies that the wing could experience.

V. Manufactured Wing Analysis Results and Discussion

The goal of this chapter is to discuss and evaluate the results of the experimentations performed on the engineered wing in Chapter 4. The results will first cover an ideal solution that does not take into account any variations in the composite material discussed in Chapter 3, and second, multiple runs of the FEA analysis were performed where the effects of the variable factors, thickness, theta orientation, θ, and placement in the laser cutter, α, were tested independently in order to compare their effects on the first and second modal frequencies of the model. Finally using the information, the experimental modal frequencies determined were matched based on observed idiosyncrasies in the composite material.

5.1. Ideal Engineered Wing

The first model solved was of the ideal engineered wing. This FEA model did not take any of the variations observed in Chapter 3 into account, and represents the engineered wing as designed. The carbon composite in the model was set to a ply orientation of [0 /90/0], with a cut angle, α, of 0°, and a thickness of 150 microns. The calculated mass of the model is shown in Table 5.1. The modal frequencies of the first four mode shapes are listed in Table 5.2.

Table 5. 1: Calculated Mass of the Ideal Engineered Wing.

Mass of the Wing			
	FEA	*Experimental*	*Difference*
Mass	51.3 mg	52.5 mg	2.3%

Table 5.2: Modal Frequencies for the Ideal Engineered Wing.

Modal Frequencies of the Ideal Engineered Wing			
Mode	*FEA Freq. [Hz]*	*Experimental Freq. [Hz]*	*Difference*
1	62.6	58.1	7.19%
2	73.0	80.3	10.0%
3	138.6	-	-
4	198.5	-	-

The first four mode shapes are shown in Figures 5.1 through 5.4. Additional images are available in Appendix J.

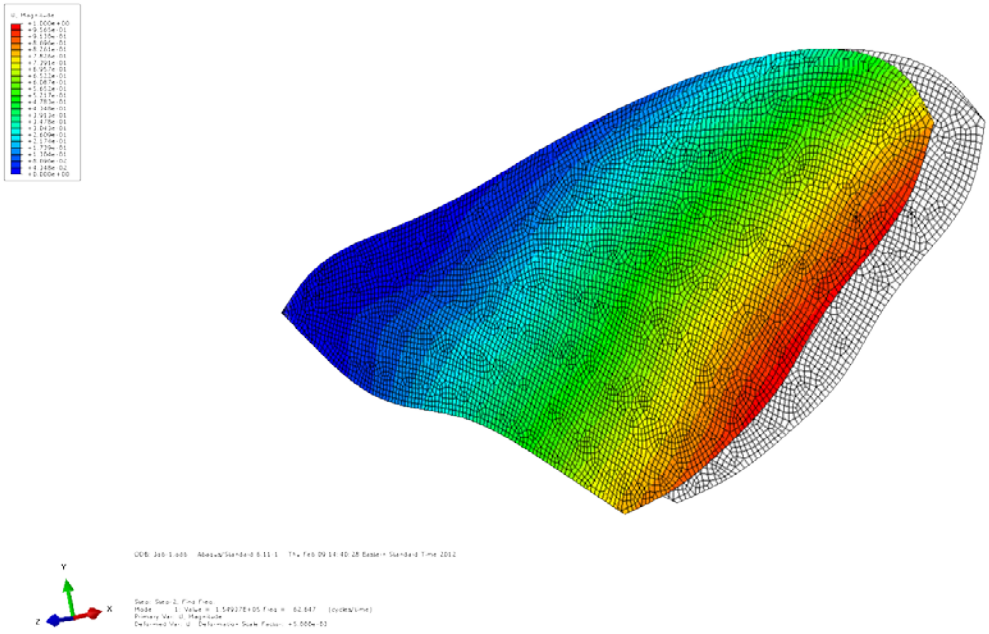

Figure 5.1: First Mode Shape of the Engineered Wing.

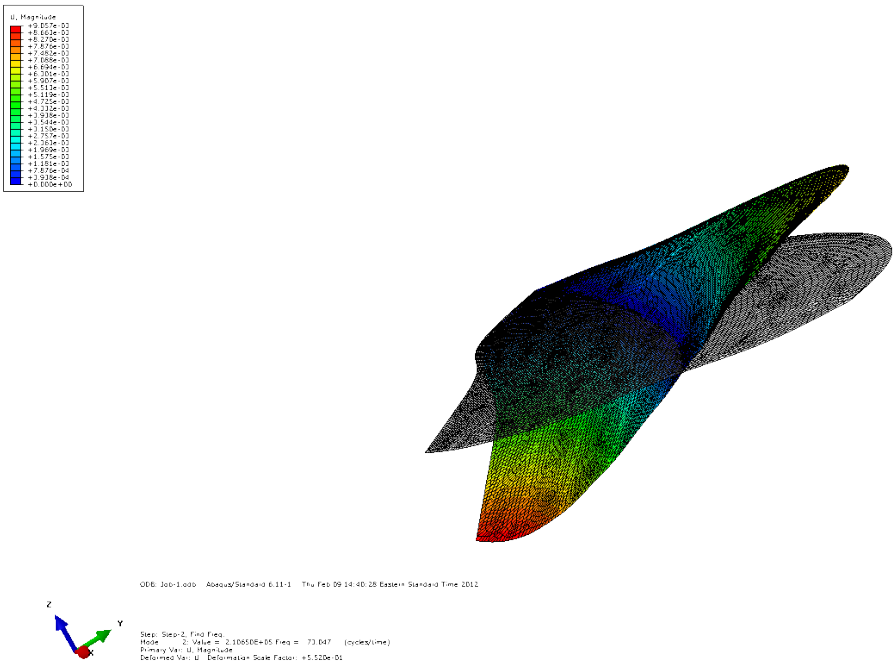

Figure 5.2: Second Mode Shape of the Engineerd Wing.

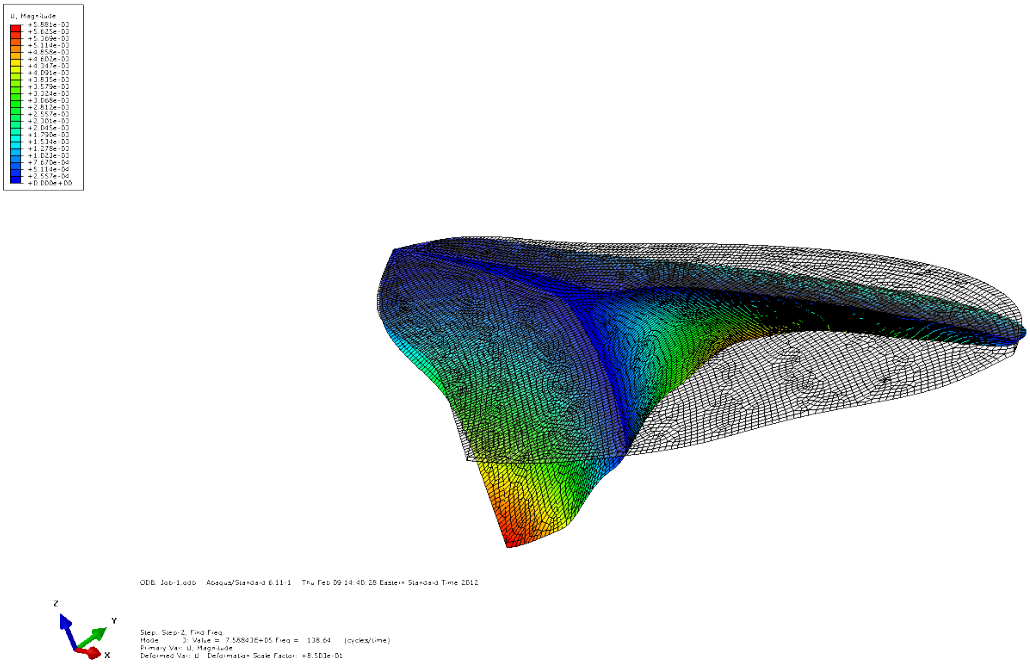

Figure 5.3: Third Mode Shape of the Engineered Wing.

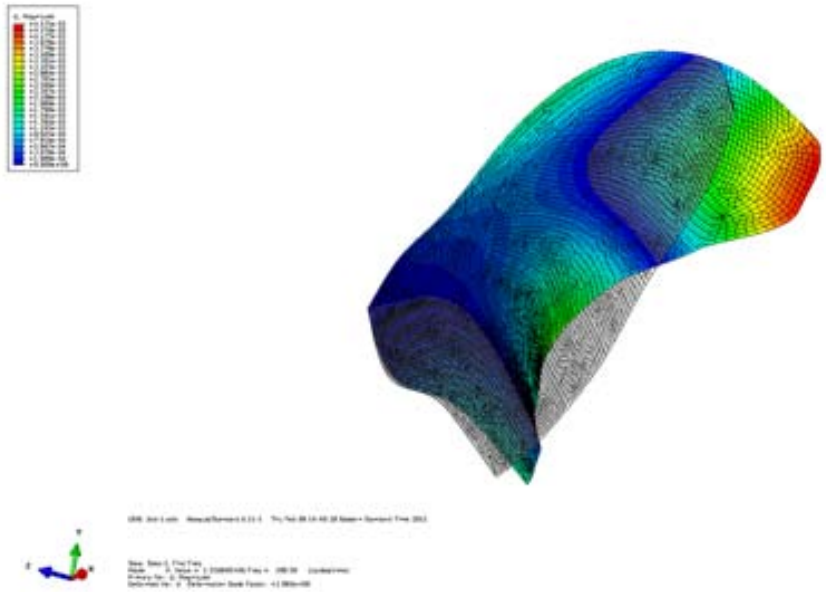

Figure 5.4: Fourth Mode Shape of the Engineered Wing.

The mode shapes determined by the FEA model closely match the *flap*, *feather*, *saddle* and *bisaddle* shapes exhibited by the biological Manduca Sexta wing and those determined experimentally of the engineered wing by DeLeon, Figure 5.5 [2]. It can also be seen that the mass of the model calculated by ABAQUS is within 2.3% of the experimentally calculated mass. The difference of 1.2 mg can be accounted for due to tolerance of the scale, or in the application of the adhesive for the Kapton membrane.

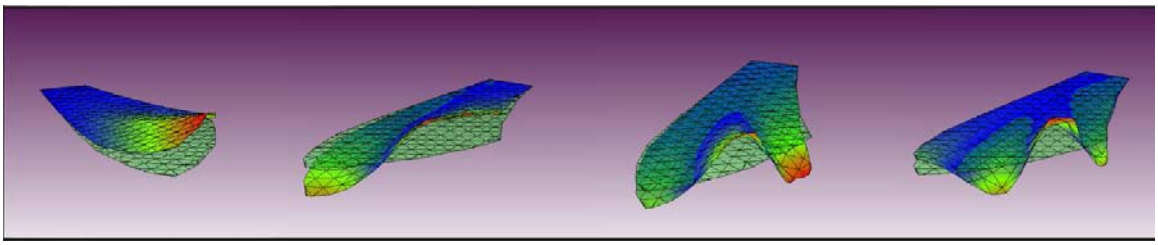

Figure 5.5: First Four Mode Shapes of the Hawkmoth Wing.

However, there is a considerable difference of 7.19% and 10.0% between the first and second modes respectively of the FEA results with the experimental results. Based on the experimental results of the composite beam structure, Chapter 3, it was considered highly probable that the variations present in the composite material could account for the difference between the experimental and FEA results. Therefore, the effects of the carbon fiber composite variations (idiosyncrasies) were examined further.

5.2. Effect of Individual Variables

In order to understand the effects the thickness, cut angle, α, and ply orientation, θ, have on the dynamic response of the wing, each of the variables was varied independently while the other variables were held at the initial ideal conditions. The first and second modal frequencies were then solved for and compared to the ideal case in order to determine the effects of each of the variables on the wing. Unlike with the beam, the angles were varied in both the positive and negative direction since a positive and negative angle of the same magnitude could have different effects that would not be present on the symmetric beam.

5.2.1. Thickness of the Composite Vein Structure

The thickness of the composite veins was varied in the FEA model between the observed 135 micron to 165 micron variation. The cut angle and ply orientation were held constant at 0, and [0/90/0] respectively. The results are shown in Figure 5.6, and Table 5.3 below. For each run, the first and second mode shape was visually determined to match the *flap* and *feather* modes exhibited in the ideal case.

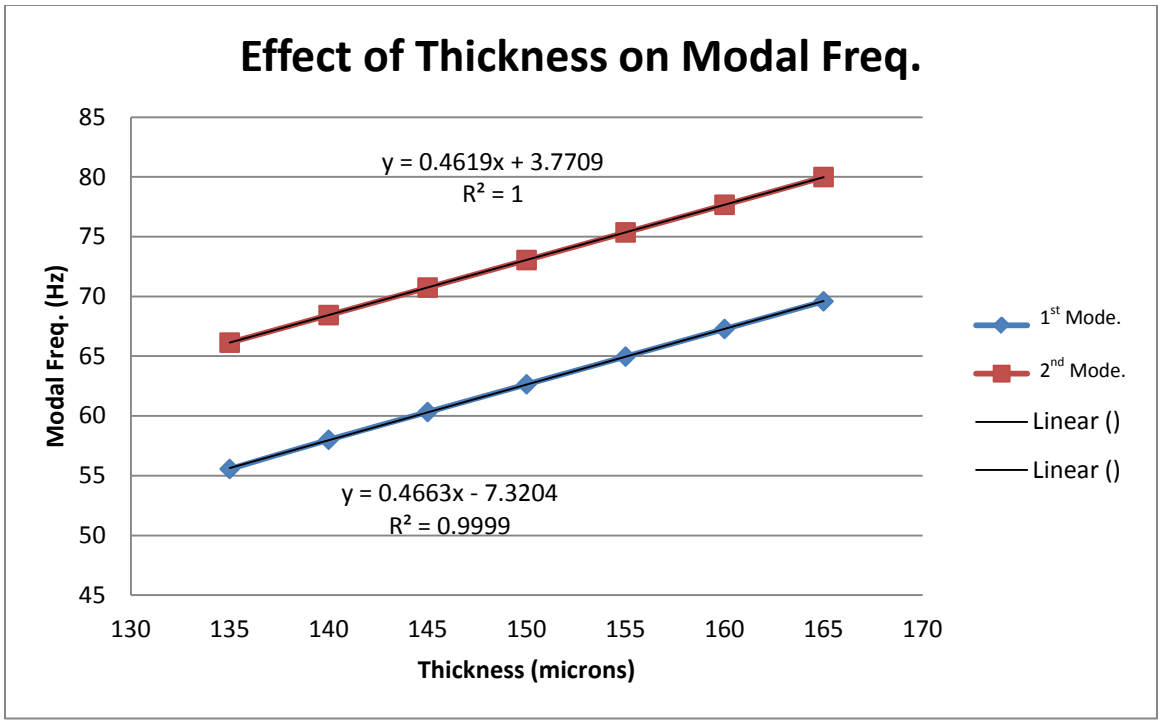

Figure 5.6: Effect of Thickness on Modal Frequencies of the Wing.

Table 5.3: Effect of Thickness on Modal Frequency.

Effect of Thickness on Modal Frequencies of the Engineered Wing		
Thickness (microns)	*First Modal Freq. (Hz)*	*Second Modal Freq. (Hz)*
135	55.6	66.1
140	58.0	68.4
145	60.3	70.7
150	62.6	73.0
155	65.0	75.4
160	67.3	77.7
165	69.6	80.0

The results show that the thickness of the composite has a significant role in determining the modal frequency of the wing. While the mode shapes retain the same shape, the first modal frequency varies between 55.68 Hz and 69.59 Hz, while the second modal frequency varies between 66.13 Hz and 79.99 Hz. Both modes increase linearly as

the thickness of the composite is increased. The equations and R-values are shown in Figure 5.6. The upward trend in frequency is expected, as a thicker beam member would have a higher moment of inertia, and therefore be more resistant to bending.

5.2.2. Ply Orientation Angles, Theta

For the variation in the ply angle, the angle of the mid-ply, and the angle of the top and bottom plies were varied in two different set of FEA runs. This was done to show the effect of the 0° plies and the 90° plies independently. Due to quasi symmetry of the actual ply, both the top and bottom plies were varied together during the analysis

The mid-ply of the FEA model was varied from 85° to 95°. The results of the FEA are shown below in Figure 5.7 and Table 5.4. The thickness of the composite was held constant at 150 microns, and the cut angle was set to 0° for each of the FEA runs.

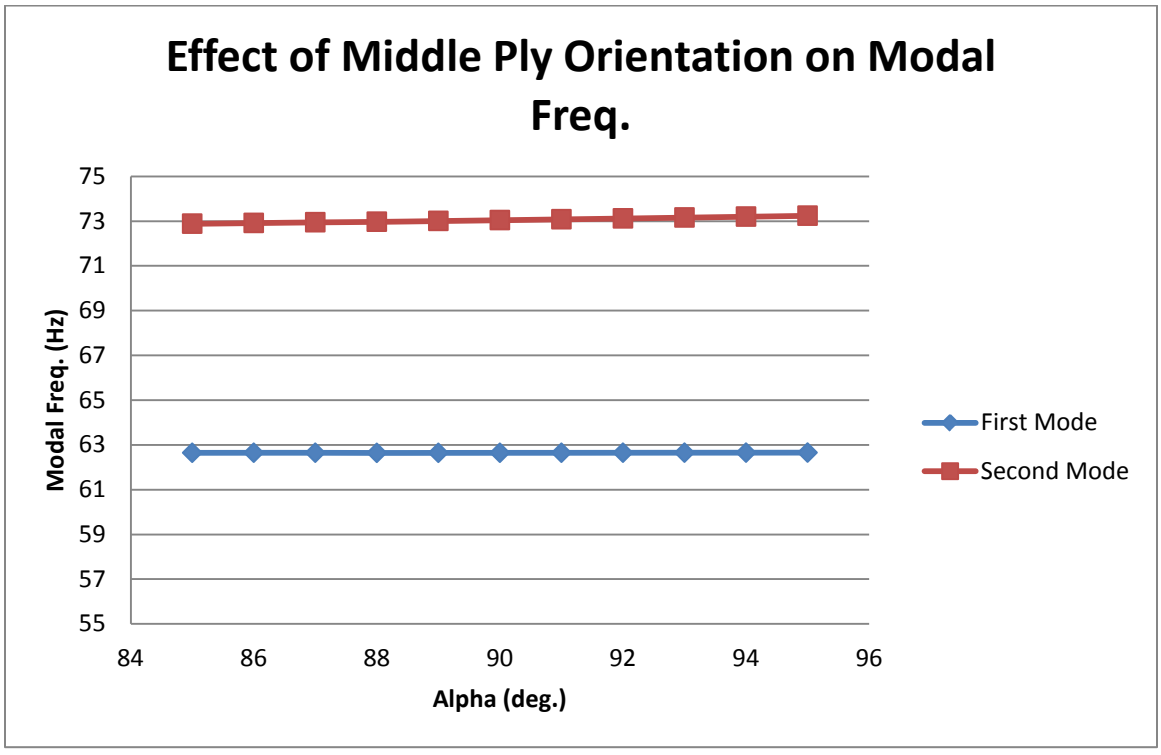

Figure 5.7: Effect of the Mid-Ply Orientation of the Wing.

Table 5.4: Effect of Mid-Ply Angle on Modal Frequencies.

Effect of Mid-Ply Orientation on Wing Modal Frequencies		
Ply Orientation (°)	*First Modal Freq. (Hz)*	*Second Modal Freq. (Hz)*
[0/85/0]	62.6	72.9
[0/86/0]	62.6	72.9
[0/87/0]	62.6	73.0
[0/88/0]	62.6	73.0
[0/89/0]	62.6	73.0
[0/90/0]	62.6	73.0
[0/91/0]	62.6	73.1
[0/92/0]	62.7	73.1
[0/93/0]	62.7	73.2
[0/94/0]	62.7	73.2
[0/95/0]	62.7	73.2

As can be seen in Figure 5.7, the orientation of the mid-ply does not have a significant effect on the modal frequency of the wing. The first modal frequency increases from 62.647 Hz to 62.655 Hz. The second mode increases from 72.887 Hz to 73.244 Hz. This is a maximum of a 0.00013% increase in the first modal frequency, and maximum of a 0.49% increase in the second modal Frequency. Variances in modal frequency this small would be hard to quantify experimentally, and does not contribute significantly to the variation measured by DeLeon and the ideal wing.

Another test was performed on the top and bottom plies of the composite vein structure. The ply angle for these lamina was varied from -5° to 5° in the FEA model. The laser cut angle was held constant at 0°, and the thickness constant at 150 microns. Figure 5.8 shows the results of the analysis.

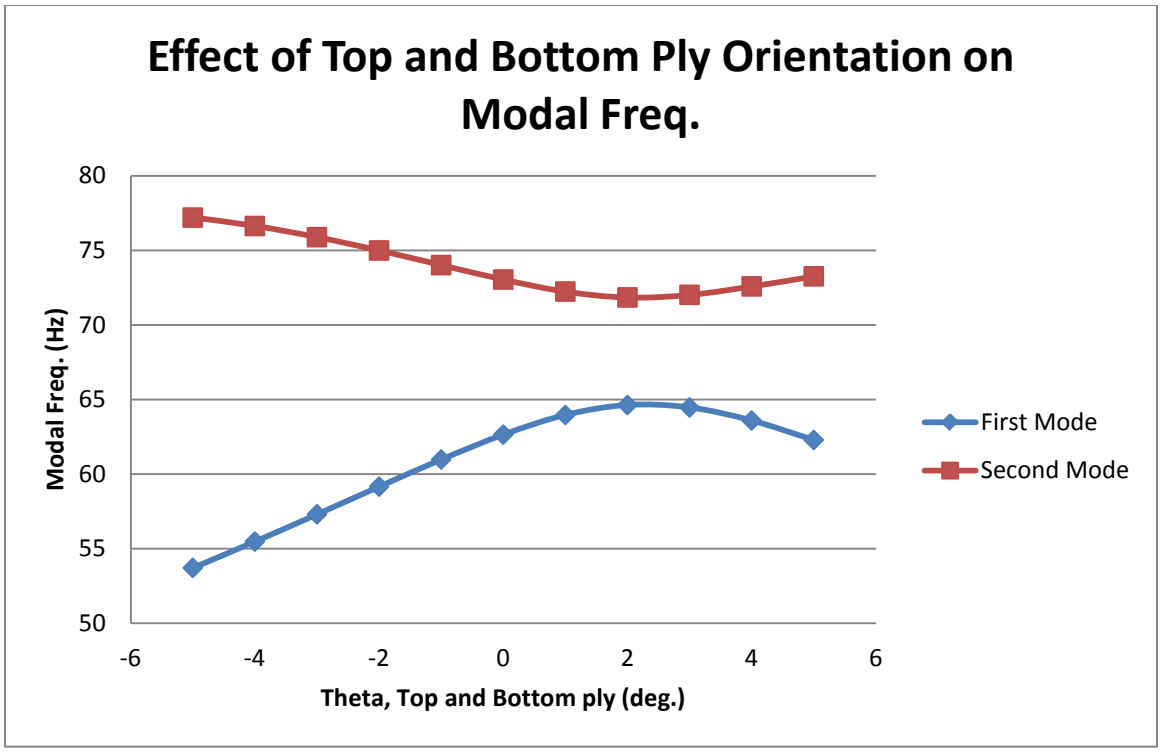

Figure 5.8: Effect of Top and Bottom Ply Orientation on the Wing.

Table 5.5: Effect of Top and Bottom Ply Orientation on Wing Modal Frequencies

Effect of Top and Bottom Ply Orientation on Wing Modal Frequencies		
Ply Orientation (°)	*First Modal Freq. (Hz)*	*Second Modal Freq. (Hz)*
[-5/90/-5]	53.7	77.2
[-4/90/-4]	55.5	76.6
[-3/90/-3]	57.3	75.9
[-2/90/-2]	59.2	75.0
[-1/90/-1]	61.0	74.0
[0/90/0]	62.6	73.0
[1/90/1]	64.0	72.2
[2/90/2]	64.6	71.8
[3/90/3]	64.5	72.0
[4/90/4]	63.6	72.6
[5/90/5]	62.3	73.3

Unlike the orientation of the mid-ply, the orientation of the top and bottom ply has a much more significant effect on the modal frequency of the wing. The first modal frequency varies from 53.719 Hz at a θ of [-5/90/-5] to 64.633 Hz at a θ of [2/90/2]. The

results form a concave down curve, peaking at approximately 2°. The opposite effect of the ply orientation can be seen on the second modal frequency. The second modal frequency varies from a high of 77.199 Hz at a θ of [-5/90/-5] to a low of 71.846 Hz at a θ of [2/902]. The results form a concave up curve with a low point of approximately 2°. The difference of 10.91 Hz and 5.353 Hz, seen on the first and second modal frequencies respectively, needed to be examined further.

These results also show that the ply orientation of the top and bottom plies not only play an important part in determining the modal frequency of the wing, but unlike the variation in the thickness of the composite, it also plays an important role in determining the modal ratio (MR, the ratio between the first and second modal frequencies) of the wing. As the orientation of the ply deviate from approximately 2°, the MR of the wing increased. This is due to the fact that as the orientation of the fibers deviate from this 2° orientation , the equations in Chapter 2 show that the fibers will have a higher elastic modulus in the chordwise direction, and a lower modulus in the spanwise direction. This would make the wing less stiff for the *flap* mode, thereby reducing the modal frequency of that mode, and stiffer against the *feather* mode, a torsion mode in the chordwise direction.

The curvature of the veins has a significant effect on the modal frequency. Since all of FEA models were run with the same geometry, the fiber angles were examined and compared to the geometry of the wing, Figure 5.9.

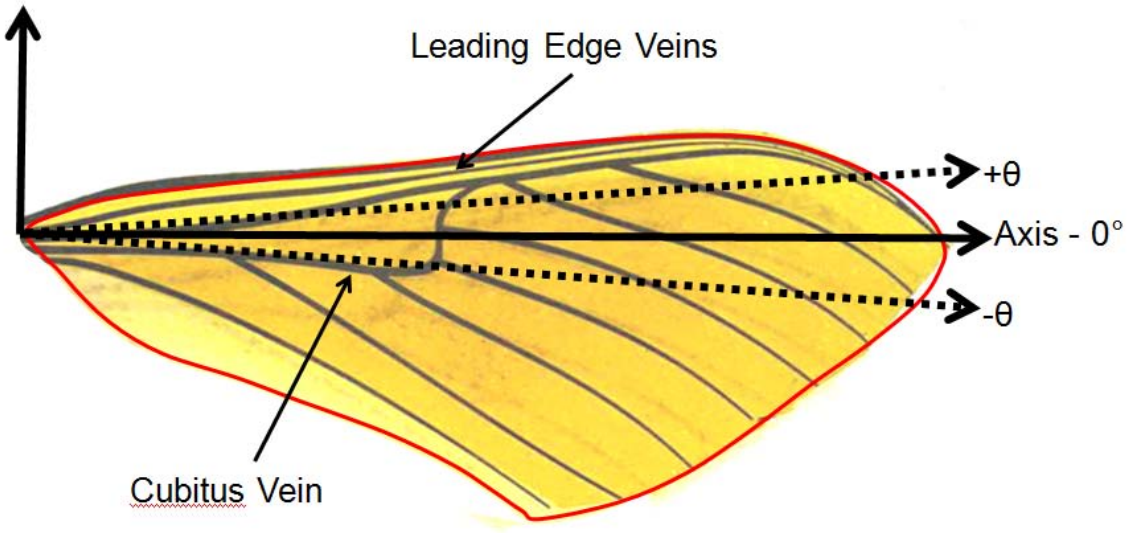

Figure 5.9: Vein Structure of the Wing Compared to Positive and Negative Ply Orientation.

As Figure 5.9 shows, as the ply orientation deviates from 0° in the negative direction, the fibers tend to run closer to parallel along the Cubitus vein, as they deviate in the positive direction, they tend to run closer to parallel along the leading edge veins. The closer the fibers are to running 0° to the local axis along either of these veins, the stiffer these veins become. Since it has been demonstrated how significantly the material properties of the veins change as the fibers approach 0° to the local axis, any positive or negative ply orientation would have a significant effect on the stiffness of these veins.

Based on these results, it can be concluded that the stiffness of these veins play an important part in determining the modal frequencies of the wing. In addition, since the fibers are unidirectional, as the fibers are orientated to stiffen one of these veins, the effect would inversely affect the other.

5.2.3. Laser Cut Angle, Alpha

The laser cut angle, α, of the composite (the angle in which the composite in placed in the laser cutter compared with the desired orientation, Figure 5.10) was varied in the FEA model between -5° and 5°. The thickness and ply orientation were held constant at 150 microns, and [0/90/0] respectively. The results displayed in Figure 5.11 and Table 5.6 below.

Figure 5.10: Figure Showing the Laser Cut Angle, α.

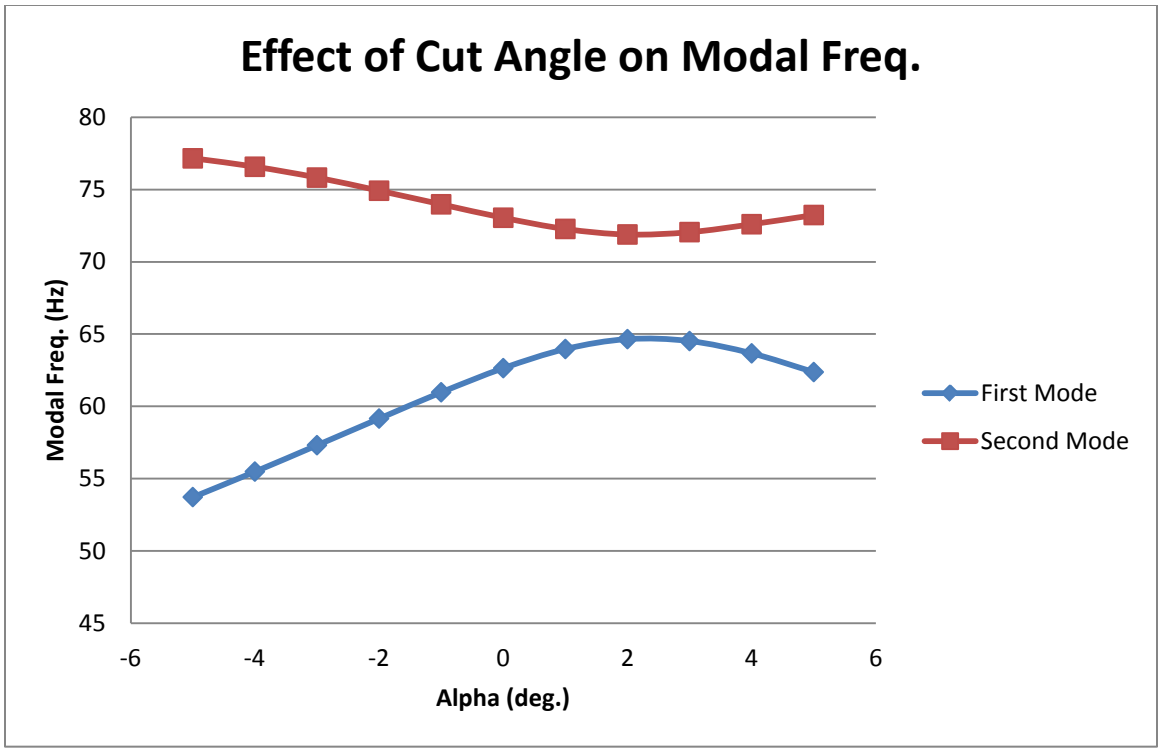

Figure 5.11: Effect of the Laser Cut Angle on the Wing

Table 5.6: Effect Of Laser Cut Angle on Engineered Wing Modal Frequencies.

Effect of Laser Cut Angle on Wing Modal Frequencies		
Laser Cut Angle (°)	*First Modal Freq. (Hz)*	*Second Modal Freq. (Hz)*
-5	53.7	77.2
-4	55.5	76.6
-3	57.3	75.8
-2	59.2	75.0
-1	61.0	74.0
0	62.6	73.0
1	64.0	72.3
2	64.7	71.9
3	64.5	72.0
4	63.7	72.6
5	62.4	73.2

As can be seen in Figure 5.11, the effect of the cut angle has a similar effect as the effect of the top and bottom plies' orientation. There is less than a 0.1 Hz difference between the results of the test that varied the top and bottom plies' orientation Table 5.5,

and the test that varied the laser cut angle. The laser cut angle simply adds or subtracts the angle to the ply orientation. Since the variation in the orientation of the mid ply has very little effect on the modal response of the wing, it can be concluded that the effect of the laser cut angle is simply having the same effect as the fiber orientations of the top and bottom plies.

5.3. Effect of Composite Thickness and Fiber Angle

Since the thickness and fiber angle of the top and bottom fibers had the most effect on the frequency response of the wing, FEA runs were performed that varied both the thickness and laser cut angle of the composite for the wing. The laser cut angle was chosen over varying the top and bottom plies' orientation because it has the same effect as varying the top and bottom ply orientations, would be simpler to modify within the program, and because the effect of the variation in the mid-ply was deemed negligible.

In order to determine the range of frequencies that could be expected within the wing, the laser cut angle was varied between -6° and 6° in increments of 1°. Since the thickness caused both the first and second modal frequency to vary linearly, the values for the thickness were only varied using the minimum and maximum values of 135 and 165 microns. Again, the results were visually checked to ensure that the mode shapes matched those exhibited in the ideal case, Section 5.1. The results for the first modal frequency is shown in Figure 5.12, and the second modal frequency in Figure 5.13, both results are shown in Table 5.7

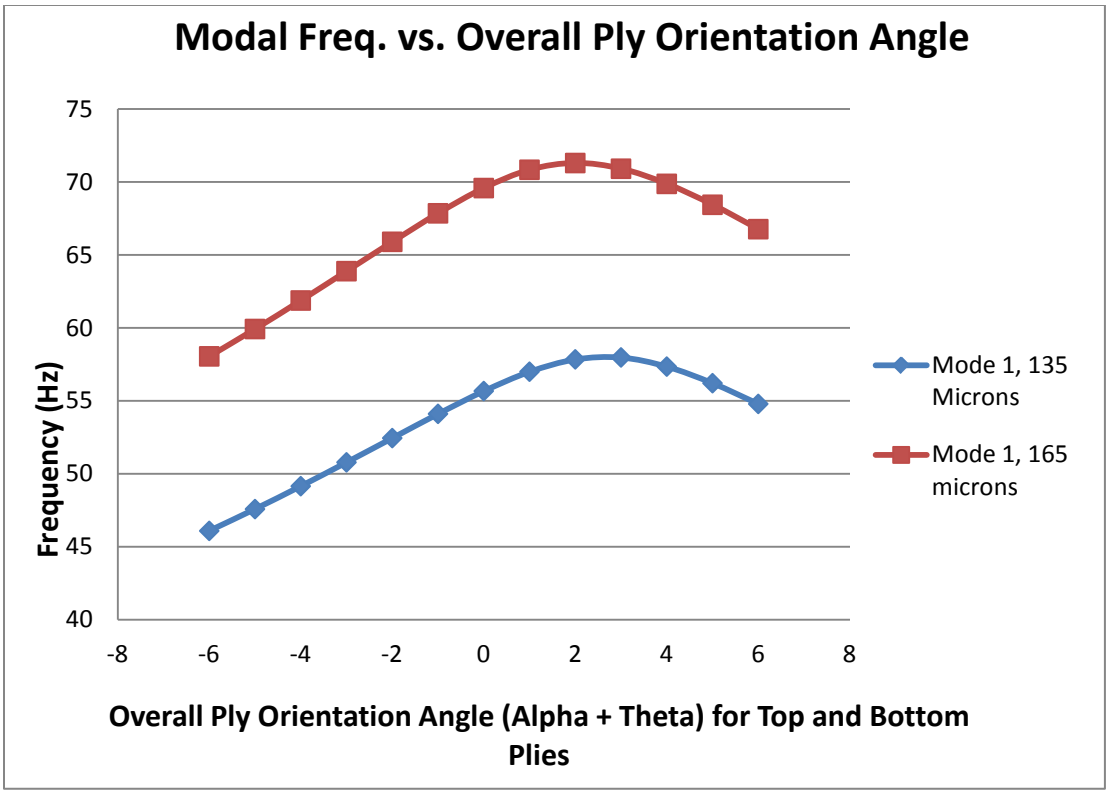

Figure 5.12: Comparison of the First Mode for Varying Thicknesses.

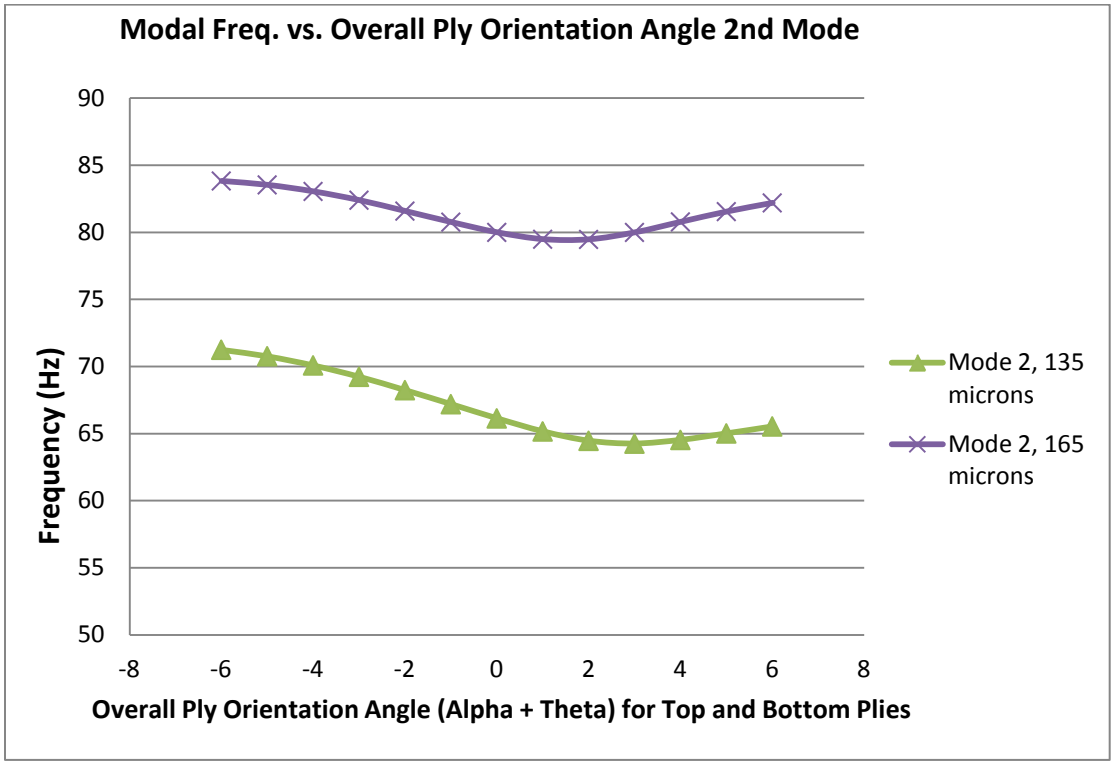

Figure 5.13: Comparison of the Second Mode For Varying Thicknesses.

Table 5.7: Effect of Laser Cut Angle and Thickness

Effect of Laser Cut Angle and Thickness on Wing Modal Frequencies				
Laser Cut Angle (°)	*1st Modal Freq. (Hz) 135 micron Thick*	*1st Modal Freq. (Hz) 165 micron Thick*	*2nd Modal Freq. (Hz) 135 micron Thick*	*2nd Modal Freq. (Hz) 165 micron Thick*
-6	46.1	58.1	71.2	83.8
-5	47.6	60.0	70.8	83.5
-4	49.2	61.9	70.1	83.0
-3	50.8	63.9	69.2	82.4
-2	52.5	65.9	68.2	81.6
-1	54.1	67.9	67.2	80.8
0	55.7	69.6	66.1	80.0
1	57.0	70.8	65.2	79.5
2	57.9	71.3	64.5	79.5
3	58.0	70.9	64.3	80.0
4	57.4	69.9	64.5	80.8
5	56.2	64.4	65.0	81.5
6	54.8	66.8	65.5	82.2

Based on the results, it can be seen that there is a significant difference present when comparing the both the first and second modal frequencies. The area between the two curves represents possible modal frequencies that could be exhibited in the engineered wing based on the current composite, and its variations due to the manufacturing process. The difference seen is similar to difference seen in Section 5.2.1, as the thickness of the composite increased, the modal frequency increased. However, it should be noted that as the thickness of the composite increases, the peak seen in the curve for the first modal frequency and the low point of the second modal frequency curves shifts from approximately a 3° α for the 135 micron composite, to approximately 2° α for the 165 micron sample.

The mean modal frequency values for this run is shown in Table 5.8, and compared to the ideal (using specific composite material property values) values and the experimental results. The results show that given the composite idiosyncrasies, the first

mean first mode will be lower than the ideal, and the mean second mode higher than the ideal. This follows the trend determined by the experimental values.

Table 5.8: Comparison of Modal Results.

Modal Frequencies			
	Result	*Ideal*	*Experimental*
First Mode	60.1 (Mean) Hz	62.6 Hz	58.1 Hz
Second Mode	74.3 (Mean) Hz	73.0 Hz	80.3 Hz
Difference	----------	----------	----------
First Mode	4.0%	-	7.2%
Second Mode	1.8%	-	10.0%

5.4. Matching the FEA to Experimental Results

With such a wide range of possible values for the modal frequencies of the wing, it is highly probable that the FEA model could be made to match the experimental results. Figure 5.14 shows the results from Section 5.3 (Figures 5.12 and 5.13) plotted on a single graph. Also plotted are two straight lines showing the first and second modal frequencies achieved experimentally.

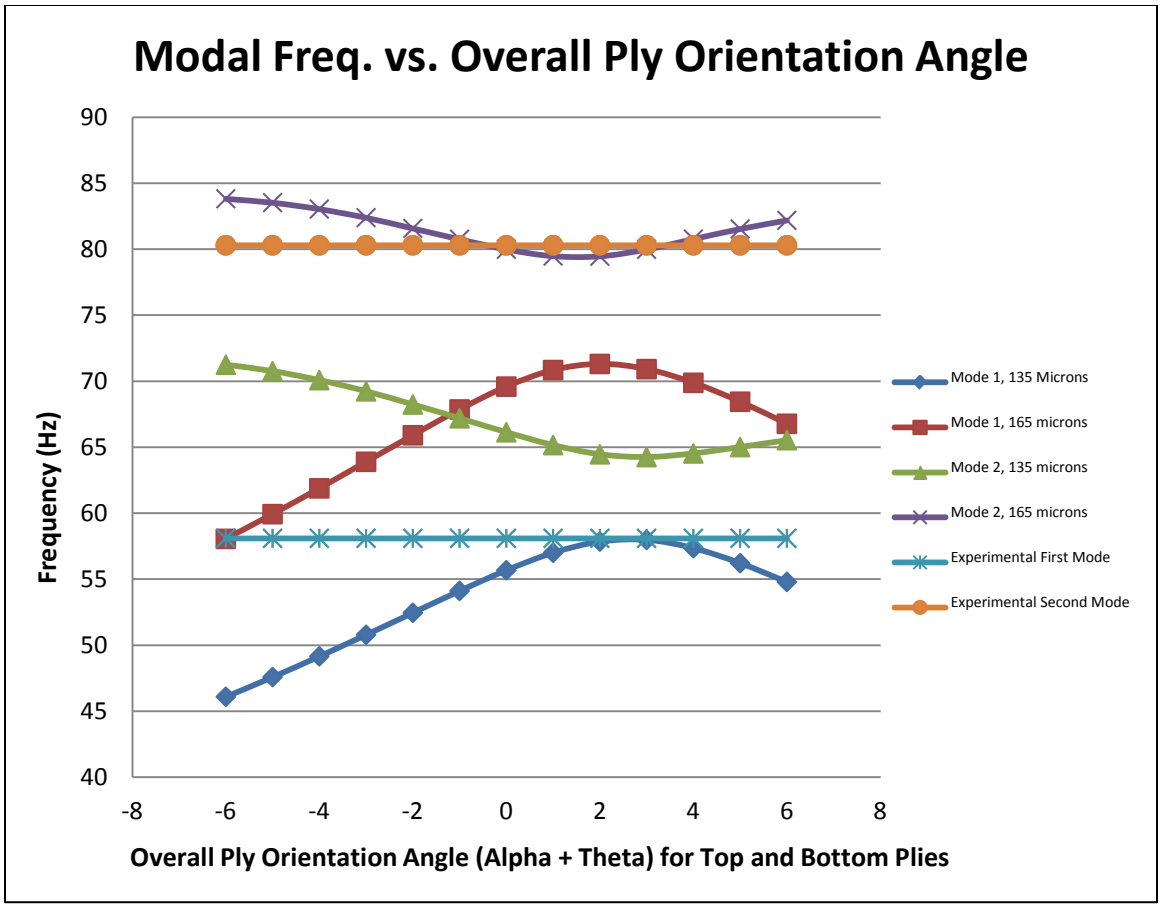

Figure 5.14: Modal Frequency Results vs. Overall Ply Orientation.

Based on these results, a trial and error method was used in an attempt to match the experimental results. Using an α of 4.5°, resulting in a ply orientation of [-4.5/85.5/-4.5], and thickness of 158 microns, a first modal frequency of 58.0 Hz, and a second modal frequency of 80.3 Hz was achieve. This represents a 0.17% difference between the first modal, and a 0% difference between the second modal frequencies of the experimental compared to the analytical FEA results. Both of these values also fell within the likely limits measured within the carbon fiber samples. In addition the mode shapes matched the same *flap* and *feather* modes seen experimentally, Figures 5.15 and

5.16. This shows that the stiffness characteristics of the model match the stiffness characteristics of the experimental analysis.

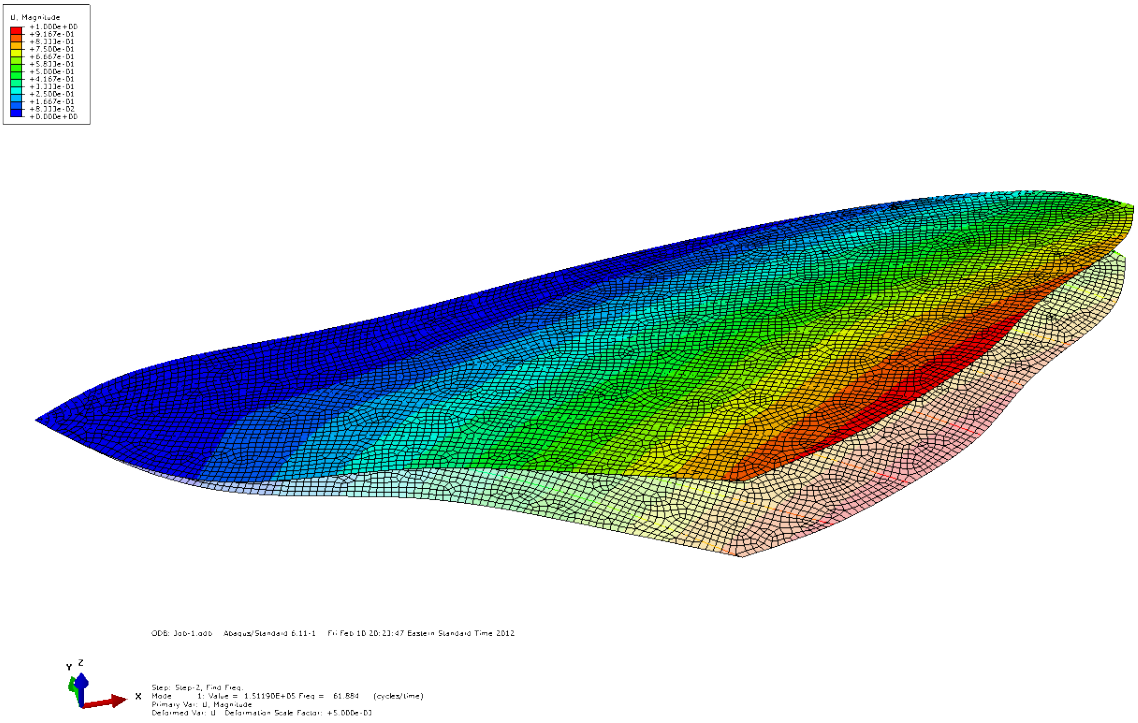

Figure 5.15: First Mode of Wing Matched to Experimental Results.

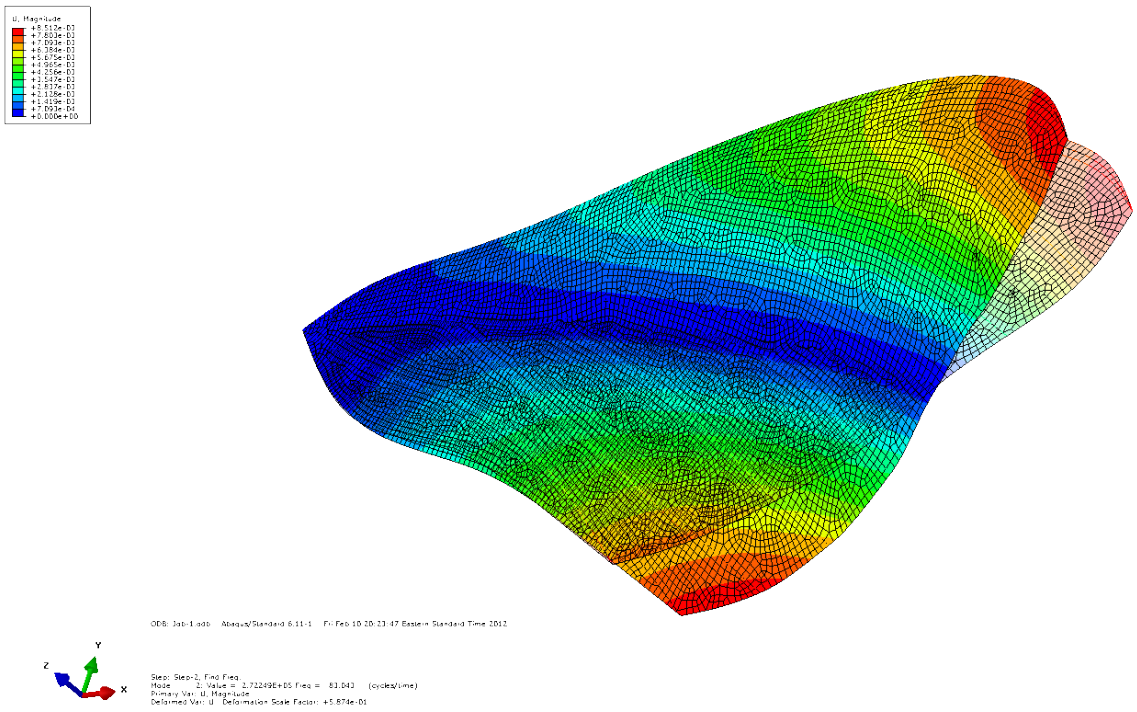

Figure 5.16: Second Mode of Wing Matched to Experimental Results.

5.5. Further Discussion

Based on the results seen with the FEA analysis, it can be determined that the errors caused in the manufacturing process play a significant role in determining the modal response of the engineered wing as would be expected. While for the case of the beam specimens in Chapter 3, this caused a significant reduction, 34.0%, in the modal frequency of the beam compared to the ideal case, the curvature of the veins resulted in a lower overall percentage reduction in the modal frequencies, up to 10%, although there is still a wide range of expected frequencies.

If a better manufacturing process could be developed, less variation in the fiber angle, and the thickness of the composite could significantly reduce the variation, although due to the small tolerances present in the manufacturing of the composite, some variation would be inevitable using the hand lay-up technique required here at AFIT.

Another method to control the fiber orientation would be to choose a ply orientation further away from the 0° that is present in two plies of the composite. This would reduce the stiffness of the model, but as seen when varying the 90° ply, less variation would occur. However this would not improve the overall stiffness of the wing without adding more plies, and thus more mass.

The FEA model does match the engineered wing, however the engineered wing does not match the biological wing, Table 5.9. This indicates that further design work still needs to be done on the wing. Given the near infinite number of possible arrangements of the composite material, possible changes in vein width to the wings, and the addition of camber to wing, the potential for an engineered wing made out of the composite is not necessarily unobtainable. This is one of the main reasons that the MATLAB code was created in order to generate the FEA model. Now that the FEA model has been matched experimentally, using the knowledge gained based on the effects of the composite material, it can be easily modified and further iterations on the design can be tested prior manufacturing.

Table 5.9: Examination of Results.

Examination of Results				
	First Mode	***Second Mode***	***Difference from Biological 1st Mode***	***Difference from Biological 2nd Mode***
Biological	86 Hz	106 Hz	-	-
Experimental	58.1 Hz	80.3 Hz	32.44%	24.25%
FEA Min	46.08 Hz	64.26 Hz	46.42%	39.38%
FEA Max	71.3 Hz	83.8 Hz	17.1%	20.94%

VI. Summary and Conclusions

The use of unidirectional carbon fiber composite material in the manufacturing of FMAV wings provides a lightweight material with a high specific strength. Previous research done at Harvard University on FMAV wings has shown that the material when laid in a [0/90/0] orientation was capable of producing a viable wing for use in a MAV. Since metals and plastics have proven to either have insufficient strength or to have too much mass, the [0/90/0] orientation of unidirectional carbon composite was chosen to form the vein structure of a FMAV wing based on the forewing of the Manduca Sexta.

The focus of this research was to develop a finite element model capable of accurately predicting the observed modes of an engineered Manduca Sexta forewing. Due to considerable variation in material properties of the [0/90/0] carbon fiber composite used in the manufacturing of the vein structure within the wing, a considerable effort was put forth in studying the effects of the off specification composite. The FEA model of the wing was used to study the effects that the material variation within the composite would have on the modal response of the engineered wing. A summary of the research performed for this project is stated below.

6.1. Summary

The manufacturing of the composite material was performed at AFIT. Sheets of unidirectional carbon fiber pre-preg were arranged in into the [0/90/0] orientation using a hand lay-up technique. This lay-up was then cured in a heatpress in order to cure the epoxy and form the composite material. A laser was then used to cut the composite into the desired vein structure shape. Using beam test specimens, the modal frequency of the

composite was evaluated using a SLV. However, the results of the SLV tests proved inconsistent with FEA results of the beam specimens.

Since the composite material has been verified using ASTM D 3039 and ASTM D 3518 standards using 20 ply test specimens, errors in the manufacturing process were investigated in order to determine the inconsistent results. Using experimental methods, the thickness, ply orientation and laser cut angle were examined. Small variations in the thickness, ply orientation and laser cut angle were each individually determined to affect the modal response of the beam specimen.

Experimental modal analysis was performed on test specimens using a SLV in order to ensure material properties of the composite material. An average value of 144.9Hz was found for the first modal frequency for the first bend mode of test composite beam specimens. FEA results had predicted a first modal response of 219.5 Hz. An investigation into the likely cause of such a difference was made. The thickness of the composite was measured and found to vary between 135 and 165 microns. Taking the thickness into account, the numerical frequency of the beam would vary from 197.6 to 234.1 Hz, a significant amount, but not enough to account for the 144.9 Hz average discovered.

The next thing looked at was hand lay-up manufacturing process of the composite material. Test specimens were measured using an optical microscope in order to determine the true orientation of the fibers. It was found that the placement of the specimens in the laser cutter could be off approximately 2.5°. This would affect the overall ply orientation of the specimen. Also investigated was the ability of the hand lay-up process to accurately manufacture the desired ply angle. Investigation of test samples

using an optical microscope again found an approximately 2.5° deviation from the specified ply angle.

Taking the thickness, laser cut angle and ply orientation of the laminate into account, a Monte Carlo solution was performed in order to determine the probable and possible first modal frequencies of the beam. The Monte Carlo solution determined that a mean value of 154.2 Hz was the most probable for the modal frequency of the beam, with the majority of solutions varying between 100 and 200 Hz. The 144.9 Hz average was well within the bell curve of the solution, showing that there was indeed off specification designs in the composite material, and that it would affect the modal frequency of structures made of the material.

Since the manufacturing of the composite material can create variations in the specified material properties of the composite, the effects that the variation of thickness, laser cut angle, and ply orientation were examined using FEA for the engineered wing. Using MATLAB, input files were created for ABAQUS in order to generate multiple FEA model.

` An FEA model of the engineered wing was constructed using a developed MATLAB code. The vein structure was modeled using B32 elements and the membrane using S8R and STRI65 elements. MATLAB was chosen in order to more easily render the material properties of the beam element representing the composite vein structure of the wing, and in order to quickly and easily incorporate the composite variations into multiple FEA simulations. Each beam in the model possessed a unique material property and profile based on its location on the curvature of the vein. The angle of the element was determined in the global axis of the model, and then the material properties of the

composite material was determined based upon that angle using the transformation equation. A homogeneous material property for the beam element was created by changing the element profile and density using the effective moment of inertia, and then calculating the mass so that it matched that of the original element with the physical square cross section. In addition, since the current engineered wing design did not fully match the modal results of the biological wing, the modal was made so that the dimensions of the veins could be easily modified, as well as the material properties.

A model was created based upon the specifications for the engineered wing. While the first four mode shapes matched the modes determined by the experimental analysis, the first and second modal frequencies were off by 7.19% and 10.0% respectively from the 58.2 and 80.3 Hz measured experimentally. The effects of off specification composite were then examined.

As with the composite beam specimen, the thickness, laser cut angle and ply orientation of the composite material was varied independently in order to determine the effects each would play on the modal response of the wing. The thickness was varied from 135 to 165 microns, resulting in a modal frequency varying between 55.6 and 69.6 Hz for the first mode, and 66.1 and 80.0 Hz for the second mode. The variation of the mid-ply orientation from 85° to 95° showed less than 1% variation in the frequency, while variation of the top and bottom plies orientation from -5° to 5° resulted in modal frequency change between 57.7 and 64.3 Hz along a concave down curve peaking at approximately 2° for the first mode, and between 71.9 and 77.2 Hz along a concave up curve with a valley at approximately 2°. Varying the laser cut angle resulted in similar results to those varying the top and bottom plies orientation. This led to the conclusion

that the effect of the top and bottom plies orientation and thickness of the composite played the most significant roles in determine the modal response of the wing.

The laser cut angle was varied between -6° to 6° for thicknesses of 135 and 165 microns. This resulted in a curve representing a range of probable values for modal frequencies that could be exhibited by the wing based on observed variations in the composite material, figure 5.13. It was shown that the experimentally observed modal frequencies of the wing fell within the probable range.

A trial and error mode was used varying the thickness and laser cut angle of the wing in order to match the experimentally observed modal characteristics of the engineered wing. It was found that a thickness of 158 microns and a laser cut angle of -4.5° resulted in a modal frequency of 58.0 Hz and 80.3 Hz for the first and second mode. This represented a 0.17% and 0.0% difference from the experimental results. The mode shapes for the modal also matched those determined experimentally.

It was determined that the experimental results of the wing fell within the bounds established by the variation in the composite material. Using a trial and error method, an FEA model of the wing with a +8 micron thickness and a -4.5° laser cut angle was created that matched the experimental modal results of the engineered within 1% variation, thus validating the assumption that the manufacturing of a [0/90/0] orientation led to major variations of the wing response.

6.2. Conclusions

6.2.1. Carbon Fiber Material

The use of the carbon fiber composite resulted in a wide range of variability in the engineered wing predicted by the FEA. It does however posses a high specific modulus not available in any isotropic material. This allows the material to be lightweight, but still have a high strength. Due to the low mass required for the wing, composites seemed to be the only viable solution due to the inertial loading caused by the flapping of the wing [2]. However this does not mean that the YSH-70-A/RS-3C composite currently used is the best solution.

There are numerous amounts of other composite materials commercially available, each with their own unique material property. Likewise, the ply lay-up and number of plies have a great affect on material properties. The [0/90/0] ply layup currently used has proven to be sensitive to ply orientation and thickness variations. Repeatable production of an engineered wing with consistent dynamic properties would not be possible given the current material and manufacturing technique.

However, if a quasi-isotropic material could be found that would still meet the mass and strength criteria required by the MAV design, it could alleviate some of the issued faced with the ply orientation. Quasi-isotropic materials are unidirectional composite materials where the laminate arranged such that the material properties in x, y, and z direction are the same. If a material and orientation could be found or developed that would provide the same axial stiffness (ability of a beam to resist bending) in both the x and y directions of the composite, then a composite material could be viable. This

material would be less sensitive to variation in ply orientation, however would most likely face the same issues due to variations in thickness.

6.2.2. Carbon Fiber Manufacturing Process

The current manufacturing process of the composite material has been attributed to the source of the ply orientation error. It is apparent that if the current 3-ply [0/90/0] orientation is to be used, the manufacturing process needs to be improved. Given the significant variations in the modal response of the wing due to small changes in angle, in order for a reliable and repeatable process for manufacturing the wing, a tolerance of only 1° would be acceptable for the total ply orientation alignment (laser cut angle + ply layup misalignment). Any further variation of the ply orientation of the material would create a variation in the modal response beyond 2.5%. This seems highly unlikely given the experimental results based on the hand layup, and the fact that this does not consider the variation due to the thickness of the composite. It should be noted that a variation of less than 5 microns would be needed to maintain the same 2.5% variation in modal response frequency, even with an ideal ply orientation. Given the large variation experimentally measured, the probability of creating a composite that would have a small variation in thickness and ply orientation using the current method would be extremely improbable. Instead, some type of automated manufacturing process would be required in order to achieve such tolerances.

6.2.3. Monte Carlo Solution

A Monte Carlo solution was used in order to evaluate the wire beam. One of the reasons behind the Monte Carlo solution is not only to find out what is possible, but also what is probable. While a Monte Carlo solution does provide useful information as to the probability of results expected in the beam specimen, the large amount of data required in order to gain a significant statistical average made it unfeasible for use on the engineered wing.

6.2.4. Effects of Composite Variation on the Wing

It is without doubt that the variation in the composite has a significant effect on the modal response of the wing. Based on such a wide range of variation that was determined, it would be difficult for a repeatable wing to be developed using the current method of manufacturing. However, it should be noted that the mode shapes of the wing are consistent, meaning that the response of the wing is the same, just the numerical frequency at which the response occurs would change. This means that while the wing does not match the stiffness of the biological wing, it shares the same characteristics, meaning that the wing should behave similarly to the biological wing, albeit at different frequencies. Getting the wing to match the biological wing would be especially be difficult given the fact that while the wing is a single entity, it would always be required to work in pairs.

This would add a complexity of having to “pair up” sets of wings together that share similar modal response. Failure to do so could cause significant control issues for a FMAV, such as having to flap two wings at different frequencies in order to generate equal amounts of lift. One possible solution to this issue would be to use vein structures

that are cut from the same general area of the composite material. Since the fibers are imbedded in the pre-preg of the epoxy matrix mechanically, the fibers are generally parallel to one another. Wings that are cut out of the same piece of composite should have less variation in the material properties compared to one another versus those cut from other sheets of the composite. This can be evident by looking at the beam samples, which were cut out of a single sheet of composite.

However, this would not account for the variation in properties, only amongst the variation between wings. It can be concluded that this would only be a feasible alternative if the variation in the MR was not as significant as long as matching sets of wings shared the same MR.

6.2.5. MATLAB to Generate FEA Model

The use of beam elements were chosen because of the ability for the geometry to easily be modified . This method was chosen as opposed to a composite shell method where the number and orientation of the plies can easily be changed, but the geometry would be difficult to do so. This decision was made at the beginning of the project prior to the composite material variations being known, when it was thought that the geometry of the wing would need to be easily changed in order to aide in the design process. This would allow the user to vary the width of the veins in a similar matter that the material orientation was varied. Multiple runs with various designs vein widths could easily be submitted and solved to determine the effect that a change in vein width would have on the overall model. While this is still a useful feature, its value to this research was limited to only fine tuning the model.

The beam elements proved to be faster to solve than the shell elements. This was especially useful for cutting down the time it took to solve the Monte Carlo solution for the sample beam specimens. They were also easier to generate the nodes because only a single line was required as a reference for the location of the vein, as opposed to the two that would be required for shell elements. This made it significantly easier if the geometry of the wing was required to change. However, the downside to beam elements was that each beam element required its own profile and material property. This meant that a MATLAB code was required in order to develop the node sets, element sets, material properties and bream profiles. This meant that more time needed to be spend "upfront" in developing the MATLAB code, as opposed to using the CAD program in ABAQUS.

The MATLAB code made the wing significantly easier to modify, enabling the geometry, beam profile and composite material variations to easily be changed. This means that the code can easily be used to modify the width of any of the veins, or even be easily modified to have a camber. The downside to the present code is that due to the I-beam shape of the composite, the beam element can only handle 3-ply lamina. This places a significant limitation on the code and its capabilities, considering the value of 2 or 4 plies may have in producing a more quasi-isotropic material. This feature can be changed to support other numbers of plies.

6.3. Suggested Future Work

Based on the results of the analysis, further modification of the engineered wing is required in order to match the characteristics of the Manduca Sexta Forewing. One thing not yet examined is different ply angles. The equations in Chapter 2 show that the

material properties of the composite change significantly as the ply orientation approaches 0°. Also, the results from Section 5.3, also confirm that the modal response of the wing can be significantly altered based on the ply orientation. Countless other ply orientations could possibly be used in the manufacturing of the vein structure that would be less susceptible to the idiosyncrasies examined for this project.

Another thing that can be examined is camber of the wing. Currently the wing is created on a flat surface. As Sims has shown, the effect of camber on the wing will have a stiffening effect without adding any additional mass [15]. Since the model was developed using a MATLAB code, imparting a camber to the wing could feasibly be done relatively easily.

Focusing on possible numerical research, a design should be created that incorporates the camber observed on the biological wing. A parametric study on various ply orientations of the composite material and vein widths should be conducted. This could be easily done by modifying the current MATLAB code that generated the FEA model of the wing. At this point, it is clear that the current manufacturing process of the composite created a significant variation in the modal response of the wing. A less susceptible design needs to be created, whether by introducing a different ply orientation, a camber, or using a different composite manufacturing process – or any combination of the three, in order to create a viable engineered wing that can be optimized to matching the biological Manduca Sexta forewing characteristics.

Appendix A. YSH-70-A/RS-3C Material Properties

NGF High Stiffness Fibers
Nominal Unid Laminate Properties

Property	Units	YS-95A	YS-90A	YS-80A	YSH-70A	YSH-70A	YSH-70A
Fiber Modulus	Msi	134	130	114	105	10500000 psi	7.2395E+11 pa	723.95
Fiber Tensile Strength	Ksi	510	510	530	530	530000 psi	3654221364 pa	3.6542
Fiber Thermal Conductivity	W/m-K	600	500	320	250			
Unid. Mechanical Properties		Epoxy	CE	Epoxy	CE			
0° Tension Modulus	Msi	83.0	79.2	72.1	60.9	6.03E+07 psi E1	4.198907E+11 pa	419.890719 gpa
0° Tension Strength	Ksi	283	272	288	291	2.91E+08 psi	2.006374E+12 pa	2006.374371 gpa
0° Compression Modulus	Msi	78.0	77.0	66.5	60.0	6.00E+07 psi	4.136854E+11 pa	413.685437 gpa
0° Compression Strength	ksi	49.4	52.0	55.4	72.3	7.23E+07 psi	4.984910E+11 pa	498.490952 gpa
0° Flexure Modulus	Msi	67.3	65.0	57.2	54.8	5.48E+07 psi	3.778327E+11 pa	377.832639 gpa
0° Flexure Strength	Ksi	94.4	92.0	92.5	96.5	9.65E+07 psi	6.653441E+11 pa	665.344078 gpa
90° Tension Modulus	Msi	0.8	0.8	0.9	0.8	8.00E+05 psi E2	5.515806E+09 pa	5.515806 gpa
90° Tension Strength	Ksi	3.1	3.5	4.7	3.4	3.40E+06 psi	2.344217E+10 pa	23.442175 gpa
SBS Strength	Ksi	8.7	9.0	9.1	8.1	8.10E+06 psi	5.584753E+10 pa	55.847534 gpa
45° In-Plane Shear Modulus	Msi	0.6	-	0.7	0.7	7.00E+05 psi G12=G13	########## pa	4.826330 gpa
45° In-Plane Shear Strength	Ksi	5.4	-	7.4	8.8	8.80E+06 psi	6.067386E+10 pa	60.673864 gpa
Lam. Thermal Conductivity (0)	W/m-K	368	303	204	160	nu12	2.800000E-01	0.000000 gpa
						G23= density	3.530116E+09 pa	3.530116 gpa

*Normalized to 60% Fiber Volume

E22 = E33, nu12=nu13, **G12=G13**, and G23= E22/(2*(1+nu23)) giving 5 independent constants. See 10.2.1 in the Users' Manual

Thomas Wong Consulting
Sep-01
Phone: 714.826.3235
Fax: 714.826.3528
tgwongconsulting@cs.com

Nippon Graphite Fiber

Property	Units	RS-3C
Fiber Modulus	Msi	
Fiber Tensile Strength	Ksi	
Fiber Thermal Conductivity	W/m-K	
Unid. Mechanical Properties		Epoxy
0° Tension Modulus	ksi	430.0
0° Tension Strength	ksi	12
0° Compression Modulus		
0° Compression Strength		
0° Flexure Modulus	Msi	481.0
0° Flexure Strength	Ksi	18.4
90° Tension Modulus		
90° Tension Strength		
SBS Strength		
45° In-Plane Shear Modulus		
45° In-Plane Shear Strength		
Lam. Thermal Conductivity (0)		

		2.965E+09
		79979185
		3.316E+09
		126863534

		pa
		pa
		pa
		pa

Mylar density 1390 g/m^3
elastic ########## pa

Appendix B. YSH-70-A/RS-3C Material Property Calculation Code

This code is the MATLAB code that was used to solve the material properties of the YSH-70-A/RS-3C composite.

```
function
[wr,Ex,Ey,Exb,Eyb,Vxy,Vyx,Gxy,Gxz,Gyz,Gxyb,E1,E2,G12]=LAMINATE_NASA_HAL
PIN_HYBRID_BASELINE_FUNC(l,b,h,alpha,theta_d,prnt)
    %
[wr,Ex,Ey,Exb,Eyb,Vxy,Vyx,Gxy,Gxz,Gyz,Gxyb,E1,E2,G12]=LAMINATE_NASA_HAL
PIN_HYBRID_BASELINE_FUNC(40E-3,2.5E-3,140E-6,0,[0 90 0],1)
    % Inputs:
    % (l)       beam length (m)
    % (b)       width of beam (m)
    % (h)       laminate thickness in meters (m)
    % (alpha)   angle of laser cut
    % (theta_d) laminate layup in degrees [0 90 0],[0 45 -45 0)
    % (prnt)    (0 = no) (1 = yes) to print values
    % ----------------------------------------
    % Outputs:
    % [wr]  First Resonant Frequency of the beam
    % [Ex]  Laminate Axial Stiffness
    % [Ey]  Laminate 90 Axial Stiffness
    % [Vxy] Laminate Poissons Ratio
    % [Vyx] Laminate Poissons Ratio
    % [Gxy] Laminate Shear Modulus x-y direction
    % [Gxz] Laminate Shear Modulus x-z direction
    % [Gxy] Laminate Shear Modulus y-z direction
    % [E1]  Lamina Axial Modulus
    % [E2]  Lamina 90 Axial Modulus
    % [G12] Lamina Shear Modulus

    %% Input Fiber and Matrix Values
    Ef = 6.55E11;      % (pa)      - Elastic Modulus of Fiber (YSH-70A)
    %Ef = 9.23E11;     % (pa)      - Elastic Modulus of Fiber (YSH-95A)
    Em = 2E9;          % (pa)      - Elastic Modulus of Matrix (RS-3C)
    Gf = 6.57E9;       % (pa)      - *Shear Modulus of the Fiber
(Estimate)
    Gm = 3.316E9;      % (pa)      - Shear Modulus of the Matrix (RS-
3C) - http://www31.ocn.ne.jp/~ngf/english/product/p1.htm
    vf = 0.3;          %    - Poisson's Ratio of the Fiber (YSH-70A)
    vm = 0.3;          %            - Poisson's Ratio of the Matrix
(RS-3C)
    df = 2140;         % (kg/m^3)  - Density of the Fiber  (YSH-70A)
    dm = 1193;         % (kg/m^3)  - Density of the Matrix (RS-3C)
    Vf = 0.639;        %           - *Fiber Volume Fraction (YSH-70A)
(estimate)
    Vm = 1 - Vf;       %           - Matrix Volume Fraction
    tf = 7E-6;         % (m)       - Fiber Diameters
    theta_d = theta_d + alpha; %- Fiber Orientation +/- Laser Cut angle
    theta_r = theta_d * pi / 180;% - Layer Fiber Orientation in Radians
   t=h/length(theta_r);%- Lamina Thickness based on Laminate Thickness
Input
    H = h/2;             - Half laminate thickness (Fig 5.2 Herakovich)
```

```
    NL = length(theta_r);           % Number of Layers
    Le = b./sin(theta_r); % (m) - Effective Fiber Length based on theta
and beam width

    %% Make Sure Le is calculated properly
    for x=1:NL
        if theta_d(x) == 0, LE = l; end %    - Account for Divide by 0
        if Le(x) > l,Le(x)=l; end %   - This is ~0-4 degrees @ 2.5 mm
    end
    %% Halpin-Tsai Calculations - Account for Fiber Orientation and
Effective Fiber Length
    %  pg 350 first paragraph
http://www.abdmatrix.com/phcdl/upload/fundamentals/Halpin-
Tsai%20Equations-A%20Review.pdf
    %  The hybrid implmentation of this only uses E1 from Halpin-Tsai,
other
    %  values follow the standard calcs from Herakovich
    %  the values suggested by the Halpin-Tsai paper produced E2,G12
values
    %  that were excessively high based on the estimate of [2 1] for
zeta.
    MAT=zeros(NL,6);         % Pre-Allocate MAT ARRAY

    if prnt==1
        fprintf('Halpin-Tsai Calculations\n')
    end

    for x=1:NL
        zeta(x,:) = [2*Le(x)/tf 1E6 1E6]; % Halpin-Tsai zeta factors
[zeta1 zeta2 zeta3]
        ada(x,:)  = (Ef-Em)./(Ef+zeta(x,:)*Em); % ada=[ada1 ada2 ada3]
        E=Em.*(1+zeta(x).*ada(x)*Vf)./(1-ada(x,:)*Vf); % E=[E1 E2 G12]
        E1=E(1);                % Only use E1, ignore E2 and G12
        E2=Em/(Vf*(Em/Ef-1)+1); %(11.14 - Herakovich)
        v12=Vf*(vf-vm)+vm;      %(11.9  - Herakovich)
        v21=E2/E1*v12;          %pg4 - http://pas.ce.wsu.edu/CE537-
1/Lectures/Rule%20of%20Mixtures.pdf
        G12=1/(Vf/Gf+Vm/Gm);    %(11.23 - Herakovich)
        G13=G12;
        G23=E2/2*(1+v12);
        Den=df*Vf+dm*Vm;
        MAT(x,:)=[E1 E2 G12 v12 v21 Den];%Store Lamina
        if prnt==1
            fprintf(' E1=%E E2=%E v12=%f G12=%E Den = %E\n',…
            [E1 E2 v12 G12 Den])
        end
    end
    %% Compute Layer Height Data
    range=zeros(1,NL+1);
    for x = 1:NL+1
        if x == 1
            range(x) = NL*t/2;
        else
            range(x) = NL*t/2-t*(x-1);
        end
    end
```

```
    %% Compute Qp Matrix
    % Q_Global based on varying Zeta Values due to Le differences for
each Lamina
    Q=zeros(3,3,NL);
    for x = 1:NL
        E1=MAT(x,1);E2=MAT(x,2);G12=MAT(x,3);v12=MAT(x,4);v21=MAT(x,5);
        Q11 = E1/(1-v12*v21);       %(4.16  - Herakovich)
        Q12 = (v12*E2)/(1-v12*v21); %(4.16  - Herakovich)
        Q22 = E2/(1-v12*v21);       %(4.16  - Herakovich)
        Q66 = G12;                  %(4.16  - Herakovich)
        Q(:,:,x)=[Q11 Q12 0;Q12 Q22 0;0 0 Q66];%Global Q for Lamina
    end
    % Init A,B,D matrices
    A=zeros(3,3);
    B=zeros(3,3);
    D=zeros(3,3);
    % Q_ply and A,B,D Matrices
    for x=1:NL
        m=cos(theta_r(x));
        n=sin(theta_r(x));
        T=[m^2 n^2 2*m*n;n^2 m^2 -2*m*n;-m*n m*n m^2-n^2];% Motavalli
p137

        QP= T*Q(:,:,x)*T'; % Motavalli p137 - QP is different for each
lamina
        A=A+QP*(range(x)-range(x+1));
        B=B+1/2*QP*(range(x)^2-range(x+1)^2);
        D=D+1/3*QP*(range(x)^3-range(x+1)^3);
    end

    %% Compute Global Laminate Properties
    %          z
    %    ______|______
    %   |      |      |
    % h |      |------|-----> y  (b = width)
    %   |______________|          (h = height)
    %          b
    % X-axis is along the length of the beam
    % Y-Axis is along the width of the beam
    % Z-Axis is along the thickness of the beam

    %% Compute Global Laminate Properties - Axial (NASA)
    ABD=[A B;B D]; % Assembled ABD Matrix
    Ex=1/h*det(ABD)/det(ABD([2 3 4 5 6],[2 3 4 5 6])); % Simplified
Using Cofactor Expansion about 1 - NASA(84)
    Ey=1/h*det(ABD)/det(ABD([1 3:6],[1 3:6])); % Simplified Using
Cofactor Expansion about 2 - NASA(85)

    astar=2*H*inv(A); %(5.80  - Herakovich)
    Vyx=-astar(1,2)/astar(1,1); % Motavalli p100
    Vxy=-astar(1,2)/astar(1,1); % Motavalli p100
    Gxy=1/h*det(ABD)/det(ABD([1 2 4 5 6],[1 2 4 5 6])); % Simplified
Using Cofactor Expansion about 3 - NASA(89)
    Gxz=Gxy;
    Gyz=Ey/2*(1+Vxy);
```

```
    %% Compute Global Laminate Properties - Bending (NASA)
    Exb=12/h^3*det(ABD)/det(ABD([1 2 3 5 6],[1 2 3 5 6]));  %
Simplified Using Cofactor Expansion about 4
    Eyb=12/h^3*det(ABD)/det(ABD([1 2 3 4 6],[1 2 3 4 6]));  %
Simplified Using Cofactor Expansion about 5
    Gxyb=12/h^3*det(ABD)/det(ABD([1 2 3 4 5],[1 2 3 4 5])); %
Simplified Using Cofactor Expansion about 6
```

Appendix C. Beam .inp File Generator Function

This Code was developed to generate the .inp file for the wire beam used in Chapter 3.

```
function [Eigen_value]=Vary_Properties_Beam(alpha,theta_original,h,t)

%Frequency
num_modes = 1; %the number of modes you wish to find
clamped_nodes = 1; %nodes you wish to clamp i.e. the base
h1= h;
den_cf = 1750;% density of the carbon-fiber composite
%% Variables
%scale nodes
%note, made root of wing = 0,0.
x_offset=0; %move nodes in x dir
y_offset=0.0; %move nodes in y dir
wing_length = 0.04; %desired length of wing in meters
%file name
File = 'Beam_Test_out'; % Name of the file created, remember to change
% on final line of code for evaluation
Node_File = 'Beam_Test';  % Name of file where nodes are located
NodesMax = 0; %number of nodes that exist (claculated later)
%% Open the File
fid2=fopen([File '.inp'],'w'); % Open file for writing, new file

%% Heading
% Standard Abaqus Heading
fprintf(fid2,'*Heading\n');
fprintf(fid2,'** Job name: BEAM_MODAL_BASELINE Model name: %s\n',date);

%% Contact
% Contact within model
fprintf(fid2,'*Preprint, echo=NO, model=NO, history=NO, contact=NO\n');
fprintf(fid2,'**\n');

%% Parts
% Parts (doesn't change for this case)
fprintf(fid2,'** PARTS\n');
fprintf(fid2,'*Part, name=WING_FIT_SHOULDER_EE_%s\n',date); % name
called up in instance
fprintf(fid2,'**\n');
fprintf(fid2,'*End Part\n');
fprintf(fid2,'**\n');
fprintf(fid2,'**');

%% Assembly
%insert the Assembly section (doesn't change for this case)
fprintf(fid2,'** ASSEMBLY\n');
fprintf(fid2,'**\n');
fprintf(fid2,'*Assembly, name=Assembly\n');
fprintf(fid2,'**\n');

%% Instance
% Insert the Instance section
```

```
fprintf(fid2,'*Instance,name=Part-1-1,
part=WING_FIT_SHOULDER_EE_%s\n',date);% name called from parts

%% Insert the nodes from the veins
%Standard Heading
fprintf(fid2,'*Node'); %heading for the nodes
fprintf(fid2,'\n');
% Take the nodes out of another inp file.
fid1=fopen([Node_File '.inp'],'r+'); % Open file for reading/writing
idx = 0;
while ~feof(fid1)
    idx = idx + 1;
    tline=fgetl(fid1);
    if isempty(strfind(tline,'*Node')) == 0 % Scan till *Nodes

        for i=1:2000000000
            tline=fgetl(fid1);
            if isempty(strfind(tline,'*')) == 0% Scan till * Found
                NodesMax=i-1;%calculate the new value of maximum nodes
                break
            else
                nodes(i,:)=sscanf(tline,'%d,%f,%f,%f')';
            end
        end
        break
    end
end
fclose(fid1);

% for loop to print nodes into the .inp file
% nodes will be scaled at this time
node_scale = wing_length/(max(nodes(:,2))); %sets scale = to desired
legnth
fprintf(fid2,'%d, %2.10f, %2.10f, %2.10f\n',[nodes(:,1),...
(nodes(:,2)-x_offset)*node_scale,
(nodes(:,3)-y_offset)*node_scale,
nodes(:,4)]');

%% Elements
% For beam elements
fprintf(fid2,'*Element, type=B32'); %heading for the elements
fprintf(fid2,'\n');

%Search Input File for *Elem Locations
fid1=fopen([Node_File '.inp'],'r+'); % Open file for reading/writing
idx = 0;
while ~feof(fid1)
    idx = idx + 1;
    tline=fgetl(fid1);
    if isempty(strfind(tline,'*Element, type=B32')) == 0 % ''
        for i=1:NodesMax                    % Scan till * Found
            tline=fgetl(fid1);
            if isempty(strfind(tline,'*')) == 0
                break
            else
```

```
elems.B32(i,:)=sscanf(tline,'%f,%f,%f,%f,%f,%f,%f,%f,%f')';
            end
        end
        break
    end
end
fclose(fid1);
% Write nodes into the program file
fprintf(fid2,'%d,%6.0f,%6.0f,%6.0f\n',[elems.B32]');

%% Read Stringer Node Sets

%Search Input File for Stringer Nsets
fid1=fopen([Node_File '.inp'],'r+'); % Open file for reading/writing
for j=1:12 %(Number of Stringers)
    idx = 0;
    Stringers(j).nset=[];
    while ~feof(fid1)
        idx = idx + 1;
        tline=fgetl(fid1);
        if isempty(strfind(tline,['*Nset, nset=_Stringer-' num2str(j)
', internal'])) == 0 % ''
            for i=1:NodesMax                    % Scan till * Found
                tline=fgetl(fid1);
                if isempty(strfind(tline,'*')) == 0
                    break
                else
                    Stringers(j).nset=[Stringers(j).nset
sscanf(tline,'%f,')'];
                end
            end
            break
        end
    end
end
fclose(fid1);

%% Calculate Angle between the Stringer B32 Elements
% needed to determine material properties.
for m = 1:(length(elems.B32(:,1)))
    %determine the first node that is part of the element i.e x
coordinate
    node_str = elems.B32(m,2);
    %determine the second (mid point) node of the element i.e y
coodiinate
    node_end = elems.B32(m,3);
    %location of first node
    loc_str =
[(nodes(node_str,2)),(nodes(node_str,3)),(nodes(node_str,4))];
    % location of the end node
    loc_end =
[(nodes(node_end,2)),(nodes(node_end,3)),(nodes(node_end,4))];
    % determine the slope of the line
    slope_2 = (loc_str(1,2) - loc_end(1,2))/(loc_str(1,1) -
loc_end(1,1));
```

```
    %determine the angle with horizontal [inf,0,0] vector from origin
    theta_elem = atand(slope_2);
    %store it!
    angle(m,1)=m; %stores the row number in angle in 1st column
    angle(m,2)= elems.B32(m,1); %the 2nd column hold element number
    angle(m,3)=theta_elem; % 3rd column holds the angle
end

%% Write Nset and Elsets
% For the beam
set_ctr=0; %counts the number of Node and Element Sets
% Create a new section for each Vein element
for x=1:length(angle)
    %create heading and pick a Nset
    fprintf(fid2,'*Nset, nset=_PickedSet%-2.0f,
internal\n',angle(x,1));
    nset_nodes = sort(elems.B32(x,2:4));%sort out the nodes in
asscending order
    %print nodes in that Nset i.e. for each element
    fprintf(fid2,'%6.0f, %6.0f,
%6.0f\n',nset_nodes(1),nset_nodes(2),nset_nodes(3));

    % for Elsets, create elset same number as corresponding Nset
    fprintf(fid2,'*Elset, elset=_PickedSet%-2.0f,
internal\n',angle(x,1));
    fprintf(fid2,'%6.0f\n',angle(x,2));

    set_ctr=set_ctr+1; %add to Set counter
end

%% Beam Sections
% The sections will start with the veins and begin with Section 1 (B32)
for x=1:length(angle) % new section for each element
    fprintf(fid2,'** Section: Section-%-2.0f  Profile: Profile-%-
2.0f\n'...
        ,x,x); % create section/profile
    fprintf(fid2,...
        '*Beam Section, elset=_PickedSet%-2.0f, material=Material-%-
2.0f, temperature=GRADIENTS, section=I\n'...
        ,x,x); % match the element with it's own elset and material

    b(x)=2.5e-3;%artificial width of the beam element

    % Generate the I beam sections
    theta = angle(x,3)+theta_original(1,:); %determine theta
    %For the top ply run a function to determine Matl Prop
    [~,Ex,Ey,~,~,Vxy,Vyx,Gxy,Gxz,Gyz,~,~,~,~]=...
        LAMINATE_NASA_HALPIN_HYBRID_BASELINE_FUNC(40E-
3,b(x),h,alpha,theta(1,1),0);
    % Capture the Mat Properties so we don't have to run this again
Matl_Ex(x,1) = Ex; Matl_Ey(x,1) = Ey; Matl_Vxy(x,1) = Vxy;
Matl_Vyx(x,1) = Vyx;
Matl_Gxy(x,1) = Gxy; Matl_Gxz(x,1) = Gxz;Matl_Gyz(x,1) = Gyz;
    %Second ply
[~,Ex,Ey,~,~,Vxy,Vyx,Gxy,Gxz,Gyz,~,~,~,~]=...
```

```
LAMINATE_NASA_HALPIN_HYBRID_BASELINE_FUNC(40E-
3,b(x),h,alpha,theta(1,2),0);
    Matl_Ex(x,2) = Ex; Matl_Ey(x,2) = Ey; Matl_Vxy(x,2) = Vxy;
Matl_Vyx(x,2) = Vyx;
    Matl_Gxy(x,2) = Gxy; Matl_Gxz(x,2) = Gxz;Matl_Gyz(x,2) = Gyz;
    %Third ply
    [~,Ex,Ey,~,~,Vxy,Vyx,Gxy,Gxz,Gyz,~,~,~,~]=...
        LAMINATE_NASA_HALPIN_HYBRID_BASELINE_FUNC(40E-
3,b(x),h,alpha,theta(1,3),0);
    Matl_Ex(x,3) = Ex; Matl_Ey(x,3) = Ey; Matl_Vxy(x,3) = Vxy;
Matl_Vyx(x,3) = Vyx;
    Matl_Gxy(x,3) = Gxy; Matl_Gxz(x,3) = Gxz;Matl_Gyz(x,3) = Gyz;

    % Use largest value of Ex to decide value for the effective modulus
    % This prevents the width of some sections from being too large.
    Eff_Mod = max(Matl_Ex(x,:)); %determines max Ex
    width(x,1)= Matl_Ex(x,1)/Eff_Mod; %makes the width of each section
a scaler, with largest being = 1
    width(x,2)= Matl_Ex(x,2)/Eff_Mod;
    width(x,3)= Matl_Ex(x,3)/Eff_Mod;

    % Prevent I(12)*2 from being > I(11)+I(22)
    if width(x,1)< width(x,2)/7.5
        width(x,1)=width(x,2);
        h_new=h/(3-(width(x,2)/(min(width(x,:)))));
        h=h_new;
    end
    if width(x,3)< width(x,2)/7.5
        width(x,3)=width(x,2);
        h_new=h1/(3-(width(x,2)/(min(width(x,:)))));
        h=h_new;
    end

    % Calculate the effective density for the Beam Sections
    real_area = h1*b(x); %real cross sectional area of the element
    faux_area = h*b(x)*(width(x,1)/3 + width(x,2)/3 + width(x,3)/3);
%area of I-beam section
    area_scale = real_area/faux_area; %scale factor to multiply density
by so mass is same for all elements
    Density(x)=den_cf*area_scale;

    % prints out in (l, h, b1(base width), b2 (top width), t1 (base),
t2(top), t3(mid width))
    fprintf(fid2,'% #6.12g, % #6.12g, % #6.12g, % #6.12g, % #6.12g, %
#6.12g, % #6.12g\n',...
        h/2,h,b(x)*width(x,3),b(x)*width(x,1),h/3,h/3,b(x)*width(x,2));
    %prints out the orientation of the beam, same for all cases
    fprintf(fid2,'0.,1.,0. \n');

    % put thickness back to original thickness
    h=h1;
end

%% End Instance
fprintf(fid2,'*End Instance\n');
fprintf(fid2,'**\n');
```

```
%% Nset for boundry conditions
%create a set of nodes where the boundry conditions will be applied
fprintf(fid2,'*Nset, nset=_PickedSet%-2.0f, internal, instance=Part-1-
1\n'...
    ,(set_ctr+3));
%Put in the nodes you wish to clamp in this case the base
fprintf(fid2,'%d,\n',clamped_nodes);

%% End Assembly
fprintf(fid2,'*End Assembly\n'); %ends the assembly portion of it
fprintf(fid2,'**\n');

%% Materials
%Standard Heading
fprintf(fid2,'** MATERIALS\n');
fprintf(fid2,'**\n');

% Determine and Assign Matl Prop for the Veins (B32 elements)
for x=1:size(angle,1)
    theta = angle(x,2)+theta_original(1,:);
    %set up material properties
    fprintf(fid2,'*Material, name=Material-%-2.0f\n',x);
    fprintf(fid2,'*Density\n');
    fprintf(fid2,'%#6.6f\n',Density(x));
    fprintf(fid2,'*Elastic, type=ENGINEERING CONSTANTS\n');

    % Use the material propertie saved from Section section
    % determine which properties to use
    ctr=max(Matl_Ex(x,:));
    if Matl_Ex(x,1) == ctr;
        ctr = 1;
    elseif Matl_Ex(x,2) == ctr;
        ctr=2;
    elseif Matl_Ex(x,3) == ctr;
        ctr=3;
    end
    fprintf(fid2,'%#12.6g, %#12.6g, %#12.6g, %#12.6g, %#12.6g, %#12.6g,
%#12.6g, %#12.6g,\n'...
        ,Matl_Ex(x,ctr),Matl_Ey(x,ctr),Matl_Ey(x,ctr),0.1,0.1,0.1,...
        Matl_Gxy(x,ctr),Matl_Gxz(x,ctr));
    fprintf(fid2,'%#12.6g,\n',Matl_Gyz(x,ctr));
end

%% Step
%Standard Heading
fprintf(fid2,'** ----------------------------------------------------------
----------\n');
fprintf(fid2,'** \n');
fprintf(fid2,'** STEP: Step-1\n');
fprintf(fid2,'**\n');

%since there is only one step and we always want to find freqency,
it'll look like this
fprintf(fid2,'*Step, name=Step-1, perturbation\n');
```

```
fprintf(fid2,'Find Freq. \n');
fprintf(fid2,'*Frequency, eigensolver=Lanczos, acoustic coupling=on,
normalization=displacement\n');
fprintf(fid2,'%6.0f, , , , ,\n',num_modes);

%% Boundry Conditions
% Standard Heading
fprintf(fid2,'** \n');
fprintf(fid2,'** BOUNDARY CONDITIONS\n');
fprintf(fid2,'** \n');

%create a boundry condition (in this case it will be fixed)
fprintf(fid2,'** Name: BC-1 Type: Displacement/Rotation\n'); %since
only one, can fix 6 dof, says type of boundry cond
fprintf(fid2,'*Boundary\n');%tells abaqus there is a boundry conditon
fprintf(fid2,'_PickedSet%-2.0f, 1, 1\n',(set_ctr+3));%hold in x or 1
dir
fprintf(fid2,'_PickedSet%-2.0f, 2, 2\n',(set_ctr+3));%hold in y or 2
dir
fprintf(fid2,'_PickedSet%-2.0f, 3, 3\n',(set_ctr+3));%hold in z or 3
dir
fprintf(fid2,'_PickedSet%-2.0f, 4, 4\n',(set_ctr+3));%hold in rot about
1 axis
fprintf(fid2,'_PickedSet%-2.0f, 5, 5\n',(set_ctr+3));%hold in rot about
2 axis
fprintf(fid2,'_PickedSet%-2.0f, 6, 6\n',(set_ctr+3));%hold in rot about
3 axis

%% Outputs
%Standard Heading
fprintf(fid2,'**\n');
fprintf(fid2,'** OUTPUT REQUESTS\n');
fprintf(fid2,'**\n');

%Frequency outputs (in this case it does not change)
fprintf(fid2,'*Restart, write, frequency=0\n');
fprintf(fid2,'** \n');
fprintf(fid2,'** FIELD OUTPUT: F-Output-1\n');
fprintf(fid2,'** \n');
fprintf(fid2,'*Output, field, variable=PRESELECT\n');

%% End Step
fprintf(fid2,'*End Step\n');

%% Close the File
fclose(fid2);
%% Run
% This line runs the completed file
eval(['dos(''abq6102 job=Beam_Test_out.inp interactive'')'])

%% Open .dat File
%Gather the results from the .dat file and store in a matrix
fid3=fopen([File '.dat'],'r+'); % Open file for reading/writing
idx = 0;
while ~feof(fid3)
```

```
    idx = idx + 1;
    tline=fgetl(fid3);
    if isempty(strfind(tline,'E I G E N V A L U E   O U T P U T '))
== 0 % Scan till *Nodes
         for i=1:5
            tline=fgetl(fid3); % Read 5 lines of blank stuff
         end
         Eigen_value_string=fgetl(fid3);%calculate the new value of
maximum nodes
         make_text =  str2num(Eigen_value_string); %converts text into
numbers MATLAB can read
         Eigen_value = make_text(1,4); % gets the Frequency from the
string of numbers
    end
end

fclose(fid3); % Close the File
```

Appendix D. Beam .inp File

This is the original .inp file that was solved for the wire beam element.

```
*Heading
** Job name: Beam_Test Model name: Model-1
** Generated by: Abaqus/CAE 6.10-2
*Preprint, echo=NO, model=NO, history=NO, contact=NO
**
** PARTS
**
*Part, name=Part-1
*End Part
**
** ASSEMBLY
**
*Assembly, name=Assembly
**
*Instance, name=Part-1-1, part=Part-1
*Node
      1,          0.,          0.,          0.
      2,          4.,          0.,          0.
      3,          8.,          0.,          0.
      4,         12.,          0.,          0.
      5,         16.,          0.,          0.
      6,         20.,          0.,          0.
      7,         24.,          0.,          0.
      8,         28.,          0.,          0.
      9,         32.,          0.,          0.
     10,         36.,          0.,          0.
     11,         40.,          0.,          0.
     12,          2.,          0.,          0.
     13,          6.,          0.,          0.
     14,         10.,          0.,          0.
     15,         14.,          0.,          0.
     16,         18.,          0.,          0.
     17,         22.,          0.,          0.
     18,         26.,          0.,          0.
     19,         30.,          0.,          0.
     20,         34.,          0.,          0.
     21,         38.,          0.,          0.
*Element, type=B32
 1,  1, 12,  2
 2,  2, 13,  3
 3,  3, 14,  4
 4,  4, 15,  5
 5,  5, 16,  6
 6,  6, 17,  7
 7,  7, 18,  8
 8,  8, 19,  9
 9,  9, 20, 10
10, 10, 21, 11
*Nset, nset=_PickedSet2, internal, generate
```

```
  1,  21,   1
*Elset, elset=_PickedSet2, internal, generate
  1,  10,   1
*Nset, nset=_PickedSet4, internal, generate
  1,  21,   1
*Elset, elset=_PickedSet4, internal, generate
  1,  10,   1
*Orientation, name=Ori-1
1., 0., 0., 0., 1., 0.
1, 0.
** Section: Section-1  Profile: Profile-1
*Beam Section, elset=_PickedSet2, material=Material-1, temperature=GRADIENTS, section=I
0.5, 1., 2.5, 2.5, 0.33, 0.33, 1.
0.,0.,-1.
*End Instance
**
*Nset, nset=_PickedSet4, internal, instance=Part-1-1
 1,
*End Assembly
**
** MATERIALS
**
*Material, name=Material-1
*Density
1785.,
*Elastic
 4.15e+09, 0.28
** ----------------------------------------------------------------
**
** STEP: Step-1
**
*Step, name=Step-1, perturbation
*Frequency, eigensolver=Lanczos, acoustic coupling=on, normalization=displacement
10, , , , ,
**
** BOUNDARY CONDITIONS
**
** Name: BC-1 Type: Displacement/Rotation
*Boundary
_PickedSet4, 1, 1
_PickedSet4, 2, 2
_PickedSet4, 3, 3
_PickedSet4, 4, 4
_PickedSet4, 5, 5
_PickedSet4, 6, 6
**
** OUTPUT REQUESTS
**
*Restart, write, frequency=0
**
** FIELD OUTPUT: F-Output-1
**
```

Appendix E. Fiber Angle Measurement MATLAB Code

This is the MATLAB code developed to measure the angle of the fibers in the images taken by the optical microscope of the carbon composite.

```
%Find the angle of the fiber orientation vs the edge
% click along the edge first, then click 5 fibers (10 clicks) on random
% fibers to find the average fiber orientation of the specimen
clc,clear,close all
%% First, let's read all the data-sets from the dam0.unv file
[FileName,PathName] = uigetfile('*.tif*','0');
File = FileName(1:findstr(FileName,'.')-1);
Ext = FileName((findstr(FileName,'.')+1):length(FileName));

%% Read in Moth image
I = imread([PathName FileName]);

%% Plot the picture in a figure
imshow(I);

%% Pick 3 Points on the image
%  location is in pixels
warndlg('Pick the first set of six Fibers!!','!! Warning !!')
[x,y]=ginput(12);
%% Save .mat file with image filename
save([File '.mat'])
%first fiber
Theta_Fiber1=abs(atand((y(2)-y(1))/(x(2)-x(1))));%pick one orientation
first
Theta_Fiber2=abs(atand((y(3)-y(4))/(x(3)-x(4))));% pick one fiber
Theta_Fiber3=abs(atand((y(5)-y(6))/(x(5)-x(6))));% pick second fiber
Theta_Fiber4=abs(atand((y(7)-y(8))/(x(7)-x(8))));% pick third fiber
Theta_Fiber5=abs(atand((y(9)-y(10))/(x(9)-x(10))));% pick fourth fiber
Theta_Fiber6=abs(atand((y(11)-y(12))/(x(11)-x(12))));% pick fifth fiber
Theta_Fiber_avg1 = (Theta_Fiber1 + Theta_Fiber2 + Theta_Fiber3 +
Theta_Fiber4...
    + Theta_Fiber5)/5;%find average

warndlg('Pick the second set of six Fibers!!','!! Warning !!')
[x,y]=ginput(12);
%second fiber
Theta_Fiber1=abs(atand((y(2)-y(1))/(x(2)-x(1))));%pick one orientation
first
Theta_Fiber2=abs(atand((y(3)-y(4))/(x(3)-x(4))));% pick one fiber
Theta_Fiber3=abs(atand((y(5)-y(6))/(x(5)-x(6))));% pick second fiber
Theta_Fiber4=abs(atand((y(7)-y(8))/(x(7)-x(8))));% pick third fiber
Theta_Fiber5=abs(atand((y(9)-y(10))/(x(9)-x(10))));% pick fourth fiber
Theta_Fiber6=abs(atand((y(11)-y(12))/(x(11)-x(12))));% pick fifth fiber
Theta_Fiber_avg2 = (Theta_Fiber1 + Theta_Fiber2 + Theta_Fiber3 +
Theta_Fiber4...
    + Theta_Fiber5)/5;%find average

Theta = abs(Theta_Fiber_avg2-Theta_Fiber_avg1)
```

Appendix F. Beam Monte Carlo Code

This developed MATLAB code was used to submit multiple .inp files used in the Monte Carlo Solution to MATLAB. Data was then stored in a matrix and plotted when the solution was finished running.

```
clc,clear all; close all;
%% Define Number of Cases to Run
NumCases=7500;
%% Definite Variation in Laser to Fiber Orientation
pm=5; %This represents +/-
nstd_alpha=1;
avg_alpha=2.5;
alpha=avg_alpha+pm*rand(NumCases,1)-pm/2;
alpha=[alpha alpha alpha];
%% Define Variation in Lamina Layup Orientation
pm=10; %This represents +/-
nstd_theta=1;
avg_theta=2.5;
theta_original = avg_theta+pm*rand(NumCases,3)-pm/2;
theta_original(:,2)=90-theta_original(:,2);
%% Define Variation in Laminate Thickness
pm=10;
nstd_t=1;
avg_thickness=145;
h = avg_thickness+pm*rand(NumCases,1)-pm/2;
h = h*1E-6; %convert from integers to microns
%% Define Parameter Estimates
[ahat,bhat,ACI,BCI] = unifit(theta_original,.01);

%% Run the Analysis
for t=1:NumCases

[Eigen_value(t,:)]=Vary_Properties_Beam(alpha(t),theta_original(t,:),h(
t),t);
end

%% Plot the Results Histogram – Modal Frequency
close all
% Open a Figure the size of the screen
scrsz = get(0,'ScreenSize');
figure('Position',[1 scrsz(2) scrsz(3) scrsz(4)])

nbins=100;
subplot(331)
hist(alpha,nbins)
grid on
xlabel(['Alpha = Mean ' num2str(avg_alpha) ' deg | std = '
num2str(nstd_alpha)])
ylabel('Bins')

subplot(332)
```

```
hist(theta_original(:,1),nbins)
grid on
xlabel(['Theta = Mean ' num2str(avg_theta) ' deg | std = '
num2str(nstd_theta)])
ylabel('Bins')

subplot(333)
hist(h(:,1)*1E6,nbins)
grid on
xlabel(['Thickness = Mean ' num2str(avg_thickness) ' um | std = '
num2str(nstd_t)])
ylabel('Bins')

subplot(3,3,4:6)
hist(Eigen_value,nbins)
grid on
xlabel('Frequency (Hz)')
ylabel('Bins')
title(['Mean freq = ' num2str(mean(Eigen_value),'%f') ' (Hz)'])

subplot(3,3,7:9)
plot(1:NumCases,Eigen_value,'.','MarkerSize',8)
grid on
xlabel('Sample')
ylabel('Frequency (Hz)')
hold on
plot([0 NumCases],mean(Eigen_value)*[1 1],'--g','LineWidth',2)
legend('Samples','Mean','Location','SouthEast')
title(['Mean freq = ' num2str(mean(Eigen_value),'%f') ' (Hz), Max freq
= ' num2str(max(Eigen_value),'%f') ' (Hz), Min freq = '
num2str(min(Eigen_value),'%f') ' (Hz)'])
hold off
```

Appendix G. Wing Develop .inp File Code

This is the code that was used to develop the FEA model of the Engineered wing.

```
function[Eigen_value1,Eigen_value2]=Final_Wing(alpha,theta_original,h,t
)
%function-Outputs = First and Second Modal Frequency
      Inputs = laser cut angle, ply orientation, thickness, run number
%File names
Input_File = 'Wing_Shoulder_Eng_Doe.inp'; % Name of the file created
with extension
Node_File = 'WING_FIT_SHOULDER_DD.inp';  % Name of file where nodes are
located with extension

%Scale Nodes
%Note, make root of wing = 0,0.
x_offset=0; %Move nodes in x dir
y_offset=0.592322826000000; %Move nodes in y dir
wing_length = 0.05; %Desired length of wing in meters

%Scale of the wing
%Begining and ending width of the vein, linearly tapering in meters x
10^5
Costa = [75 20]; %Costa Vein
Radius = [80 60]; % Radius Veins
Archulus = [60 35];% Archulus
RMCA = [55 15]; % Rest of the veins

StringersWidth=[Costa; % Stringer 1 - Leading Edge Vein
                Costa; % Stringer 2
                Costa; % Stringer 3
                Radius; % Stringer 4 - Medial Vein
                Archulus; % Stringer 5 - Arculus Vein
                RMCA; % Stringer 6
                RMCA; % Stringer 7
                RMCA; % Stringer 8
                RMCA; % Stringer 9
                RMCA; % Stringer 10
                RMCA; % Stringer 11
                RMCA;]*1E-5; % Stringer 12

%Material Properties
%Carbon fiber – IDEAL VALUES
% alpha = 0; %Angle misallignment placed in laser
% theta_original= [0 90 0]; %Fiber orientation
% h = 150e-6; %Thickness

%Material Properties
%Carbon fiber
h1 = h; %Thickness part 2, must be same as h (used to reset h in some
calc)
den_cf = 1790*0.88;% Density of the carbon-fiber composite
%Membrane
shell_thick = 20.0e-6; %Thickness of the membrane (um)
```

```
den_sh = 1420*0.88; %Density of the Mylar membrane (kg/m^3)
shell_E = 2.5E9; %Modulus of Membrane (GPa)
shell_v = 0.3; %Poisson's Ratio of Membrane

%Nodes
Base_Node_Loc= [2,48,51,280,283,942,1269]; %Node number where you want
to apply the Boundry Condition.
Pt_Node_Loc = 1108; % Node number where Pt load is applied

%Frequency
num_modes = 9; %The number of modes you wish to find

%Point Load
Pt_Load = -0.001; %The force you want to put on the tip of the wing

%% Open the File
fid2=fopen(Input_File,'w'); % Open file for writing, new file

%% Heading
% Standard Abaqus Heading
fprintf(fid2,'*Heading\n');
fprintf(fid2,'** Job name: BEAM_MODAL_BASELINE Model name: %s\n',date);

%% Contact
% Contact within model
fprintf(fid2,'*Preprint, echo=NO, model=NO, history=NO, contact=NO\n');
fprintf(fid2,'**\n');

%% Parts
% Parts (doesn't change for this case)
fprintf(fid2,'** PARTS\n');
fprintf(fid2,'*Part, name=WING_FIT_SHOULDER_EE_%s\n',date); % name
called up in instance
fprintf(fid2,'**\n');
fprintf(fid2,'*End Part\n');
fprintf(fid2,'**\n');
fprintf(fid2,'**');

%% Assembly
%insert the Assembly section (doesn't change for this case)
fprintf(fid2,'** ASSEMBLY\n');
fprintf(fid2,'**\n');
fprintf(fid2,'*Assembly, name=Assembly\n');
fprintf(fid2,'**\n');

%% Instance
% Insert the Instance section
fprintf(fid2,'*Instance, name=Part-1-1,
part=WING_FIT_SHOULDER_EE_%s\n',date);% name called from parts

%% Insert the nodes from the veins
%Standard Heading
fprintf(fid2,'*Node'); %heading for the nodes
fprintf(fid2,'\n');
```

```
NodesMax = 0; %Placeholder for number of nodes counter (cacl later)

% Take the nodes out of another inp file.
fid1=fopen(Node_File,'r+'); % Open file for reading/writing
idx = 0;
while ~feof(fid1)
    idx = idx + 1;
    tline=fgetl(fid1);
    if isempty(strfind(tline,'*Node')) == 0 % Scan till *Nodes

        for i=1:2000000000 % Scan till * Found
            tline=fgetl(fid1);
            if isempty(strfind(tline,'*')) == 0
                NodesMax=i-1;%calculate the new value of maximum nodes
                break
            else
                nodes(i,:)=sscanf(tline,'%d,%f,%f,%f')';
            end
        end
        break
    end
end
fclose(fid1);

% for loop to print nodes into the .inp file
% nodes will be scaled at this time
node_scale = wing_length/(max(nodes(:,2))); %sets scale = to desired
legnth
fprintf(fid2,'%d, %2.10f, %2.10f, %2.10f\n',[nodes(:,1),...
                                             (nodes(:,2)-
x_offset)*node_scale,...
                                             (nodes(:,3)-
y_offset)*node_scale,...
                                              nodes(:,4)]');


%% Elements
% For beam elements
fprintf(fid2,'*Element, type=B32'); %heading for the elements
fprintf(fid2,'\n');

%Search Input File for *Elem Locations
fid1=fopen(Node_File,'r+'); % Open file for reading/writing
idx = 0;
while ~feof(fid1)
    idx = idx + 1;
    tline=fgetl(fid1);
    if isempty(strfind(tline,'*Element, type=B32')) == 0 % ''
        for i=1:NodesMax                  % Scan till * Found
            tline=fgetl(fid1);
            if isempty(strfind(tline,'*')) == 0
                break
            else

elems.B32(i,:)=sscanf(tline,'%f,%f,%f,%f,%f,%f,%f,%f,%f')';
            end
        end
```

```
        break
    end
end
fclose(fid1);
% Write nodes into the program file
fprintf(fid2,'%d,%6.0f,%6.0f,%6.0f\n',[elems.B32]');

% Heading for quad elements membrane section
fprintf(fid2,'*Element, type=S8R'); %heading for the elements
fprintf(fid2,'\n');

%Search Input File for *Elem Locations
fid1=fopen(Node_File,'r+');
idx = 0;
while ~feof(fid1)
    idx = idx + 1;
    tline=fgetl(fid1);
    if isempty(strfind(tline,'*Element, type=S8R')) == 0 % Scan till ''
        for i=1:NodesMax
            tline=fgetl(fid1);
            if isempty(strfind(tline,'*')) == 0
                break
            else

elems.S8R(i,:)=sscanf(tline,'%f,%f,%f,%f,%f,%f,%f,%f,%f')';
            end
        end
        break
    end
end
fclose(fid1);

%Write the Elements to the File
fprintf(fid2,'%d,%6.0f,%6.0f,%6.0f,%6.0f,%6.0f,%6.0f,%6.0f,%6.0f\n',[el
ems.S8R(:,:)]');

% For tri elements membrane section
fprintf(fid2,'*Element, type=STRI65'); %heading for the elements
fprintf(fid2,'\n');

%Search Input File for *Elem Locations
fid1=fopen(Node_File,'r+'); % Open file for reading/writing
idx = 0;
while ~feof(fid1)
    idx = idx + 1;
    tline=fgetl(fid1);
    if isempty(strfind(tline,'*Element, type=STRI65')) == 0 % Scan till
        for i=1:NodesMax
            tline=fgetl(fid1);
            if isempty(strfind(tline,'*')) == 0
                break
            else

elems.STRI65(i,:)=sscanf(tline,'%f,%f,%f,%f,%f,%f,%f,%f,%f')';
            end
        end
```

```
        break
    end
end
fclose(fid1);

% Print Tri Elements to the Program
fprintf(fid2,'%d,%6.0f,%6.0f,%6.0f,%6.0f,%6.0f,%6.0f\n',elems.STRI65');
%% Read Stringer Node Sets
%Search Input File for Stringer Nsets
fid1=fopen(Node_File,'r+'); % Open file for reading/writing
for j=1:12 %(Number of Stringers)
    idx = 0;
    Stringers(j).nset=[];
    while ~feof(fid1)
        idx = idx + 1;
        tline=fgetl(fid1);
        if isempty(strfind(tline,['*Nset, nset=_Stringer-' num2str(j)
', internal'])) == 0 % ''
            for i=1:NodesMax                    % Scan till * Found
                tline=fgetl(fid1);
                if isempty(strfind(tline,'*')) == 0
                    break
                else
                    Stringers(j).nset=[Stringers(j).nset
sscanf(tline,'%f,')'];
                end
            end
            break
        end
    end
end
fclose(fid1);

%% Read Stringer Element Sets
%Search Input File for Stringer Elsets
fid1=fopen(Node_File,'r+'); % Open file for reading/writing
for j=1:12 %(Number of Stringers)
    idx = 0;
    Stringers(j).elset=[];
    while ~feof(fid1)
        idx = idx + 1;
        tline=fgetl(fid1);
        if isempty(strfind(tline,['*Elset, elset=_Stringer-' num2str(j)
', internal, generate'])) == 0 % ''
            for i=1:NodesMax                    % Scan till * Found
                tline=fgetl(fid1);
                if isempty(strfind(tline,'*')) == 0
                    break
                else
                    Stringers(j).elset=[Stringers(j).elset
sscanf(tline,'%f,')'];
                end
            end
            break
        end
    end
```

```
end
fclose(fid1);

%% Process Stringer Element Sets
for j=1:12

Stringers(j).vect=[Stringers(j).elset(1):Stringers(j).elset(3):Stringer
s(j).elset(2)]'; %Vector of Elements

    % Find Index of Stringer Elements within the subset of all the
Model Elements
    [c, ia, ib]=intersect(elems.B32(:,1),Stringers(j).vect); % c =
common values, ia = index values in A, ib = index values in b

    % Assign Stringer Nodes to Elements
    Stringers(j).elems=elems.B32(ia,1:end);

    % Assign Midpoint Node Location to Elems
    Stringers(j).elems=[Stringers(j).elems
nodes(Stringers(j).elems(:,3),2:end)];

    % Sort Elems based on Midpoint Nodes X-Location
    if j ~= 5
        [Stringers(j).elems]=sortrows(Stringers(j).elems,5); % Sort
veins based on X-Location
    else
        [Stringers(j).elems]=sortrows(Stringers(j).elems,6); % Sort
Arculus based on Y-Location
    end
end

for j=1:12

Stringers(j).widths=linspace(StringersWidth(j,1),StringersWidth(j,2),si
ze(Stringers(j).elems,1))';
    [Stringers(j).elems]=[Stringers(j).elems Stringers(j).widths]; %
Assign widths to last column
end

%% Rearrange Structured Stringers Variable into new Unstructured
Variable
elems.Stringers=[]; % [Elem #,StartNode,MidNode,EndNode,Width,(add
angle later in code)]
for j=1:12
    elems.Stringers=[elems.Stringers; Stringers(j).elems(:,[1:4,8])];
end

elems.Stringers=sortrows(elems.Stringers,1); % Sort Elems by Elem#

%% Calculate Angle between the Stringer B32 Elements
% needed to determine material properties.
for m = 1:(length(elems.B32(:,1)))
    %determine the first node that is part of the element i.e x
coordinate
    node_str = elems.B32(m,2);
```

```
    %determine the second (mid point) node of the element i.e y
coodiinate
    node_end = elems.B32(m,3);
    %location of first node
    loc_str =
[(nodes(node_str,2)),(nodes(node_str,3)),(nodes(node_str,4))];
    % location of the end node
    loc_end =
[(nodes(node_end,2)),(nodes(node_end,3)),(nodes(node_end,4))];
    % determine the slope of the line
    slope_2 = (loc_str(1,2) - loc_end(1,2))/(loc_str(1,1) -
loc_end(1,1));
    %determine the angle with horizontal [inf,0,0] vector from origin
    theta_elem = atand(slope_2);
    %store it!
    angle(m,1)=m; %stores the row number in angle in 1st column
    angle(m,2)= elems.B32(m,1); %the 2nd column hold element number
    angle(m,3)=theta_elem; % 3rd column holds the angle
end

elems.Stringers=[elems.Stringers angle(:,3)]; % Append Angle Data

%% Write Nset and Elsets
% For the beam
set_ctr=0; %counts the number of Node and Element Sets
% Create a new section for each Vein element
for x=1:length(angle)
    %create heading and pick a Nset
    fprintf(fid2,'*Nset, nset=_PickedSet%-2.0f,
internal\n',angle(x,1));
    nset_nodes = sort(elems.B32(x,2:4));%sort out the nodes in
asscending order
    %print nodes in that Nset i.e. for each element
    fprintf(fid2,'%6.0f, %6.0f,
%6.0f\n',nset_nodes(1),nset_nodes(2),nset_nodes(3));

    % for Elsets, create elset same number as corresponding Nset
    fprintf(fid2,'*Elset, elset=_PickedSet%-2.0f,
internal\n',angle(x,1));
    fprintf(fid2,'%6.0f\n',angle(x,2));

    set_ctr=set_ctr+1; %add to Set counter
end

% For the Membrane
% Quad S8R elements
% Sort the nodes in order, using unique to get rid of duplicates
s8r_node=sort(unique(elems.S8R));
fprintf(fid2,'*Nset, nset=_PickedSet%-2.0f, internal\n',(set_ctr+1));
fprintf(fid2,'%d, %d, %d, %d, %d, %d, %d, %d, %d, %d, %d, %d, %d, %d,
%d, %d\n',s8r_node(:,1));
fprintf(fid2,'\n');
% sort the elements in order
s8r_elem=sort(elems.S8R(:,1));
% for Elsets, create elset same number as corresponding Nset
fprintf(fid2,'*Elset, elset=_PickedSet%-2.0f, internal\n',(set_ctr+1));
```

```
fprintf(fid2,'%d, %d, %d, %d, %d, %d, %d, %d, %d, %d, %d, %d, %d, %d,
%d, %d\n',s8r_elem(:,1));
fprintf(fid2,'\n');

% Tri STRI65 elements
% Sort the nodes in order, using unique to get rid of duplicates
tri_node=sort(elems.STRI65);
fprintf(fid2,'*Nset, nset=_PickedSet%-2.0f, internal\n',(set_ctr+2));
fprintf(fid2,'%d, %d, %d, %d, %d, %d, %d, %d, %d, %d, %d, %d, %d, %d,
%d, %d\n',tri_node(:,1));
fprintf(fid2,'\n');
% sort the elements in order
tri_elem=sort((elems.STRI65(:,1)));
% for Elsets, create elset same number as corresponding Nset
fprintf(fid2,'*Elset, elset=_PickedSet%-2.0f, internal\n',(set_ctr+2));
fprintf(fid2,'%d, %d, %d, %d, %d, %d, %d, %d, %d, %d, %d, %d, %d, %d,
%d, %d\n',tri_elem(:,1));
fprintf(fid2,'\n');

%% Beam Sections
% The sections will start with the veins and begin with Section 1 (B32)
for x=1:length(angle) % new section for each element
    fprintf(fid2,'** Section: Section-%-2.0f  Profile: Profile-%-
2.0f\n'...
        ,x,x); % create section/profile
    fprintf(fid2,...
        '*Beam Section, elset=_PickedSet%-2.0f, material=Material-%-
2.0f, temperature=GRADIENTS, section=I\n'...
        ,x,x); % match the element with it's own elset and material

    b(x)=elems.Stringers(x,5);%artificial width of the beam element

    % Generate the I beam sections
    % Generate the I beam sections
    theta = angle(x,3)+theta_original(1,:); %determine theta
    %For the top ply run a function to determine Matl Prop
    [~,Ex,Ey,~,~,Vxy,Vyx,Gxy,Gxz,Gyz,~,~,~,~]=...
        LAMINATE_NASA_HALPIN_HYBRID_BASELINE_FUNC(40E-
3,b(x),h,alpha,theta(1,1),0);
    % Capture the Mat Properties so we don't have to run this again
    Matl_Ex(x,1) = Ex; Matl_Ey(x,1) = Ey; Matl_Vxy(x,1) = Vxy;
Matl_Vyx(x,1) = Vyx;
    Matl_Gxy(x,1) = Gxy; Matl_Gxz(x,1) = Gxz;Matl_Gyz(x,1) = Gyz;
    %Second ply
    [~,Ex,Ey,~,~,Vxy,Vyx,Gxy,Gxz,Gyz,~,~,~,~]=...
        LAMINATE_NASA_HALPIN_HYBRID_BASELINE_FUNC(40E-
3,b(x),h,alpha,theta(1,2),0);
    Matl_Ex(x,2) = Ex; Matl_Ey(x,2) = Ey; Matl_Vxy(x,2) = Vxy;
Matl_Vyx(x,2) = Vyx;
    Matl_Gxy(x,2) = Gxy; Matl_Gxz(x,2) = Gxz;Matl_Gyz(x,2) = Gyz;
    %Third ply
    [~,Ex,Ey,~,~,Vxy,Vyx,Gxy,Gxz,Gyz,~,~,~,~]=...
        LAMINATE_NASA_HALPIN_HYBRID_BASELINE_FUNC(40E-
3,b(x),h,alpha,theta(1,3),0);
    Matl_Ex(x,3) = Ex; Matl_Ey(x,3) = Ey; Matl_Vxy(x,3) = Vxy;
Matl_Vyx(x,3) = Vyx;
```

```
    Matl_Gxy(x,3) = Gxy; Matl_Gxz(x,3) = Gxz;Matl_Gyz(x,3) = Gyz;

    % Use largest value of Ex to decide value for the effective modulus
    % This prevents the width of some sections from being too large.
    Eff_Mod = max(Matl_Ex(x,:)); %determines max Ex
    width(x,1)= Matl_Ex(x,1)/Eff_Mod; %makes the width of each section
a scaler, with largest being = 1
    width(x,2)= Matl_Ex(x,2)/Eff_Mod;
    width(x,3)= Matl_Ex(x,3)/Eff_Mod;

    % Prevent I(12)*2 from being > I(11)+I(22)
    if width(x,1)< width(x,2)/2.5
        width(x,1)=width(x,2);
        h_new=h/(3-(width(x,2)/(min(width(x,:)))));
        h=h_new;
    end
    if width(x,3)< width(x,2)/2.5
        width(x,3)=width(x,2);
        h_new=h1/(3-(width(x,2)/(min(width(x,:)))));
        h=h_new;
    end

    % Calculate the effective density for the Beam Sections
    real_area = h1*b(x); %real cross sectional area of the element
    faux_area = h*b(x)*(width(x,1)/3 + width(x,2)/3 + width(x,3)/3);
%area of I-beam section for the element
    area_scale = real_area/faux_area; %scale factor to multiply density
by so mass is same for all elements
    Density(x)=den_cf*area_scale;

    % prints out in (l, h, b1(base width), b2 (top width), t1 (base),
t2(top), t3(mid width))
    fprintf(fid2,'% #6.12g, % #6.12g, % #6.12g, % #6.12g, % #6.12g, %
#6.12g, % #6.12g\n',...
        h/2,h,b(x)*width(x,3),b(x)*width(x,1),h/3,h/3,b(x)*width(x,2));
    %prints out the orientation of the beam, same for all cases
    fprintf(fid2,'0.,1.,0. \n');

    % put thickness back to original thickness
    h=h1;
end

% This section is for the Quad (S8R) elements
fprintf(fid2,'** Section: Section-%-2.0f\n',(set_ctr+1)); % create
section/profile
fprintf(fid2,'*Shell Section, elset=_PickedSet%-2.0f,
material=Material-%-2.0f\n'...
    ,(set_ctr+1),(set_ctr+1));
fprintf(fid2,'%6.12g,  %d\n',shell_thick,5);

% This section is for the TRI (STRI65) elements
fprintf(fid2,'** Section: Section-%-2.0f\n',(set_ctr+2)); % create
section/profile
fprintf(fid2,'*Shell Section, elset=_PickedSet%-2.0f,
material=Material-%-2.0f\n'...
```

```
    ,(set_ctr+2),(set_ctr+2));
fprintf(fid2,'%6.12g, %d\n',shell_thick,5);

%% End Instance
fprintf(fid2,'*End Instance\n');
fprintf(fid2,'**\n');

%% Nset for Boundry Conditions and Point Load
%Create a set of nodes where the boundry conditions will be applied
fprintf(fid2,'*Nset, nset=_PickedSet%-2.0f, internal, instance=Part-1-
1\n'...
    ,(set_ctr+3));
%Put in the nodes you wish to clamp in this case the base
fprintf(fid2,'%d,\n',Base_Node_Loc);

%Creat a set for the Pt Load to be applied
fprintf(fid2,'*Nset, nset=_PickedSet%-2.0f, internal, instance=Part-1-
1\n'...
    ,(set_ctr+4));
%Put in the node where you want the force applied.
fprintf(fid2,'%d,\n',Pt_Node_Loc);

%% End Assembly
fprintf(fid2,'*End Assembly\n'); %ends the assembly portion of it
fprintf(fid2,'**\n');

%% Materials
%Standard Heading
fprintf(fid2,'** MATERIALS\n');
fprintf(fid2,'**\n');

% Determine and Assign Matl Prop for the Veins (B32 elements)
for x=1:size(angle,1)
    theta = angle(x,2)+theta_original(1,:);
    %set up material properties
    fprintf(fid2,'*Material, name=Material-%-2.0f\n',x);
    fprintf(fid2,'*Density\n');
    fprintf(fid2,'%#6.6f\n',Density(x));
    fprintf(fid2,'*Elastic, type=ENGINEERING CONSTANTS\n');

    % Use the material propertie saved from Section section
    % determine which properties to use
    ctr=max(Matl_Ex(x,:));
    if Matl_Ex(x,1) == ctr;
        ctr = 1;
    elseif Matl_Ex(x,2) == ctr;
        ctr=2;
    elseif Matl_Ex(x,3) == ctr;
        ctr=3;
    end
    fprintf(fid2,'%#12.6g, %#12.6g, %#12.6g, %#12.6g, %#12.6g, %#12.6g,
%#12.6g, %#12.6g,\n'...
        ,Matl_Ex(x,ctr),Matl_Ey(x,ctr),Matl_Ey(x,ctr),0.1,0.1,0.1,...
        Matl_Gxy(x,ctr),Matl_Gxz(x,ctr));
    fprintf(fid2,'%#12.6g,\n',Matl_Gyz(x,ctr));
```

```
end

% Assign the Matl Prop to the Quad elements (S8R)
fprintf(fid2,'*Material, name=Material-%-2.0f\n',(set_ctr+1));
fprintf(fid2,'*Density\n');
fprintf(fid2,'%#6.6f\n',den_sh);
fprintf(fid2,'*Elastic\n');
fprintf(fid2,'%#12.6g, %#6.6f\n',[shell_E shell_v]);

% Assign the Matl Prop to the TRI elements (STRI65)
fprintf(fid2,'*Material, name=Material-%-2.0f\n',(set_ctr+2));
fprintf(fid2,'*Density\n');
fprintf(fid2,'%#6.6f\n',den_sh);
fprintf(fid2,'*Elastic\n');
fprintf(fid2,'%#12.6g,%#6.6f\n',[shell_E shell_v]);

%% Steps
%create the steps to output the Eignevector/Eigenvalue and Point load
%response

%% Step 1 Point Load
%Create a static step to evaluate a point load located on the wing
%Standard Heading
fprintf(fid2,'** ----------------------------------------------------
----------\n');
fprintf(fid2,'** \n');
fprintf(fid2,'** STEP: Step-1\n');
fprintf(fid2,'**\n');

%Since we want a static load it will look like this
fprintf(fid2,'*Step, name=Step-1, perturbation\n'); % perturbation must
be set otherwise step will carry over loads
fprintf(fid2,'*Static\n');

%Boundry Conditions
%Standard Heading
fprintf(fid2,'** \n');
fprintf(fid2,'** BOUNDARY CONDITIONS\n');
fprintf(fid2,'** \n');

%create a boundry condition (in this case it will be clamped)
fprintf(fid2,'** Name: BC-1 Type: Displacement/Rotation\n'); %since
only one, can fix 6 dof, says type of boundry cond
fprintf(fid2,'*Boundary\n');%tells abaqus there is a boundry conditon
fprintf(fid2,'_PickedSet%-2.0f, 1, 1\n',(set_ctr+3)); %hold in x or 1
dir
fprintf(fid2,'_PickedSet%-2.0f, 2, 2\n',(set_ctr+3)); %hold in y or 2
dir
fprintf(fid2,'_PickedSet%-2.0f, 3, 3\n',(set_ctr+3)); %hold in z or 3
dir
fprintf(fid2,'_PickedSet%-2.0f, 4, 4\n',(set_ctr+3)); %hold in rot
about 1 axis
fprintf(fid2,'_PickedSet%-2.0f, 5, 5\n',(set_ctr+3)); %hold in rot
about 2 axis
```

```
fprintf(fid2,'_PickedSet%-2.0f, 6, 6\n',(set_ctr+3)); %hold in rot
about 3 axis

% Loads
%Heading
fprintf(fid2,'**\n');
fprintf(fid2,'** LOADS\n');
fprintf(fid2,'**\n');

%Apply they type of load, a concentrated node
fprintf(fid2,'** Name: Load-1   Type: Concentrated force\n');%name of
load
fprintf(fid2,'*Cload\n');% type = concentrated
fprintf(fid2,'_PickedSet%-2.0f, 3, %d\n',(set_ctr+4), Pt_Load);

% Outputs
%Standard Heading
fprintf(fid2,'**\n');
fprintf(fid2,'** OUTPUT REQUESTS\n');
fprintf(fid2,'**\n');

%Displacement/Stress outputs (in this case it does not change)
fprintf(fid2,'** FIELD OUTPUT: F-Output-1\n');
fprintf(fid2,'** \n');
fprintf(fid2,'*Output, field, variable=PRESELECT\n');

%History Output
fprintf(fid2,'**\n');
fprintf(fid2,'** HISTORY OUTPUT: H-Output-1\n');
fprintf(fid2,'**\n');
fprintf(fid2,'*Output, history, variable=PRESELECT\n');

% End Step
fprintf(fid2,'*End Step\n');

%% Step 2 Frequency
%Create a step that wil levaluate Eigenvectors/Eigenvalues of the wing
%Standard Heading
fprintf(fid2,'** ----------------------------------------------------
----------\n');
fprintf(fid2,'** \n');
fprintf(fid2,'** STEP: Step-2\n');
fprintf(fid2,'**\n');

%Since we want to find freqency, it'll look like this
fprintf(fid2,'*Step, name=Step-2, perturbation\n');
fprintf(fid2,'Find Freq. \n');
fprintf(fid2,'*Frequency, eigensolver=Lanczos, acoustic coupling=on,
normalization=displacement\n');
fprintf(fid2,'%6.0f, , , , ,\n',num_modes);

%Boundry Conditions
%Standard Heading
fprintf(fid2,'** \n');
fprintf(fid2,'** BOUNDARY CONDITIONS\n');
```

```
fprintf(fid2,'** \n');

%create a boundry condition (in this case it will be clamped)
fprintf(fid2,'** Name: BC-1 Type: Displacement/Rotation\n'); %since
only one, can fix 6 dof, says type of boundry cond
fprintf(fid2,'*Boundary\n');%tells abaqus there is a boundry conditon
fprintf(fid2,'_PickedSet%-2.0f, 1, 1\n',(set_ctr+3)); %hold in x or 1
dir
fprintf(fid2,'_PickedSet%-2.0f, 2, 2\n',(set_ctr+3)); %hold in y or 2
dir
fprintf(fid2,'_PickedSet%-2.0f, 3, 3\n',(set_ctr+3)); %hold in z or 3
dir
fprintf(fid2,'_PickedSet%-2.0f, 4, 4\n',(set_ctr+3)); %hold in rot
about 1 axis
fprintf(fid2,'_PickedSet%-2.0f, 5, 5\n',(set_ctr+3)); %hold in rot
about 2 axis
fprintf(fid2,'_PickedSet%-2.0f, 6, 6\n',(set_ctr+3)); %hold in rot
about 3 axis

%Outputs
%Standard Heading
fprintf(fid2,'**\n');
fprintf(fid2,'** OUTPUT REQUESTS\n');
fprintf(fid2,'**\n');

%Frequency outputs (in this case it does not change)
fprintf(fid2,'*Restart, write, frequency=0\n');
fprintf(fid2,'** \n');
fprintf(fid2,'** FIELD OUTPUT: F-Output-2\n');
fprintf(fid2,'** \n');
fprintf(fid2,'*Output, field, variable=PRESELECT\n');

%End First Step
fprintf(fid2,'*End Step\n');

%% Close the File
fclose(fid2);

%% Run
% This line runs the completed file
 %Make matlab slow down so Abaqus doesn't crash
 pause(5)
eval(['dos(''abq6111 job=' Input_File ' interactive'')'])

%% Open .dat File
%Gather the results from the .dat file and store in a matrix
fid3=fopen([Input_File(1:length(Input_File)-4) '.dat'],'r+'); % Opens
.dat file for reading/writing
idx = 0;
while ~feof(fid3)
    idx = idx + 1;
    tline=fgetl(fid3);
    if isempty(strfind(tline,'E I G E N V A L U E    O U T P U T  '))
== 0 % Scan till *Nodes
        for i=1:5
```

```
            tline=fgetl(fid3); % Read 5 lines of blank stuff
        end
        for i=1:1 % for i = 1 to the number of modes you wish to get
            %Get the 1st Modal Freq.
            Eigen_value_string(i,:)=fgetl(fid3);%Grabs the
eigenvector/value date from .dat file
            make_text =  str2num(Eigen_value_string); %converts text
into numbers MATLAB can read
            Eigen_value1 = make_text(1,4); % gets the Frequency from
the string of numbers
            %Get the 2nd Modal Freq.
            Eigen_value_string(i,:)=fgetl(fid3);%Grabs the
eigenvector/value date from .dat file
            make_text =  str2num(Eigen_value_string); %converts text
into numbers MATLAB can read
            Eigen_value2 = make_text(1,4); % gets the Frequency from
the string of numbers
        end
    end
end

fclose(fid3); % Closes the File
```

Appendix H. Wing .inp File

Appendix H contains a condensed version of the .inp file submitted to ABAQUS in order to solve the engineered wing FEA Model. Redundant information has been replaced by the symbol [snip]… because the original .inp file would take approximately 658 pages to illustrate due to the vast number of element sets and material properties.

```
*Heading
** Job name: BEAM_MODAL_BASELINE Model name: 08-Feb-2012
*Preprint, echo=NO, model=NO, history=NO, contact=NO
**
** PARTS
*Part, name=WING_FIT_SHOULDER_EE_08-Feb-2012
**
*End Part
**
**** ASSEMBLY
**
*Assembly, name=Assembly
**
*Instance, name=Part-1-1, part=WING_FIT_SHOULDER_EE_08-Feb-2012
*Node
1, 0.0111069997, -0.0007809994, 0.0000000000
2, 0.0000000000, 0.0000000000, 0.0000000000
3, 0.0253340003, 0.0031570005, 0.0000000000
4, 0.0224740005, 0.0004820003, 0.0000000000
5, 0.0223999998, -0.0012629998, 0.0000000000

[snip]…

22247, 0.0405554337, 0.0051652824, 0.0000000000
22248, 0.0307590264, 0.0053330138, 0.0000000000
**
*Element, type=B32
7356,  1105, 21460,    15
7357,  1106, 21477,  1105

[snip]…

8447,   380,  8626,   381
8448,   381,  8579,     7
**
*Element, type=S8R
14,    18,    19,  1356,  1363,  7487,  7488,  7489,  7490
15,  1356,  1357,  1502,  1308,  7491,  7492,  7493,  7494

[snip]…

7354,  7433,  7445,  7446,  7430, 22002, 21771, 22234, 22229
7355,  7293,  7244,  7357,  7292, 22126, 21749, 22038, 21846
**
```

```
*Element, type=STRI65
1,  1674,  1444,  1304,  7448,  7449,  7450
2,    49,     2,    50,  7451,  7452,  7453

[snip]…

6963,  7431,  7419,  7328, 21470, 21471, 21472
6964,  7392,  7418,  7233, 21473, 21474, 21475
**
*Nset, nset=_PickedSet1 , internal
    15,   1105,  21460
*Elset, elset=_PickedSet1 , internal
  7356
*Nset, nset=_PickedSet2 , internal
  1105,   1106,  21477
*Elset, elset=_PickedSet2 , internal
  7357

[snip]…

*Nset, nset=_PickedSet1093, internal
     7,    381,   8579
*Elset, elset=_PickedSet1093, internal
  8448
*Nset, nset=_PickedSet1094, internal
1, 3, 4, 5, 6, 7, 8, 9, 10, 11, 12, 13, 14, 15, 16, 17
18, 19, 20, 21, 22, 23, 24, 25, 26, 27, 28, 29, 30, 31, 32, 33
34, 35, 36, 37, 38, 39, 40, 41, 42, 43, 44, 45, 46, 47, 48, 49
50, 51, 52, 53, 54, 55, 56, 57, 58, 59, 60, 61, 62, 63, 64, 65
66, 67, 68, 69, 70, 71, 72, 73, 74, 75, 76, 77, 78, 79, 80, 81
82, 83, 84, 85, 86, 87, 88, 89, 90, 91, 92, 93, 94, 95, 96, 97
98, 99, 100, 101, 102, 103, 104, 105, 106, 107, 108, 109, 110, 111,
112, 113

[snip]…

22238, 22239, 22240, 22241, 22242, 22243, 22244, 22245, 22246, 22247,
22248,
**
*Elset, elset=_PickedSet1094, internal
14, 15, 16, 17, 18, 19, 20, 21, 22, 23, 24, 25, 26, 27, 28, 29
30, 31, 32, 33, 34, 35, 36, 37, 38, 39, 40, 41, 42, 43, 44, 45
46, 47, 48, 49, 50, 51, 52, 53, 54, 55, 56, 57, 58, 59, 60, 61
62, 63, 64, 65, 66, 67, 68, 69, 70, 71, 72, 73, 74, 75, 76, 77
78, 79, 80, 81, 82, 83, 84, 85, 86, 87, 88, 89, 90, 91, 92, 93
94, 95, 96, 97, 98, 99, 100, 101, 102, 103, 104, 105, 106, 107, 108,
109
110, 111, 112, 113, 114, 115, 116, 117, 118, 119, 120, 121, 122, 123,
124,

[snip]…
7341, 7342, 7343, 7344, 7345, 7346, 7347, 7348, 7349, 7350, 7351, 7352,
7353, 7354, 7355,
**
*Nset, nset=_PickedSet1095, internal
1, 2, 3, 4, 5, 6, 7, 8, 9, 10, 11, 12, 13, 524, 525, 526
```

```
527, 528, 529, 530, 531, 532, 533, 534, 535, 536, 537, 538, 539, 540,
1153,

[snip]…

6549, 6550, 6551
6552, 6553, 6955, 6956, 6957, 6958, 6959, 6960, 6961, 6962, 6963, 6964,
**
*Elset, elset=_PickedSet1095, internal
1, 2, 3, 4, 5, 6, 7, 8, 9, 10, 11, 12, 13, 524, 525, 526
527, 528, 529, 530, 531, 532, 533, 534, 535, 536, 537, 538, 539, 540,
1153,

[snip]…

6552, 6553, 6955, 6956, 6957, 6958, 6959, 6960, 6961, 6962, 6963, 6964,
**
** Section: Section-1   Profile: Profile-1
*Beam Section, elset=_PickedSet1 , material=Material-1 ,
temperature=GRADIENTS, section=I
 3.75000000000e-005,  7.50000000000e-005,  0.000200000000000,
0.000200000000000,  2.50000000000e-005,  2.50000000000e-005,
0.000200000000000
0.,1.,0.
** Section: Section-2   Profile: Profile-2

[snip]…

** Section: Section-1093  Profile: Profile-1093
*Beam Section, elset=_PickedSet1093, material=Material-1093,
temperature=GRADIENTS, section=I
 7.50000000000e-005,  0.000150000000000,  0.000150000000000,
0.000150000000000,  5.00000000000e-005,  5.00000000000e-005,
0.000125086683873
0.,1.,0.
** Section: Section-1094
*Shell Section, elset=_PickedSet1094, material=Material-1094
2e-005,  5
** Section: Section-1095
*Shell Section, elset=_PickedSet1095, material=Material-1095
2e-005, 5
*End Instance
**
*Nset, nset=_PickedSet1096, internal, instance=Part-1-1
2,
48,
51,
280,
283,
942,
1269,
*Nset, nset=_PickedSet1097, internal, instance=Part-1-1
1108,
*End Assembly
**
** MATERIALS
**
```

```
*Material, name=Material-1
*Density
3150.400000
*Elastic, type=ENGINEERING CONSTANTS
2.09090e+010, 6.92733e+009, 6.92733e+009,     0.100000,     0.100000,
0.100000, 5.15227e+009, 5.15227e+009,
3.78346e+009,
*Material, name=Material-2

[snip]…

*Material, name=Material-1093
*Density
1667.518713
*Elastic, type=ENGINEERING CONSTANTS
1.13487e+010, 9.51111e+009, 9.51111e+009,     0.100000,     0.100000,
0.100000, 5.60787e+009, 5.60787e+009,
5.09636e+009,
*Material, name=Material-1094
*Density
1249.600000
*Elastic
2.50000e+009, 0.300000
*Material, name=Material-1095
*Density
1249.600000
*Elastic
2.50000e+009,0.300000
** ----------------------------------------------------------------
**
** STEP: Step-1
**
*Step, name=Step-1, perturbation
*Static
**
** BOUNDARY CONDITIONS
**
** Name: BC-1 Type: Displacement/Rotation
*Boundary
_PickedSet1096, 1, 1
_PickedSet1096, 2, 2
_PickedSet1096, 3, 3
_PickedSet1096, 4, 4
_PickedSet1096, 5, 5
_PickedSet1096, 6, 6
**
** LOADS
**
** Name: Load-1   Type: Concentrated force
*Cload
_PickedSet1097, 3, -1.000000e-003
**
** OUTPUT REQUESTS
**
** FIELD OUTPUT: F-Output-1
**
*Output, field, variable=PRESELECT
```

```
**
** HISTORY OUTPUT: H-Output-1
**
*Output, history, variable=PRESELECT
*End Step
** ----------------------------------------------------------------
**
** STEP: Step-2
**
*Step, name=Step-2, perturbation
Find Freq.
*Frequency, eigensolver=Lanczos, acoustic coupling=on,
normalization=displacement
     9, , , , ,
**
** BOUNDARY CONDITIONS
**
** Name: BC-1 Type: Displacement/Rotation
*Boundary
_PickedSet1096, 1, 1
_PickedSet1096, 2, 2
_PickedSet1096, 3, 3
_PickedSet1096, 4, 4
_PickedSet1096, 5, 5
_PickedSet1096, 6, 6
**
** OUTPUT REQUESTS
**
*Restart, write, frequency=0
**
** FIELD OUTPUT: F-Output-2
**
*Output, field, variable=PRESELECT
*End Step
```

Appendix I. Wing Multi-Run Code

This code was used to create multiple runs of the wing code, and plot the results.

This Case is set to vary the laser cut angle.

```
clc; clear all; close all;
%% Define Number of Cases to Run
NumCases=13;
%% Definite Variation in Laser to Fiber Orientation
nstd_alpha=1;
avg_alpha=0;
alpha=[-6;-5;-4;-3;-2;-1;0;1;2;3;4;5;6]
alpha=[alpha];
%% Define Variation in Lamina Layup Orientation
nstd_theta=1;
avg_theta=0;
theta_original(:,2)=90-theta_original(:,2);
%% Define Variation in Laminate Thickness
nstd_t=1;
avg_thickness=150;
h = avg_thickness;
h = h*1E-6; %convert from integers to microns
%% Define Parameter Estimates
[ahat,bhat,ACI,BCI] = unifit(theta_original,.01);

%% Run the Analysis
 for t=1:NumCases
[Eigen_value1(t,:),Eigen_value2(t,:)]=Final_Wing(alpha(t),theta_origina
l(t,:),h(t),t);
 end

%% Plot the Results Histogram
close all
%% First Modal Frequency
% Open a Figure the size of the screen
scrsz = get(0,'ScreenSize');
figure('Position',[1 scrsz(2) scrsz(3) scrsz(4)])

nbins=100;
subplot(331)
hist(alpha,nbins)
grid on
xlabel(['Alpha = Mean ' num2str(avg_alpha) ' deg | std = '
num2str(nstd_alpha)])
ylabel('Bins')

subplot(332)
hist(theta_original(:,1),nbins)
grid on
xlabel(['Theta = Mean ' num2str(avg_theta) ' deg | std = '
num2str(nstd_theta)])
ylabel('Bins')
```

```
subplot(333)
hist(h(:,1)*1E6,nbins)
grid on
xlabel(['Thickness = Mean ' num2str(avg_thickness) ' um | std = '
num2str(nstd_t)])
ylabel('Bins')

subplot(3,3,4:6)
hist(Eigen_value1,nbins)
grid on
xlabel('1st Modal Frequency (Hz)')
ylabel('Bins')
title(['Mean freq = ' num2str(mean(Eigen_value1),'%f') ' (Hz)'])

subplot(3,3,7:9)
plot(1:NumCases,Eigen_value1,'.','MarkerSize',8)
grid on
xlabel('Sample')
ylabel('Frequency (Hz)')
hold on
plot([0 NumCases],mean(Eigen_value1)*[1 1],'--g','LineWidth',2)
legend('Samples','Mean','Location','SouthEast')
title(['Mean freq = ' num2str(mean(Eigen_value1),'%f') ' (Hz), Max freq
= ' num2str(max(Eigen_value1),'%f') ' (Hz), Min freq = '
num2str(min(Eigen_value1),'%f') ' (Hz)'])
hold off


%% 2nd Modal Frequency
scrsz = get(0,'ScreenSize');
figure('Position',[1 scrsz(2) scrsz(3) scrsz(4)])

nbins=100;
subplot(331)
hist(alpha,nbins)
grid on
xlabel(['Alpha = Mean ' num2str(avg_alpha) ' deg | std = '
num2str(nstd_alpha)])
ylabel('Bins')

subplot(332)
hist(theta_original(:,1),nbins)
grid on
xlabel(['Theta = Mean ' num2str(avg_theta) ' deg | std = '
num2str(nstd_theta)])
ylabel('Bins')

subplot(333)
hist(h(:,1)*1E6,nbins)
grid on
xlabel(['Thickness = Mean ' num2str(avg_thickness) ' um | std = '
num2str(nstd_t)])
ylabel('Bins')

subplot(3,3,4:6)
```

```
hist(Eigen_value2,nbins)
grid on
xlabel('2nd Modal Frequency (Hz)')
ylabel('Bins')
title(['Mean freq = ' num2str(mean(Eigen_value2),'%f') ' (Hz)'])

subplot(3,3,7:9)
plot(1:NumCases,Eigen_value2,'.','MarkerSize',8)
grid on
xlabel('Sample')
ylabel('Frequency (Hz)')
hold on
plot([0 NumCases],mean(Eigen_value2)*[1 1],'--g','LineWidth',2)
legend('Samples','Mean','Location','SouthEast')
title(['Mean freq = ' num2str(mean(Eigen_value2),'%f') ' (Hz), Max freq
= ' num2str(max(Eigen_value2),'%f') ' (Hz), Min freq = '
num2str(min(Eigen_value2),'%f') ' (Hz)'])
hold off
```

Appendix J. Additional Ideal Wing Mode Shape Images

First mode shape:

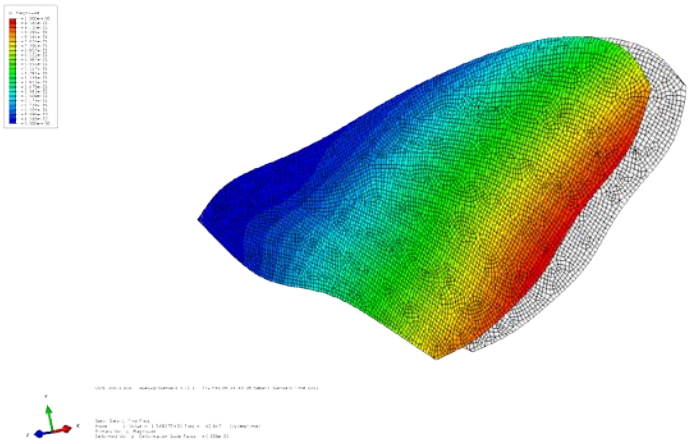

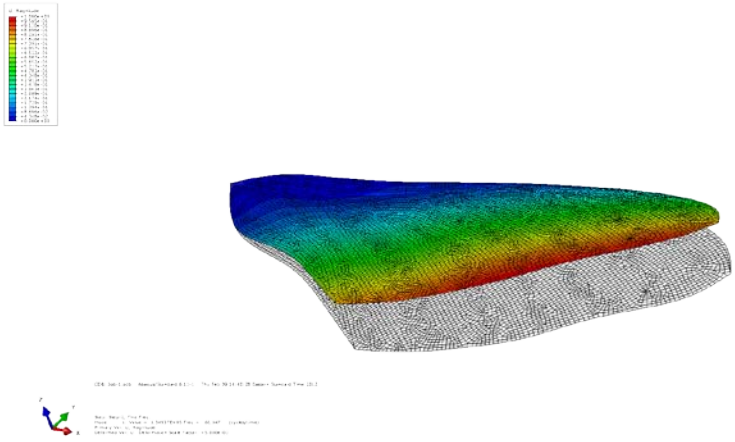

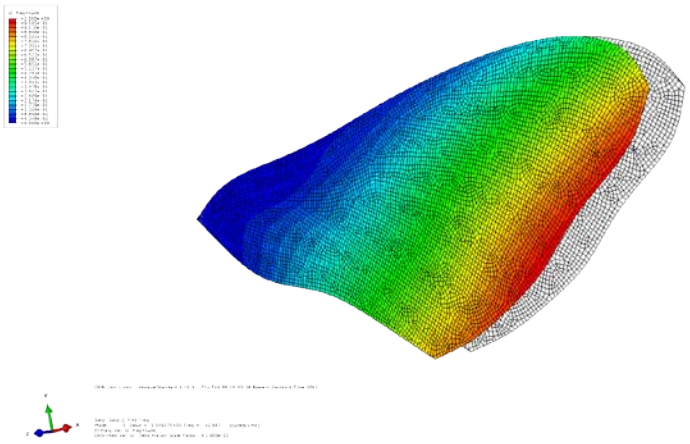

Second mode shape:

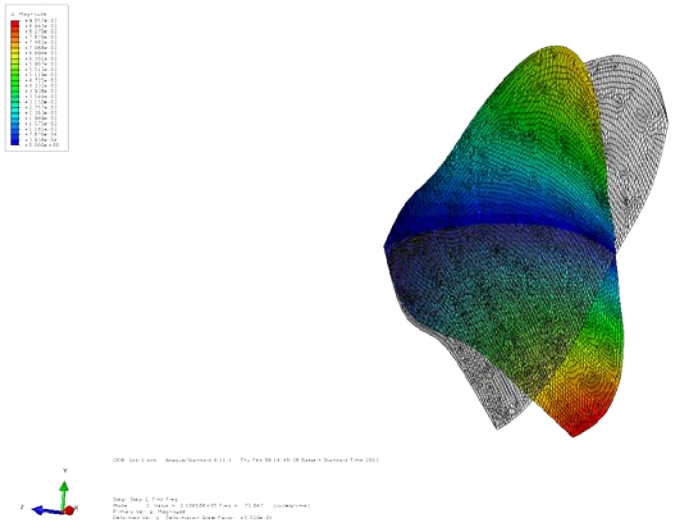

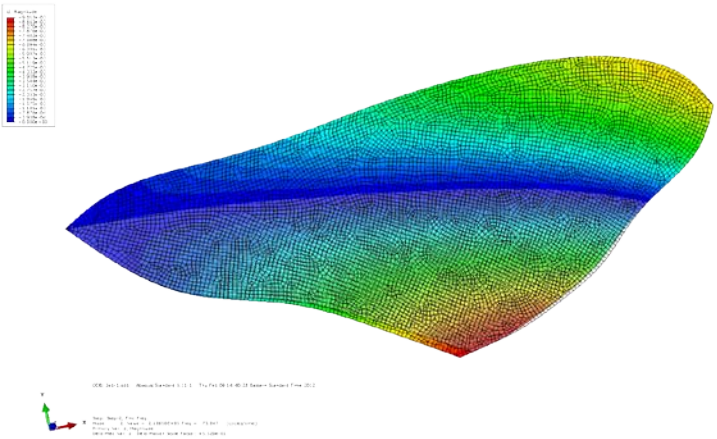

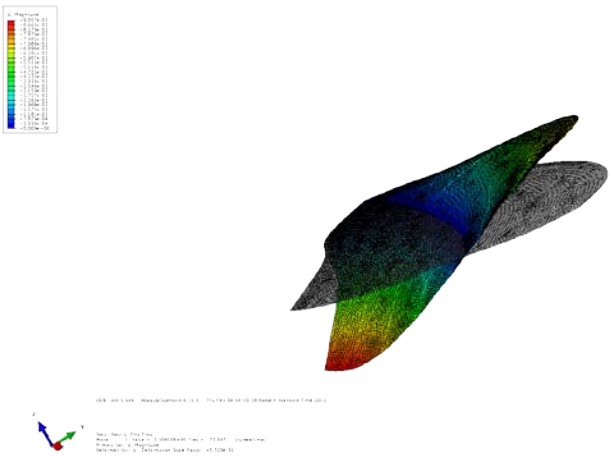

Third mode shape:

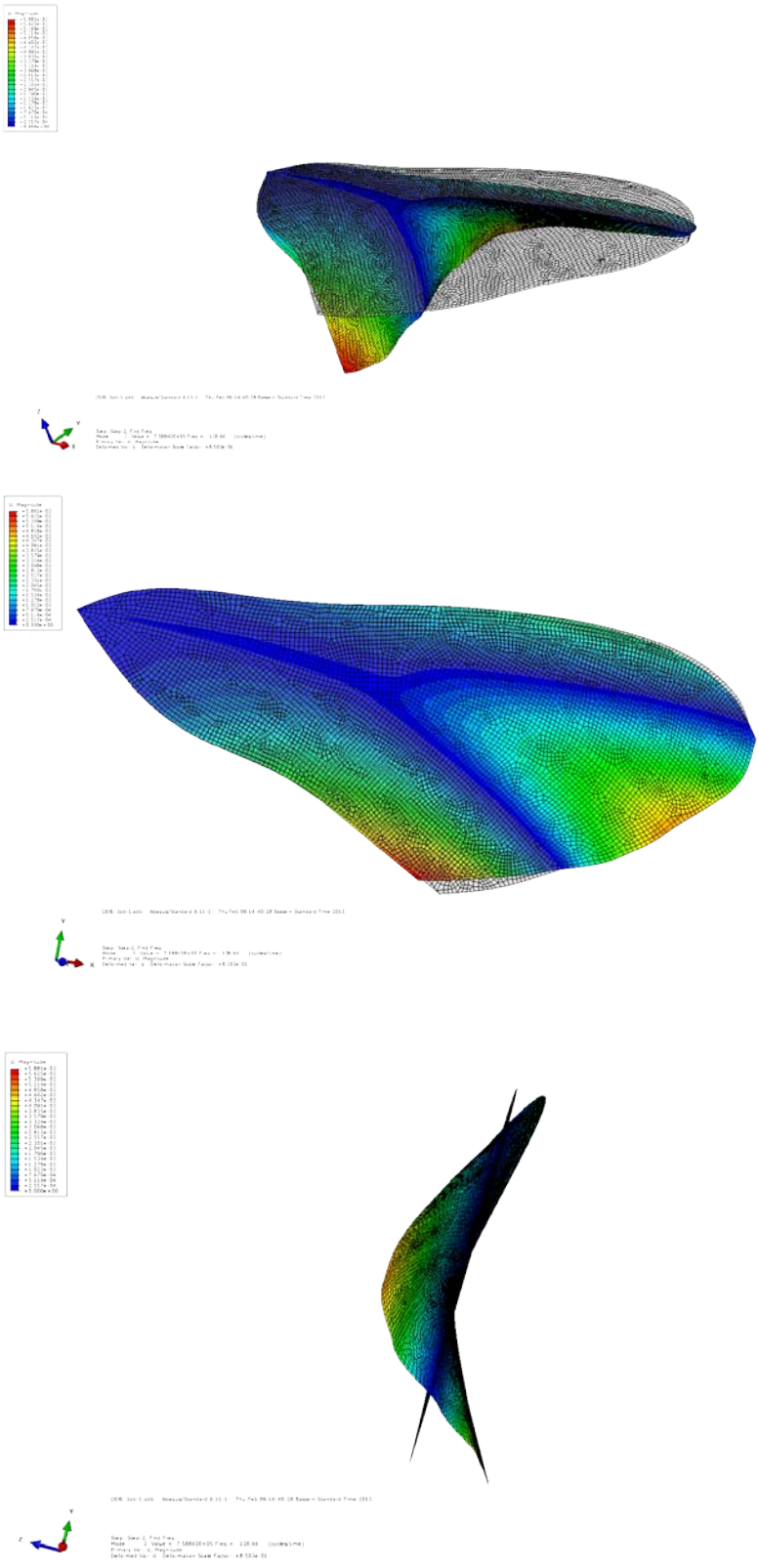

Fourth mode shape:

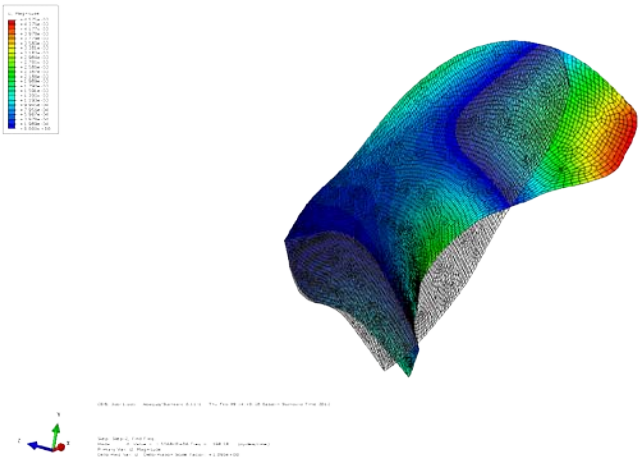

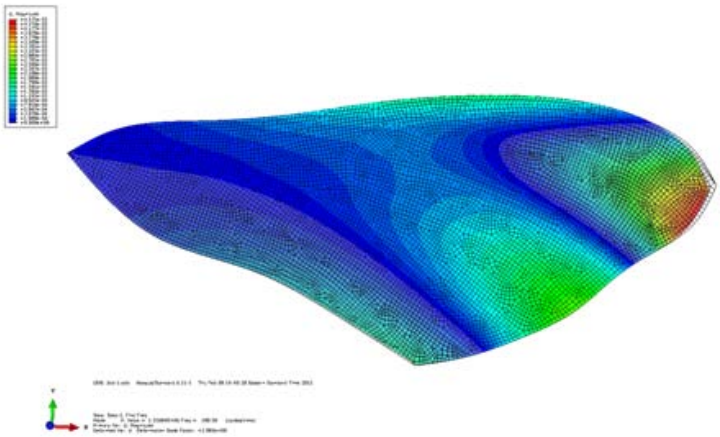

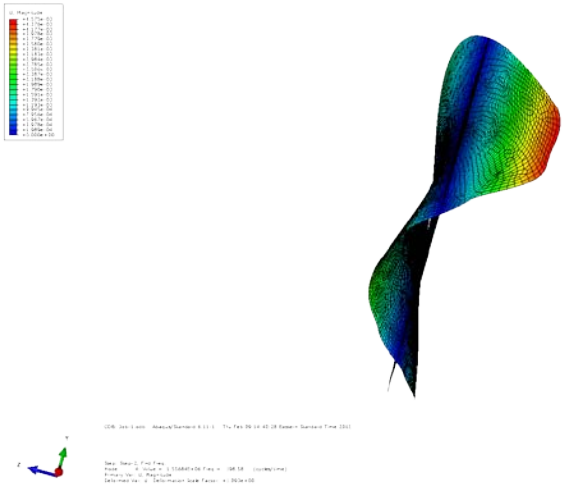

Bibliography

[1] R. O'Hara, "The Material Property and Structural Dynamic Characterization of the Manduca Sexta Forewing for Application to Flapping Micro Air Vehicle Design, Dissertation Prospectus," Air Force Institute of Technology, 2011.

[2] N. E. DeLeon, "Manufacturing and Evaluation of a Biologically Inspired Engineered MAV Wing Compared to the Manduca Sexta Wing Under Simulated Flapping Conditions," Air Force Institute of Technology, Master's Thesis, 2011.

[3] L. Xie, P. Wu and P. Ifju, "Advanced Flapping Wing Structure Fabrication for Biologically-Inspired Hovering Flight," 51st AIAA/ASME/ASCE/AHS/ASC Structures, Structural Dynamics, and Materials Converence, AIAA, 2010.

[4] R. C. Michelson and S. Reece, "Update on Flapping Wing Micro Air Vehicle Research," in *13th Bristol International RPV Conference*, 1998.

[5] A. Norris, "Investigation of Reinforced Membrane Wings for Use in Micro Air Vehicles," Air Force Institute of Technology, Dissertation Prospectus AFIT/GA/ENYDSY-09S, 2008.

[6] T. Sims, A. Palazotto and A. Norris, "A Strucural Dynamic Analysis of a Manduca Sexta Forewing," *International Journal of Micro Air Vehicles*, vol. 2, no. 3, September 2010.

[7] A. Norris, A. Palazotto and R. Cobb, "Structural Dynamic Characterization of an Insect Wing: Towards the Developement of Bug Sized Flapping Wing Micro Air Vehicles," *American Institute of Aeronautics and Astronautics*, 2006.

[8] E. v. Holst and D. Kuechemann, "Biologishe und Aerodynamische Probleme des Tierfluges," *Die Naturewissenshaften*, no. Neunundszwanzigster Jahrgang 1941, pp. 348-362, 1941.

[9] J. Meyer, External Atatomy: Wings.

[10] S. Hwang and C. Chang, "Determination of Elastic Constants of Materials by Vibration Testing," *Composite Structures*, pp. 49:183-190, 2000.

[11] A. Nettles, "Basic Mechanics of Laminated Composite Plates," in *NASA, Reference Publication 1351*, 1994.

[12] C. T. Herakovich, Mechanics of Fibrous Composites, New York, NY: John Wiley & Sons, 1998.

[13] R. Wood, "Design Fabrication and Analysis of a 3DOF 3cm Flapping Wing MAV," in *Conference on Intelligent Robots and Systems, IEEE*, San Diego, CA, USA, 2007.

[14] T. Storage, "Composite Fiber Database," August, 2011.

[15] T. Sims, "A Structural Dynamic Analysis of a Manduca Sexta Forewing," *Master's Thesis, Air Force Institute of Technology*, March, 2010.

[16] S. Combes and T. Daniels, "Flexural Stiffness in Insect Wings I. Scaling and the Influence of Wing Venation," *Jornal of Experimental Biology*, vol. 206, 2003.

[17] J. Marrocco, S. Venkataraman and L. Demasi, "Biomimetic Design of a Flexible Wing," in *ACCESS*, San Diego, 2009.

[18] A. Malik and B. Qureshi, "Vibration Analysis of Flapping Wing Micro Air Vehicle Using Finite Element Methods," in *Proceedings of the World Congress on Engineering 2010 Vol II*, 2004.

[19] J. C. Halpin and J. L. Kardos, "The Halpin-Tasi Equations: a Review".

[20] SIMULIA/ABAQUS, "Answers to Common ABAQUS Questions," Simulia, 1994. [Online]. Available: http://www.simulia.com/reference/epaper/answers_summer_94.pdf. [Accessed January 2012].

[21] S. 6.11-1, "ABAQUS 6.11-1 ABAQUS Users Manual, Vol. IV: Elements," Simulia, 2011. [Online]. Available: https://www.sharcnet.ca/Software/Abaqus/6.11.2/pdf_books/ANALYSIS_4.pdf. [Accessed October 2011].

[22] A. Tobias, "Experimental Methods to Characterize Nonlinear Vibration of Flapping Wing Micro Air Vehciles," *Master's Thesis, Air Force Insitute of Technology*, 2005.

[23] B. Singh, M. Ramasamy and I. Chopra, "Experimental Studies on Insect-Based Flapping Wings for Micro Hovering Air Vehicles," *American Institute of Aeronautics and Astronautics*, unk..

[24] P. Masarati, M. Morandini, G. Quaranta and R. Vescovini, "Multibody Analysis of a Micro-Aierial Vehicle Flapping Wing," MULTIBODY DYNAMICS, ECCOMAS Thematic Conference, 2011.

REPORT DOCUMENTATION PAGE

Form Approved
OMB No. 074-0188

1. REPORT DATE *(DD-MM-YYYY)*	**2. REPORT TYPE**	**3. DATES COVERED** *(From – To)*
22-03-2012	Master's Thesis	January 2011 – March 2012

4. TITLE AND SUBTITLE

A Finite Element Analysis of a Carbon Fiber Composite Micro Air Vehicle Wing

5a. CONTRACT NUMBER

5b. GRANT NUMBER

5c. PROGRAM ELEMENT NUMBER

6. AUTHOR(S)

Theodore A. Szelag

5d. PROJECT NUMBER

5e. TASK NUMBER

5f. WORK UNIT NUMBER

7. PERFORMING ORGANIZATION NAMES(S) AND ADDRESS(S)
Air Force Institute of Technology
Graduate School of Engineering and Management (AFIT/ENY)
2950 Hobson Way, Building 640
WPAFB OH 45433-8865

8. PERFORMING ORGANIZATION REPORT NUMBER

AFIT/GAE/ENY/12-M44

9. SPONSORING/MONITORING AGENCY NAME(S) AND ADDRESS(ES)
Dr. Douglas Smith AFOSR (703) 696-6219
DSN 426-6219 FAX (703) 696-7320
E-mail: douglas.smith@afosr.af.mil
Air Force Office of Scientific Research
Arlington VA 22203

10. SPONSOR/MONITOR'S ACRONYM(S)
AFOSR

11. SPONSOR/MONITOR'S REPORT NUMBER(S)

12. DISTRIBUTION/AVAILABILITY STATEMENT
APPROVED FOR PUBLIC RELEASE; DISTRIBUTION UNLIMITED.

13. SUPPLEMENTARY NOTES
This material is declared a work of the U.S. Government and is not subject to copyright protection in the United States.

14. ABSTRACT

Inaccuracies in the composite fiber orientation result in variations in the material properties. Experimental vibration data of manufactured three-ply [0/90/0] non-homogenous composite samples varied 33% from analytical results. Since the material was used in the manufacturing of a micro-air vehicle (MAV) based upon the Manduca Sexta, variance in the measured material properties and the effects on the manufacturing of the MAV wing needed to be understood.

An analysis was performed on the material taken into account inaccuracies; ply orientation, cut angle, and material thickness. Using finite element analysis (FEA), misalignment in fiber orientation of less than 5° was determined to account for the difference between analytical and experimental results. Using optical techniques, observed variances in the ply orientation confirmed FEA results.

A FEA model of the MAV wing was developed. To allow for quick changes to the model, the FEA model was generated using a developed MATLAB code that generated input files to be solved using ABAQUS, a finite element program. This MATLAB code generated beam cross-sections and corrected densities for the composite beam elements based upon the ply orientations and inaccuracies. An analysis was performed to determine the effects of the ply orientation misalignment on the FEA wing model.

15. SUBJECT TERMS
Micro Air Vehicle, Structural Dynamics, Unidirectional Carbon Composite, Finite Element, Manduca Sexta

16. SECURITY CLASSIFICATION OF:			**17. LIMITATION OF ABSTRACT**	**18.NUMBER OF PAGES**	**19a. NAME OF RESPONSIBLE PERSON**
a. REPORT	**b. ABSTRACT**	**c.THIS PAGE**			**Dr. Anthony N. Palazotto, PE, ADVISOR**
U	**U**	**U**	**UU**	**195**	**19b. TELEPHONE NUMBER** *(Include area code)* (937) 255-6565, ext 4599 (anthony.palazotto@afit.edu)

Standard Form 298 (Rev. 8-98)
Prescribed by ANSI Std. Z39-18